# Preparation and Characterization of Carbon Molecular Sieve (CMS) / SPEEK bilayer Membranes and SPEEK / Polyimide (PI) Blend Membranes for Direct Alcohols Fuel Cell (DAFC) performance

***Dissertation***

zur Erlangung des akademischen Grades

Doktor der Ingenieurwissenschaften

(Dr. –Ing.)

der Technischen Fakultät

der Christian-Albrechts-Universität zu Kiel

***Husnul Maab***

***Kiel***

***2009***

1. Gutachter Prof  Dr. Volker Abetz
2. Gutachter Prof  Dr. Rainer Adelung
3. Gutachter Prof Dr. Mady Elbahri

*Datum der mündlichen Prüfung: 25th September 2009*

# *Dedication*

*Germany is among those few countries who offer Free Education to the people from all over the world irrespective of their race and religion or any other identity. That shows the intention of this great nation for the technical and moral development of other nations of the world and to put human being on a more civilized path and peace. Fortunately I was among one of those who availed this opportunity and educated myself from the best scientific team inside GKSS Research Centre Geesthacht GmbH Germany.*

*I dedicate this research work to the German Nation and Government and hope that they will provide maximum opportunities to the students and researchers from Pakistan.*

# Table of contents


| | | | |
|---|---|---|---|
| Table of contents | | | i |
| List of Figures | | | vi |
| List of Tables | | | x |
| Chapter 1 | | Introduction | 1 |
| 1.0 | | History of fuel cell | 6 |
| 1.1 | | Fuel cell as an emerging technology | 8 |
| 1.2 | | Direct methanol fuel cell (DMFC ) | 12 |
| 1.3 | | Membranes for fuel cell | 20 |
| | 1.3.1 | Types of membranes materials for fuel cell | 21 |
| | 1.3.2 | Membranes characteristics for DMFC applications | 23 |
| | 1.3.3 | Factors affecting the performance of the membrane | 24 |
| | | *1.3.3.1 Hydration* | 24 |
| | | *1.3.3.2 Thickness* | 24 |
| 1.4 | | Sulfonated poly (ether ether ketone) (SPEEK) membranes | 25 |
| 1.5 | | Main Objective of the present work | 28 |
| | 1.5.1 | CMS coated SPEEK Bilayer membranes | 28 |
| | 1.5.2 | SPEEK / Polyimide (PI) Blend membranes | 29 |
| 1.6 | | References | 31 |
| Chapter 2 | | Theoretical background | 34 |
| 2.0 | | Proton transportation | 34 |
| 2.1 | | Electrical work, Potential and Efficiency of Fuel cell | 38 |
| | 2.1.1 | Theoretical electrical work | 38 |
| | 2.1.2 | Theoretical potential of fuel cell | 40 |
| | 2.1.3 | Theoretical fuel cell efficiency | 42 |

2.1.4 Actual efficiency of fuel cell 43
2.1.5 Comparasion of Carnot and fuel cell efficiencies 44
2.2 References 46
Chapter 3 Characterization Methods 48
3.0 Impedance measurements 48
3.1 Pervaporation of alcohols / water mixtures 56
3.1.1 Diffusion through polymeric membranes 58
3.1.2 Permeability, flux and selectivity 58
3.2 References 62
3.3 Electro-oxidation of fuel during fuel cell performance 64
3.3.1 Electro-oxidation of Hydrogen during fuel cell performance 64
3.3.2 Electro-oxidation of methanol fuel during (DMFC) test 65
3.3.3 Electro-oxidation of ethanol fuel during (DEFC) test 67
3.3.4 Oxygen reduction reaction 69
3.4 FTIR-ATR Spectroscopy 70
3.5 Atomic force microscopy 71
3.6 Scanning electron microscopy (SEM) 71
3.7 Thermal properties 72
3.7.1 Dynamics mechanical thermal analysis (DMTA) 72
3.7.2 Differential scanning calorimetry (DSC) 73
3.7.3 Thermogravimetric analysis (TGA) 73
3.8 References 74

| | | | |
|---|---|---|---|
| Chapter 4 | | Experimental Part | 76 |
| | | Preparation and characterization of Bilayer carbon molecular sieves (CMS) / SPEEK membranes; CMS as a fuel barrier and catalysts support. | 76 |
| 4.1 | | Introduction | 76 |
| 4.2 | | Experimental Work | 81 |
| | 4.2.1 | Materials | 81 |
| | 4.2.2 | Preparation of Carbon Molecular Sieve (CMS) layer | 81 |
| | 4.2.3 | Preparation of bilayer membranes | 82 |
| | 4.2.4 | FTIR-ATR Spectroscopy | 83 |
| | 4.2.5 | Morphology of bilyer membranes | 83 |
| | 4.2.6 | Pervaporation measurements | 83 |
| | 4.2.7 | Impedance measurements | 84 |
| | 4.2.8 | Membranes electrodes assembly (MEA) preparation | 84 |
| | 4.2.9 | Fuel cell tests | 85 |
| 4.3 | | Results and discussion | 86 |
| | 4.3.1 | CMS preparation by pyrolysis | 86 |
| | 4.3.2 | Morphology of CMS layer and bilayer membranes | 87 |
| | 4.3.3 | Pervaporation of alcohols and water through bilayer CMS /SPEEK membranes | 90 |
| | | *4.3.3.1 Effect of the pyrolysis temperature on the permeability of bilayer membranes* | 90 |
| | | *4.3.3.2 Effect of alcohols concentration and CMS layer thickness* | 92 |
| | | *4.3.3.3 Effect of alcohols molecular size* | 93 |
| 4.4 | | Characterization of bilayer membranes for fuel cell application | 97 |
| | 4.4.1 | Proton conductivity | 97 |
| | 4.4.2 | DMFC tests with standard electrodes | 97 |
| | 4.4.3 | Fuel cell results with integrated catalysts in the CMS layer | 99 |

| | | | |
|---|---|---|---|
| 4.5 | | Conclusion | 102 |
| 4.6 | | References | 103 |
| Chapter 5 | | Experimental Part | 111 |
| | | Preparation and characterization of SPEEK / Polyimide blends for proton conductive membranes | 111 |
| 5.1 | | Introduction | 111 |
| 5.2 | | Experimental Work | 112 |
| | 5.2.1 | Materials | 112 |
| | 5.2.2 | Molar mass distribution measurements by GPC | 113 |
| | 5.2.3 | Preparation of SPEEK / Polyimide (PI) blends | 113 |
| | 5.2.4 | Morphology | 113 |
| | 5.2.5 | FTIR-ATR Spectroscopy | 113 |
| | 5.2.6 | Water and Mixture uptake (%) | 114 |
| | 5.2.7 | Thermal properties | 115 |
| | | *5.2.7.1 Dynamic Mechanical Thermal Analysis (DMTA)* | 115 |
| | | *5.2.7.2 Differential Scanning Calometry (DSC)* | 115 |
| | | *5.2.7.3 Thermogravimetric analysis (TGA)* | 116 |
| | 5.2.7 | Pervaporation measurements | 116 |
| | 5.2.8 | Impedance measurements | 116 |
| | 5.2.9 | Membranes electrode assembly (MEA) preparation | 117 |
| | 5.2.10 | Fuel cell tests | 117 |
| 5.3 | | Results and discussion | 118 |
| | 5.3.1 | Membranes preparation and morphology | 118 |
| | 5.3.2 | FTIR-ATR study | 122 |
| | 5.3.3 | Water and Mixture uptake (%) | 123 |
| | 5.3.4 | Thermal properties | 123 |
| | 5.3.5 | Pervaporation of alcohol and water | 127 |
| | 5.3.6 | Proton conductivity | 129 |

5.3.7 DMFC tests 131

5.4 Conclusion 132

5.5 References 133

Chapter 6 Experimental Part 139

CMS coated SPEEK bilayer and SPEEK / Polyimide (PI) blends membranes for Direct Ethanol fuel cell (DEFC) performance 139

6.1 Introduction 139

6.2 Experimental Part 141

6.2.1 Materials and membranes preparation 141

6.2.2 Water and mixture uptake (%) 141

6.2.3 Pervaporation measurements 141

6.2.4 Membrane electrode assembly (MEA) preparation 142

6.2.5 Direct Ethanol Fuel Cell (DEFC) tests 142

6.3 Results and discussion 143

6.3.1 Water and mixture uptake (%) 143

6.3.2 Pervaporation of alcohol and water 144

6.3.3 Direct Ethanol Fuel cell (DEFC) tests 147

6.4 Conclusions 153

6.5 References 154

Chapter 7 Summary 157

7.1 Summary 157

7.2 Zusammenfassungen 161

Chapter 8 Acknowledgment 166

8.1 Acknowledgment 166

8.2 Curriculum Vitae (CV) 168

8.3 Pictures 171

# List of Figures


| | | |
|---|---|---|
| Figure 1.1: | Long term World population growth from 1750 to 2050 | 2 |
| Figure 1.2: | Satellite radar composite view of melting of Arctic ice from 1979 to 2005 (NASA) | 3 |
| Figure 1.3: | Schematic of a typical Fuel cell | 5 |
| Figure 1.4: | (a) Grove's Gas battery (Fuel cell) (1839) and (b) Grove's gas chain powering an electrolyzer (1842). | 7 |
| Figure 1.5: | Number of fuel cell papers from different countries during 1983 – 2007 [data from the web of science]. | 9 |
| Figure 1.6: | Comparasion of energy density of compressed Hydrogen (3000 psi) Vs Lithium-ion battery and lead-acid battery. | 10 |
| Figure 1.7: | Trend in the burning capacity of fuel and Hydrogen is the best one | 10 |
| Figure 1.8: | (a) Sources from where methanol can be produced and applications onwards and (b) fire accidents comparasion between gasoline and methanol using as fuel in vehicles. | 12 |
| Figure 1.9: | General schematics of direct methanol fuel cell (DMFC). | 14 |
| Figure 1.10: | (a) Number of research publications published about development in DMFC and membranes for DMFC, (b) Number of Patents after 1991. | 15 |
| Figure 1.11: | (a) DMFC Stacks developed by Smart Fuel Cell (SFC) EFOY (Energy for You) for Motor Bike (presented at Hannover Messe 2007) and (b) 500 W DMFC Stack developed by Forschunzentrum Julich GmbH. | 17 |
| Figure1.12: | (a) DMFC Potential Uses and (b) Estimated sales of FCV each year | 19 |
| Figure 1.13: | Classification of membranes materials for fuel cell. | 22 |
| Figure 1.14: | Some of the typical representative of poly (aryl ether ketone). | 25 |
| Figure 1.15: | Sulfonated poly ether ether ketone (SPEEK) | 25 |
| Figure 2.1: | Simple schematic of proton transportation along with hydrogen bonding. | 34 |
| Figure 2.2: | Simple schematic of vehicle mechanism for transportation of protons | 35 |

| | | |
|---|---|---|
| Figure 2.3: | Proton conduction through hydrogen-bond pattern, which diffuses by hydrogen bond breaking and forming process | 35 |
| Figure 2.4: | Comparasion of structure of Nafion and Sulfonated poly (etheretherketon) SPEEK and proton transfer mechanism | 36 |
| Figure 2.5: | Theoretical Hydrogen fuel cell efficiency at standard pressure based on HHV | 43 |
| Figure 2.6: | Theoretical efficiencies of Carnot engine and fuel cell as a function of temperature. | 45 |
| Figure 3.1: | Sinusoidal current response in linear system | 49 |
| Figure 3.2: | origin of Lissajous Figure | 50 |
| Figure 3.3: | (a) Nyquist plot with impedance vector and (b) simple equivalent circuit with one time constant. | 52 |
| Figure 3.4: | Bode Plot with one time constant. | 52 |
| Figure 3.5: | Current Vs Voltage curve showing Pseudo-linearity. | 53 |
| Figure 3.6: | (a) represents impedance in series and (b) impedance in parallel. | 53 |
| Figure 3.7: | (a) Pervaporation process and (b) pervaporation apparatus. | 57 |
| Figure 3.8: | Electro-oxidation mechanism of methanol on Pt-catalyst. | 66 |
| Figure 3.9: | Simple schematic of DEFC. | 67 |
| Figure 3.10: | Probable reaction mechanism of electro-oxidation of ethanol | 69 |
| Figure 3.11: | ORR on platinum catalyst. | 70 |
| Figure 4.1: | Schemematic diagram showing the membrane electrode assembly for fuel cells based on a bilayer CMS/SPEEK membrane. | 80 |
| Figure 4.2: | FTIR Spectrum of Matrimid® 5218 film, (a) before, (b) after pyrolysis at 500 and (c) 800 ºC. For the comparison of pyrolyzed specimens' spectra to that/those of the pristine Matrimid® the values for the line (b) were multiplied by a factor of 5 and for the line (c) by a factor of 10. | 87 |
| Figure 4.3: | (a) Height and (b) phase contrast and (c) 3D Image; atomic force microscopy of the synthesized carbon molecular sieves. | 88 |
| Figure 4.4: | Protuberances (on CMS surface) size distribution determined along the diagonal line in the phase contrast image. | 89 |

| | | |
|---|---|---|
| Figure 4.5: | SEM image (secondary electrons) of a bilayer carbon/SPEEK membrane. | 90 |
| Figure 4.6: | Effect of pyrolysis temperature on: (a) methanol and water permeability and (b) the water/methanol selectivity. | 91– 92 |
| Figure 4.7: | Effect of the CMS thickness on the permeability of bilayer CMS/SPEEK membranes. Feed: 5, 10 and 20 wt % methanol aqueous solutions. | 93 |
| Figure 4.8: | Effect of penetrant molecule size (kinetic diameter) on (a) the permeability of alcohols and (b) water/alcohol selectivity. Feed: 5 wt % alcohol aqueous solution. | 94-95 |
| Figure 4.9: | Effect of penetrant molecule size on (a) the permeability of alcohols and (b) water/alcohol selectivity. Feed: 10 wt % alcohol aqueous solution. | 96 |
| Figure 4.10: | Proton conductivities of SPEEK and CMS/SPEEK membranes as a function of temperature at 100% RH. | 97 |
| Figure 4.11: | (a) Polarization and power density curves for plain SPEEK and bilayer CMS/SPEEK membranes and (b) $CO_2$ concentration | 98-99 |
| Figure 4.12: | Scanning electron microscopy (backscattered electrons image) of the CMS layer containing dispersed Pt as catalyst. | 100 |
| Figure 4.13: | Hydrogen fuel cell (single cell) tests with the membrane-electrode-assembly prepared as depicted in Figure 4.1 and using the CMS layer with dispersed Pt shown in (Figure 4.12) | 101 |
| Figure 5.1: | Chemical structure of (a) polyimide (Matrimid 5218) and (b) home made sulfonated poly ether ether ketone (SPEEK) | 113 |
| Figure 5.2: | SEM images of SPEEK/PI blend membranes cast at different temperatures: (a, c, e) at 130 °C and (b, d, f) at 80 °C; membranes with different PI content: (a. b) 10 wt. %, (c, d) 20 wt. %, and (e, f) 30 wt. %. | 119 |
| Figure 5.3: | (■) Theoretical phase diagram; Experimental observations: (○) transparent and (●) turbid films after solvent evaporation. | 121 |
| Figure 5.4: | FTIR spectrum of polyimide, SPEEK and a 70/PI SPEEK/PI film cast at 130$^{o}$C. | 122 |
| Figure 5.5: | Water and mixture uptake of SPEEK and SPEEK/PI films cast at 130 °C. | 123 |
| Figure 5.6: | DMTA analysis (Tan δ vs. Temperature/$^{o}$C) of PI, SPEEK and 70/30 SPEEK/PI cast at 80 and 130$^{o}$C. | 124 |
| Figure 5.7: | (a)DSC thermograms of PI, SPEEK and 70/30 SPEEK/PI cast at 80 and 130$^{o}$C & (b) DSC thermograms of three SPEEK/PI blends (90/10, 80/20 and 70/30) SPEEK/PI membranes. | 125 |
| Figure 5.8: | TGA curves of PI, SPEEK and 70/30 SPEEK/PI cast at 80 and 130$^{o}$C. | 127 |

| | | |
|---|---|---|
| Figure 5.9: | (a) Effect of polyimide contents (membrane cast at 130$^{o}$C) on the methanol and water permeability measured at 55$^{o}$C and (b) selectivity of water/alcohol Feed solution: 5 wt. % methanol aqueous solutions. | 128 |
| Figure 5.10: | Proton conductivity as a function of temperature for PI, SPEEK and blends measured at 100 % relative humidity. | 129 |
| Figure5.11: | Polarization and power density curves for plain SPEEK and SPEEK/PI membranes. | 131 |
| Figure 6.1: | Water and solution uptake results for Nafion 117, pure SPEEK and (90/10), (80/20), (70/30) SPEEK/ PI blends cast at 130 °C. | 143 |
| Figure 6.2: | Permeabilities of (ethanol and water) for Nafion 117 and pure SPEEK membranes at 60 °C | 144 |
| Figure 6.3: | (a) Effect of polyimide contents on permeability of ethanol and (b) water/ethanol selectivity. Feed solution: 5 wt. % ethanol aqueous solution. | 145 |
| Figure 6.4: | (a) Effect of CMS layer (180 nm and 400 nm) on permeability of ethanol and (b) water/ethanol selectivity. Feed solution: 5 wt. % ethanol aqueous solution. | 146 |
| Figure 6.5: | Polarization and power density curves at operating temperature of 25 °C (a)Nafion 117, pure SPEEK and (90/10), (80/20), (70/30) SPEEK/PI blends and (b) Nafion 117, pure SPEEK, CMS (180 nm and 400 nm) coated SPEEK. | 147 |
| Figure 6.6: | Polarization and power density curves at operating temperature of 60 °C (a) Nafion 117, pure SPEEK and (90/10), (80/20), (70/30) SPEEK/PI blends membranes and (b) Nafion 117, pure SPEEK, CMS (180 nm and 400 nm) / SPEEK membranes. | 149 |
| Figure 6.7: | Polarization and power density curves at operating temperature of 90 °C (a) Nafion 117, pure SPEEK and (90/10), (80/20), (70/30) SPEEK/PI membranes and (b) Nafion 117, pure SPEEK, CMS (180 nm and 400 nm)/SPEEK membranes. | 151 |
| Figure 6.8: | Comparasion of $CO_2$ (crossover) results during DEFC test at 25 °C, 60 °C and 90 °C. | 152 |
| Figure 6.9: | Comparasion of $CO_2$ (crossover) results during DEFC test at 25 °C , 60 °C and 90 °C (a) Nafion 117, pure SPEEK and (90/10), (80/20) and (70/30) SPEEK/PI membranes and (b) Nafion 117, pure SPEEK, CMS (180 nm and 400 nm)/ SPEEK membranes. | 152 |

# List of Tables


| | | |
|---|---|---|
| Table 1.1: | Total final consumption of fuel (World wide) in millions tons of oil equivalents (MTOE): Evaluation from 1973 to 2006. | 1 |
| Table 1.2: | $CO_2$ emission from fuel combustion only: Evaluation from 1973 to 2006 | 3 |
| Table 1.3: | DMFC Stack developers | 16 |
| Table 1.4: | Potential applications of DMFC | 16 |
| Table 1.5: | What's coming out of Cars. | 19 |
| Table 1.6: | Structure properties relation and in-situ performance of polymeric membranes. | 22 |
| Table 2.1: | Enthalpies and entropies of formation of fuel cell reactants and products. | 39 |
| Table 3.1: | Current voltage relationships of common electrical elements. | 54 |
| Table 3.2: | Exchange current density of hydrogen evolution reaction at different electrodes materials. | 64 |
| Table 5.1: | Proton conductivity, methanol permeability and relative selectivity for the membranes prepared and discussed in this chapter compared to other membranes from the literature. | 130 |
| Table 7.1: | Methanol and Ethanol permeability at 55 °C and proton conductivity at 60 °C and 100% R.H. | 159 |
| Table 7.2: | Methanol and Ethanol permeability at 55 °C and proton conductivity at 60 °C and 100% R.H. | 160 |
| Tabelle 7.3: | Methanol- und Ethanoldurchlässikeit (P) bei 55 °C und Protonenleitfähigkeit bei 60 °C und 100% r.F. | 164 |
| Tabelle 7.4 | Methanol- und Ethanoldurchlässikeit (P) bei 55 °C und Protonenleitfähigkeit bei 60 °C und 100% r.F. | 165 |

# Chapter 1. Introduction

Life on earth is driven by ENERGY. Human beings have been using different forms of energy in day to day life activity since very long. Before the 20$^{th}$ century the main source of fuel was from the natural world; burning of wood or agricultural waste but the 20$^{th}$ Century inventions of modern technologies brought a fortune to mankind and hidden treasures of coal, oil and gases beneath the soil explored and were utilized in almost every field of life. The life standard was totally changed due to rapid growth in industrial, transportation and residential sectors. But a dramatic increase was observed in consumption of fuel from 4672 MTOE (millions tons of oil equivalent) in the year 1973 to 8082 MTOE in 2006 that correspond to almost double consumption of fuel in just 33 years [1]. This difference can be seen in Table 1.1.

*Table 1.1: Total final consumption of fuel (World wide) in millions tons of oil equivalent (MTOE); Evaluation from 1973 to 2006.*

| **Fuel source** | **(MTOE in 1973)** | **(%)** | **(MTOE in 2006)** | **(%)** |
|---|---|---|---|---|
| Oil | 2247 | 48.1 | 3484 | 43.1 |
| Gas | 673 | 14.4 | 1237 | 15.3 |
| Coal | 621 | 13.3 | 695 | 8.6 |
| Electricity | 439 | 9.4 | 1350 | 16.7 |
| (CRW) | 617 | 13.2 | 1043 | 12.9 |
| Others | 75 | 1.6 | 275 | 3.4 |
| Total | 4672 | 100 | 8084 | 100 |

(CRW); Combustible, Renewable and waste

Others; Solar, Geothermal, Wind, Heat etc.

The increase in the fuel consumption is not only because of developments in different sectors but also because of a tremendous increase in human population after the 17th century. Specifically the 20th century has witnessed extraordinary population growth from 1.65 billions to 6 billions and experienced a high rate population growth (2.04 %) annualy. It is expected that inspite of the present annual growth rate of 1.3 %, the population will be around 10 billion in 2200 demanding more MTOE of fuels [2].

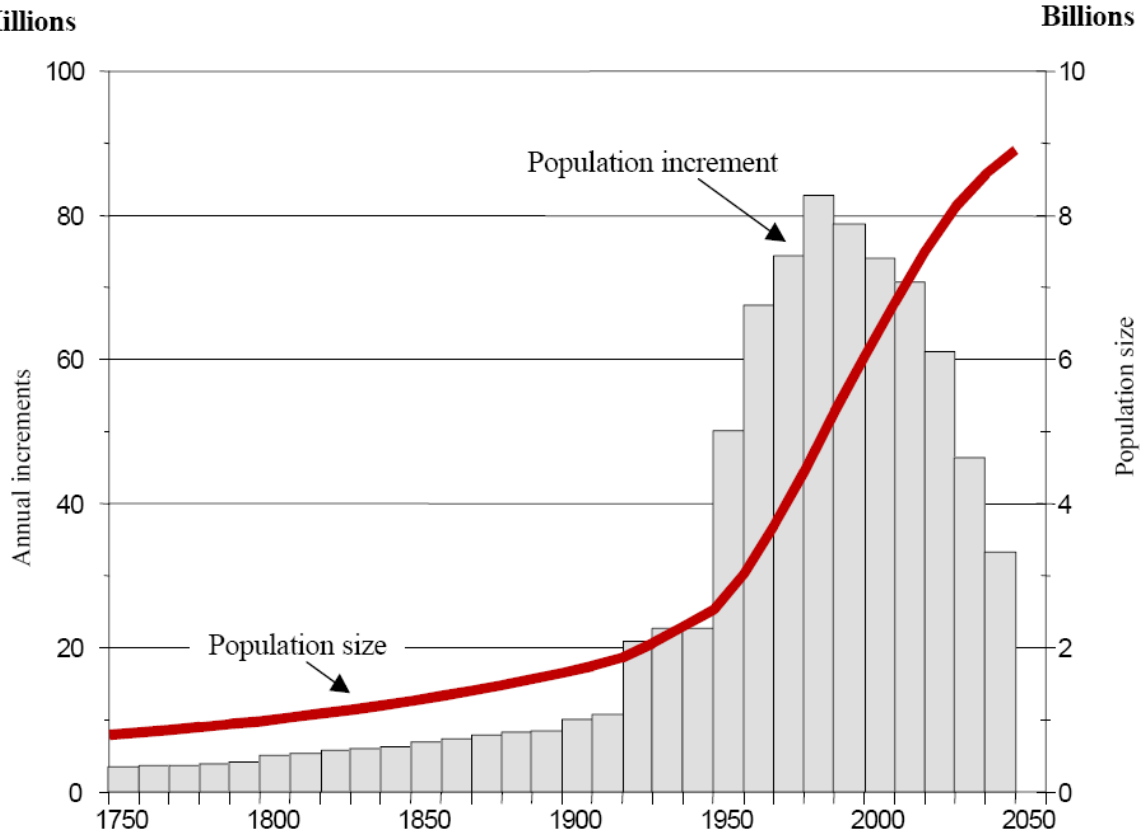


*Figure 1.1: Long term World population growth from 1750 to 2050 [2]*

Production and consumption of almost any type of energy have environmental impacts. Global warming due to increase in $CO_2$ concentration is the hot and challenging topic of the day and fears that it might lead to change the world of flora and fauna. Table 1.2 shows the global $CO_2$ emission from different sources of fuel from 1973 to 2006 [1].

*Table 1.2: $CO_2$ emission from fuel combustion only; Evaluation from 1973 to 2006.*

| **Fuel Source** | **Mt in 1973** | **(%)** | **(Mt in 2006)** | **(%)** |
|---|---|---|---|---|
| Oil | 7914 | 50.6 | 10781 | 38.5 |
| Gas | 2252 | 14.4 | 5433 | 19.4 |
| Coal | 5458 | 34.9 | 11677 | 41.7 |
| Others | 16 | 0.1 | 112 | 0.4 |
| Total | 15640 | 100 | 28003 | 100 |

In the last 33 years the emission of $CO_2$ increased by a double factor (1.8) from 15642 Mega Tons (Mt) to 28003 Mt from 1973 to 2006 respectively due to combustion of intensive amount of fossil fuels and definitely it will produce an increase in the average surface temperature of earth over time. Rising temperature may in turn produce changes in precipitation pattern, melting of glaciers, storm severity and sea level that will challenge the life on the coastal areas all over the world [3].

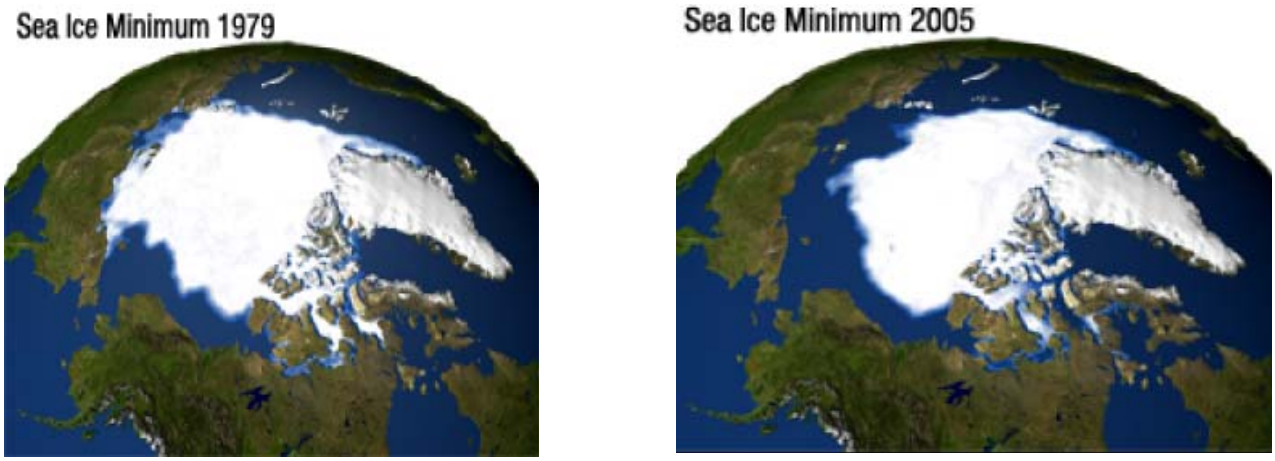


*Figure 1.2: satellite radar composite view of melting of Arctic ice from 1979 to 2005 (NASA)*

Apart from the pollution problem; now the oil production will start to decline at a rate of several percents per year. Because 33 out of 48 largest oil producing countries have already

passed the peak and that compelled King Abdullah of Saudi Arabia to state "*the oil boom is over and will not return*". All of us need to get used to some different style of life [4]. The same kind of statement was also issued by the Chevron: "*the Era of Oil is over*". By the year 2020 and even more 2030, global oil supply will be dramatically lower and this will create a supply gap. This can be hardly compensated with the growing contribution from the alternative energy sources like nuclear, wind, solar and etc. [5].

Keeping in view all these now the world is looking for the alternative energy sources with

(1) Minimum or $CO_2$ free production

(2) High energy conversion efficiency

(3) Extremely low noise or acoustical pollution

(4) Extremely low emission of pollutants

(5) Process simplicity for conversion of chemical energy to electrical energy.

The motivation is to provide a chance to reduce the $CO_2$ emission, clean the air and put the human civilization on a more sustainable footing. Countries around the world are using their efforts to improve their energy security and spur the economic development. More than 65 countries now have goals for their own renewable energy future and many renewable technologies and industries have been growing at rate of 20 to 60 % each year. This also encouraged the investment of more than 100 billions US$ (in 2007) for energy production assets, manufacturing, research and development; a true global milestone [6].

The $20^{th}$ century was the century of internal combustion engine and hopefully the $21^{st}$ century will be the century of fuel cell and hydrogen technology. Fuel cells produce electrical energy without going through combustion and the final product are the heat and water if pure hydrogen is used as fuel. In case of using bio-fuels the $CO_2$ concentration will be much less as compared to combustion engine and so hopefully the amount of green house gases will be reduced to a maximum level making the world safe and a clean place for living. The basic design of a fuel cell system contains;

(1) Electrolyte medium for transportation of protons

(2) Cathode as an electrode on one side of the electrolyte medium

(3) Anode as an electrode on other side of the electrolyte medium

(4) Fuel source (Hydrogen or bio-fuels)

(5) Pure Air or Oxygen

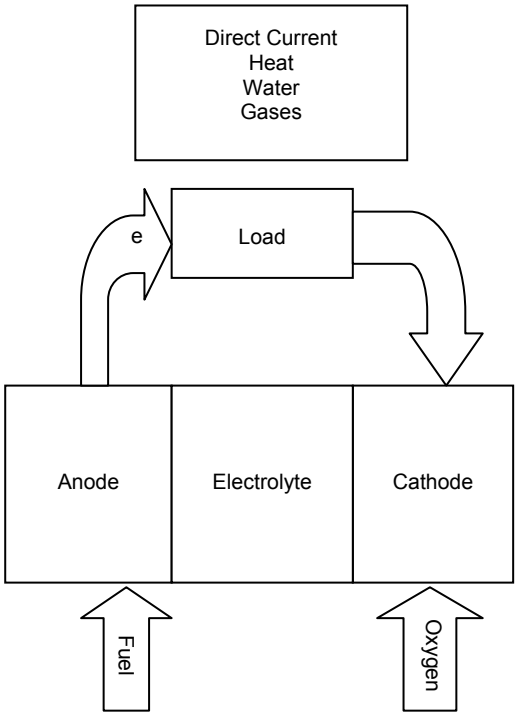


*Figure 1.3: Schematic of a typical Fuel cell.*

Fuel cells are usually classified based on the types of electrolytes employed in that cell which in turn also determine the kind of chemical reaction taking place inside the cell, kind of catalysts required, temperature range for the cell operation, the kind of fuel required and etc. There are several types of fuel cells currently under development each with its own advantages and disadvantages and potential applications [7 - 11]. Most prominent of all these are:

(i) Proton Exchange Membranes (PEM)

(ii) Direct Methanol Fuel Cell (DMFC)

(iii) Direct Ethanol Fuel cell (DEFC)

(iv) Direct Formic Acid Fuel Cell (DFAFC)

(v) Phosphoric acid Fuel Cell (PAFC)

(vi) Solid Oxide Fuel Cell (SOFC)

(vii) Molten Carbonate Fuel Cell (MCFC)

(viii) Alkaline Fuel Cell (AFC)

(ix) Zinc Air Fuel Cell (ZAFC)

(x) Regenerative

(xi) Aluminium Air Fuel Cell (AAFC)

(xii) Formic Acid Fuel Cell (FAFC)

(xiii) Microbial Fuel Cell (MFC)

## 1.0 History of Fuel Cell

***Sir William Robert Grove*** (1811 – 1896) was the first to recognise the importance of three phase contact (Gas, electrolyte and platinum) to energy generation and that made him the first inventor of the Fuel Cell in 1839. He concluded that the opposite reaction of electrolysis (water) would produce an electric current and for that purpose he developed a device that could combine hydrogen and oxygen to produce electricity. He developed the world first gas battery and to day it is known as Fuel Cell.

***Ludwig Mond*** (1839 – 1909) and ***Carl Langer*** conducted experiments with hydrogen as fuel and that produced a current of 6 amp per square foot at 0.73 V. They used earthenware plates saturated with dilute sulphuric acid.

***Friedrich Wilhelm Ostwald*** (1852 – 1932) founder of the physical chemistry experimentally determined the relationships between different components of a fuel cell; electrodes and electrolytes, oxidizing and reducing agents, anions and cations. His works opened the door to fuel cell researchers of the future by supplying these informations.

***Emil Baur*** (1873 – 1944) conducted research in collaboration with Braunschweig and Zurich on the fuel cell devices to be operated at high temperature and used molten silver as electrolyte.

***Francis Thomas Bacon*** (1904 – 1992) worked on high pressure fuel cells and thus was successful in developing a fuel cell that used Nickel gauze electrodes and operated at high pressure up to 3000 psi. During the World War II he developed a fuel cell to be used the in the Royal navy submarine. His developments were so successful that it gained the interest of Pratt & Whitney, and his work was licensed and used in Apollo spacecraft fuel cell. Similar technology is still in use in space technology.

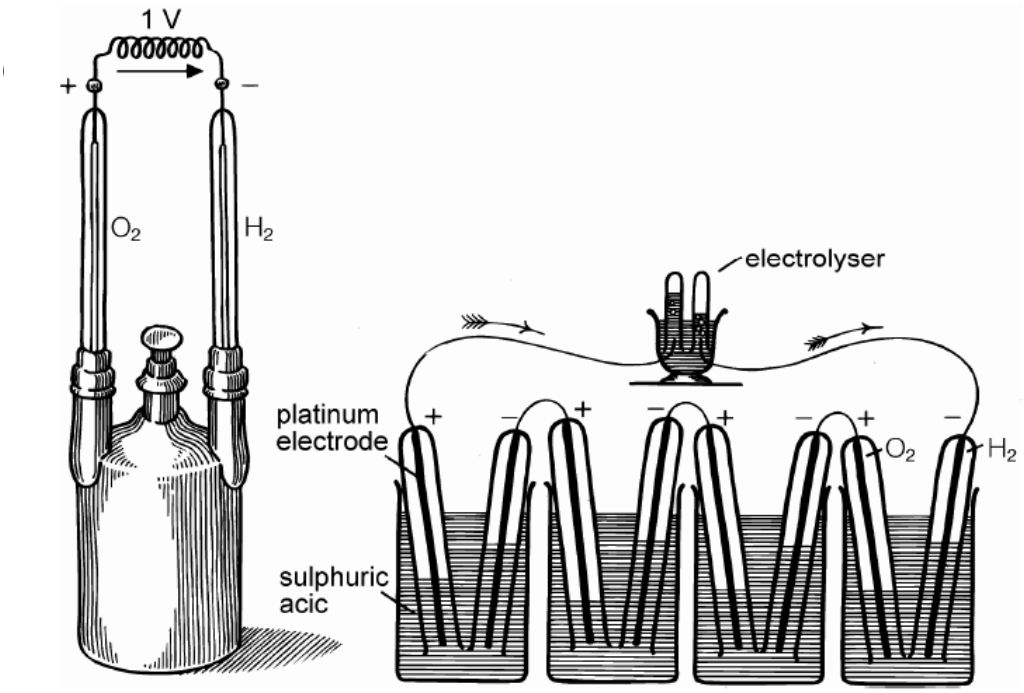


*(a)* *(b)*

*Figure 1.4: (a) Grove's Gas battery (Fuel cell) (1839) and (b) Grove's gas chain powering an electrolyzer (1842) [15].*

Currently a lot of research works are being carried out to solve the engineering problems that prevent fuel cell becoming commercially available at the markets. Some of these problems can be summarized as:

1. High initial cost of manufacturing of fuel cells
2. The lack of an infra-structure to deliver fuel
3. Unfamiliarity of industries with fuel cells

These problems encourage working intensively on three areas; first industry must reduce the cost of manufacturing fuel cells. Such problems are mainly associated with engineering or manufacturing problems associated with almost all types of fuel cells. The second issue is relevant to the engineering technology for manufacturing of fuel cells and implementation of one policy. To develop an infra-structure for fuel cell, first a specific type of fuel cell is to be manufactured and chosen. Policy matters regarding standardization, safety code and regulation for production of fuel cells need to be changed if necessary. And finally the most important one is that the industrial sectors must recognize the fuel cell technology as an emerging technology.

### 1.1 Fuel Cell as an emerging technology

The fuel cells will become a dominant technology of energy conversion only when the barrier of their cost is broken. They are extremely efficient, simple, have no emission and during operation produce no sound or noise. The current efficiency of a fuel cell when operated alone is around 40 – 50% but when used with the CHP (combined heat / power) then efficiencies increases to 80%. This shows a dramatic improvement of fuel cell over internal combustion engine which is limited to an efficiency of about 30% [13, 14]. They have no moving parts and in most cases are made up of solid parts and this makes their repair more simple and easy. The simpler is fuel cell the longer is the durability in long operational periods. The cell converts energy through a chemical process unlike internal combustion process (mechanical

process) and therefore the sound emission is virtually zero and so its application in vehicles is highly appreciated by the consumers and researchers. All such advantages make fuel cells an excellent choice of the future of power generation. The growth in fuel cell research all over the world can be viewed also from the numbers of papers published from 1983 to 2007 in the following figure 1.5. This shows a drastic increase with the passage of time and in future the rise in numbers might be in times.

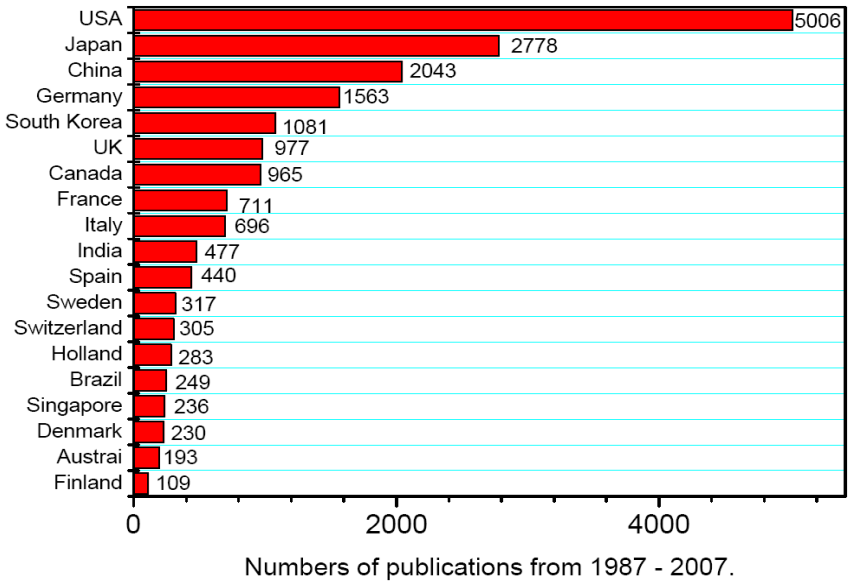


*Figure 1.5: Number of fuel cell papers from different countries during 1983 – 2007. [web of Science]*

Fuel cells also have advantages over other batteries when compared with the energy density. Portable instruments having fuel cells will be lighter and smaller. The size, weight and cost of energy storage for fuel cell power plant can easily compete with other batteries presently in use. Batteries discharge over time very fast if the environment is colder. Also the re-charging capacity of these batteries decreases with the number of time of discharge and recharge. A fuel cell will not discharge over time if the fuel is provided regularly and maintaining it full charge capacity almost indefinitely [15]. A comparasion of energy densities for fuel cell, lithium ion battery and lead acid battery is shown in figure 1.6 showing FC technology

performance better than other sources of power generators. Also from figure 1.7 it is quite evident the fuel of the future will be 100 % hydrogen.

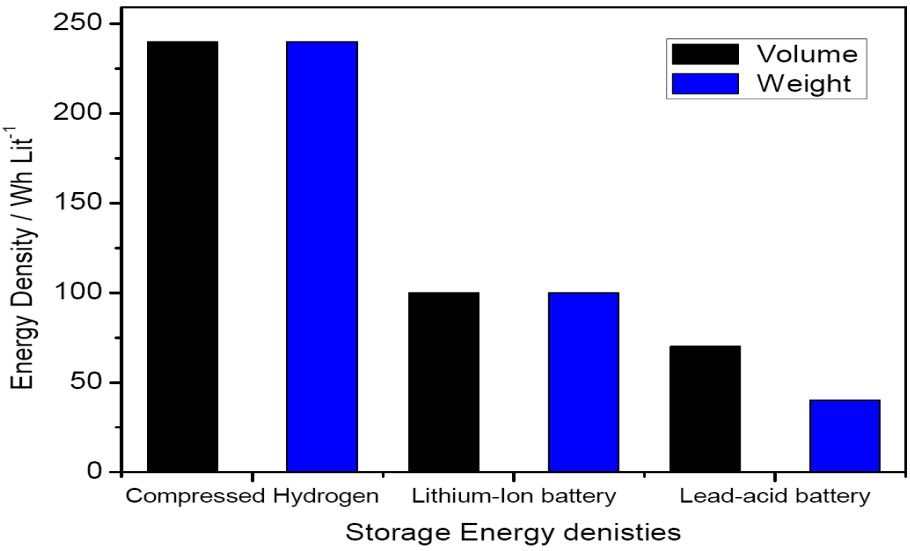


*Figure 1.6: Comparasion of energy density of compressed Hydrogen (3000 psi) Vs Lithium-ion battery and lead-acid battery [15].*

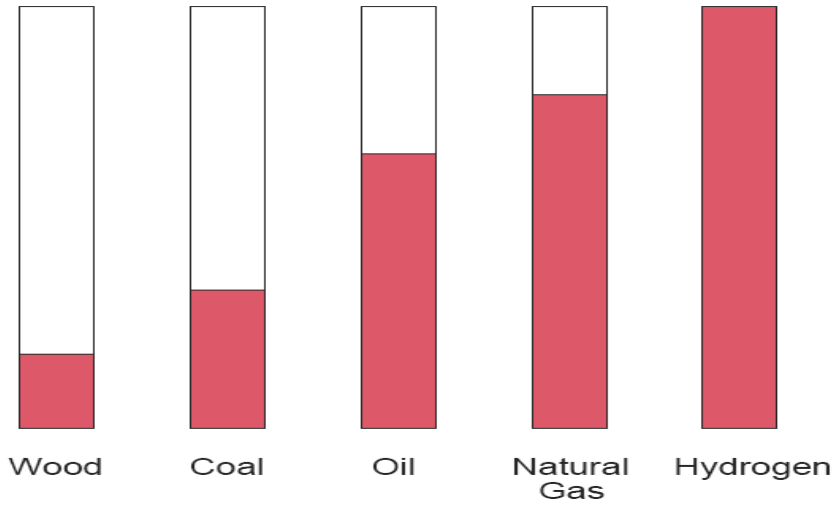


*Figure 1.7: Trend in the burning capacity of different fuels; Hydrogen is the best one [15].*

Hydrogen can be produced by reforming process from other hydrocarbon or from electrolysis of water. The compression of hydrogen gas is a costly thermodynamic process and for a state

of art around 10 and 17 MJ are needed to compress ONE kilogram of hydrogen from atmospheric pressure to 20 and 80 MPa (200 and 800 bar) respectively. This is between 8 and 13% of the HHV (Higher Heating Values) energy content of hydrogen. The heavier methane can be compressed at seven times lower consumption of energy. And even more energy is required for compact hydrogen liquefaction. Moreover liquid hydrogen storage systems lose hydrogen gas due unavoidable heat leakage and this must be prevented for safety reasons [16]. *All these things are making the use of hydrogen as a fuel quite difficult and more costly. Therefore search for alternative fuel to be fed directly to the cell is the target.*

Methanol is one of the safest and environmentally friendly sound fuels. Since methanol is liquid at STP (boils at 65 °C and 1 atm), it can be handled much like gasoline or diesel fuel and can also be fed through the same filling station infra-structure with only minor modifications. According to USA-EPA a switch to methanol fuel will reduce the fire incidents (by gasoline) by 90%, saving 720 lives and preventing 3,900 serious injuries. Pure methanol (M 100) is much harder to ignite as compared to gasoline and burns at much slower rate of about 60 % less than gasoline and after burning it release energy one-fifth to that of gasoline. Unlike gasoline fire, methanol fire can be extinguished simply and quickly by dousing it with water. Based on such reasons methanol is a safer fuel to be used in vehicles.

Presently large amount of methanol is produced from the conversion of natural gases into alcohols. But other than natural gases, methanol production from land-fill gases, biomass, municipal solid wastes (MSW), coal and etc are very effective and feasible. Methanol can be fed directly to fuel cell without any reforming process and thus can be a better substitutive to hydrogen gas. The type of cell fed with direct methanol is called as direct methanol fuel cell (DMFC).

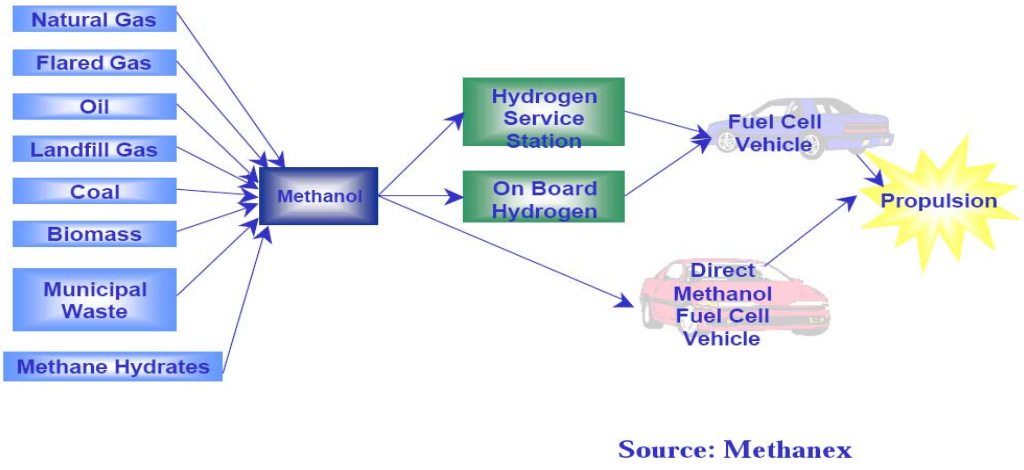


(a)

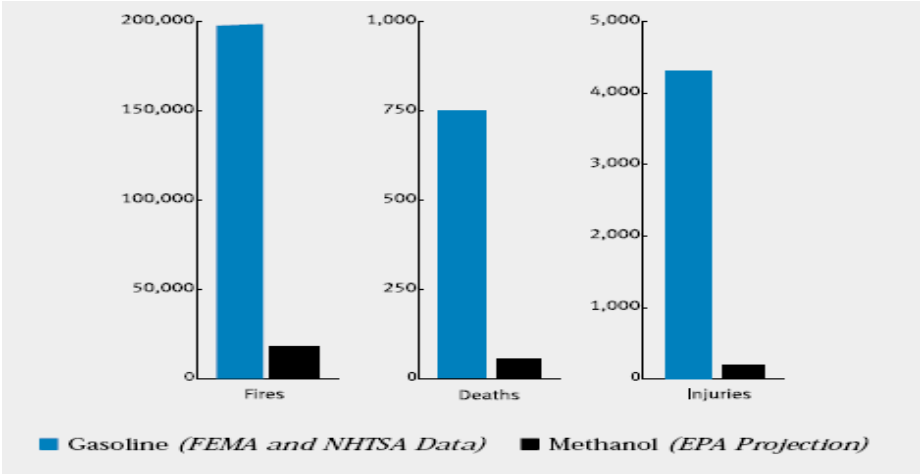


(b)

*Figure 1.8: (a) Sources from where methanol can be produced and applications onwards and (b) fire accidents comparasion between gasoline and methanol using as fuel in vehicles [22]*

### 1.2 Direct Methanol fuel cell (DMFC)

The fundamentals of DMFC were first demonstrated in 1922. However the first direct methanol fuel cell (DMFC) were invented and developed in the year 1959 at the Jet Propulsion Laboratory (JPL) at Pasadena, California; to supply electricity for the field forces

and for application with NASA. Usually DMFC are designed to be operated at lower temperature ranges (60 – 150 °C) being advantageous for portable devices such as cell phones, laptop and etc. because DMFC holds great promise for reducing size, weight, cost, emission and improving energy efficiency (10 times higher than Lithium-ion battery) for a broad array of applications [13, 15]. Therefore much more preference is given to the development of DMFC by different companies like Smart fuel cell (SFC), Toshiba, Hitachi, Fujitsu and Sanyo all have developed a prototype laptop, cellular phones and personal digital assistants empowered by DMFC [17].

The components of a DMFC are three including a proton conducting membrane, an anode and a cathode. All these three components together after heat pressing are called membrane electrode assembly (MEA), a single cell-fuel ready to be used in DMFC test. During DMFC test the fuel methanol (methanol / water mixture) is fed directly to the cell on the anode side without any reforming process and oxygen on the cathode side. Direct combination of fuel and oxygen is prevented by the polymer electrolyte membranes, but after electro-oxidation of fuel on the catalyst anode the proton ($H^+$ ion) is desired to pass through the membranes towards the cathode side for the completion of reaction. The flow of protons through the membranes must be balanced by the flow of electric charge through an out side circuit and because of this balance it produces power. It is worth mentioning that the polymer electrolyte membranes must be conductive for protons only and not for electric circuit. A simple schematic of DMFC is presented in figure 1.9.

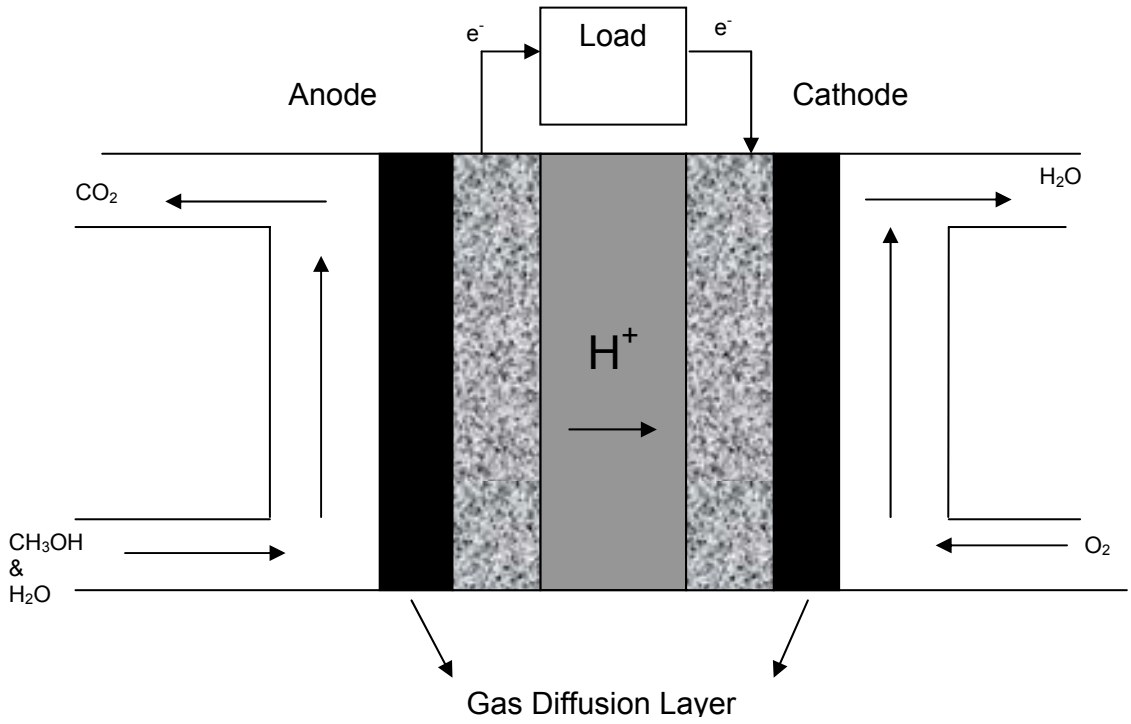


*Figure 1.9: General schematics of direct methanol fuel cell (DMFC).*

During the last two decades a lot of research works were carried out on the development of DMFC or membranes for DMFC. Figure 1.10 (a) shows the number of publications for these two purposes. Solid bars represent research works focused on DMFC while shaded bars show the articles relevant to membranes development for DMFC [17]. However the first patent was issued in 1990 and up till now 10,000 units are shipped world wide for producing power in leisure markets (Camping & Yachting). The total numbers of patents issued since 1990 are listed into the figure 1.10 (b). From 1991 to 2000 a very less number of patents were published on the DMFC development but it was the period during which the fundamentals of DMFC were developed. The earliest DMFC with the membranes as PEM were adapted to run on direct methanol with higher catalysts loading and balance of plant than pure hydrogen with PEM. But with the passage of time and development both the loading and balance of plant were reduced with some of most recent DMFC patents covering novel catalysts that allows for water recycling. After 2000, a real take off in the number of patents around 100 publications by the 2002 and 160 in 2006 were observed respectively [19].

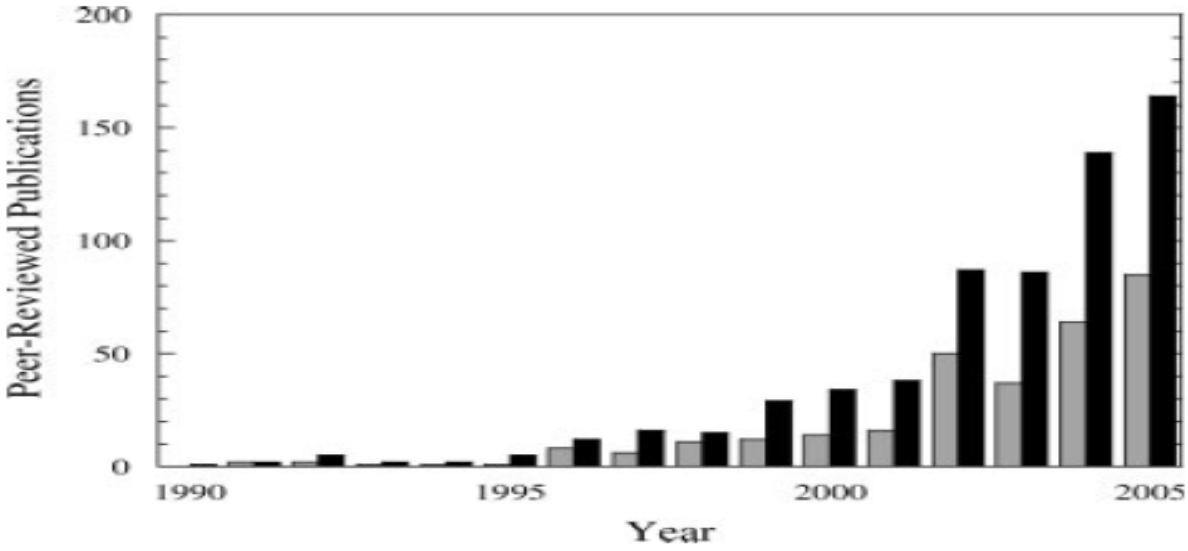


(a)

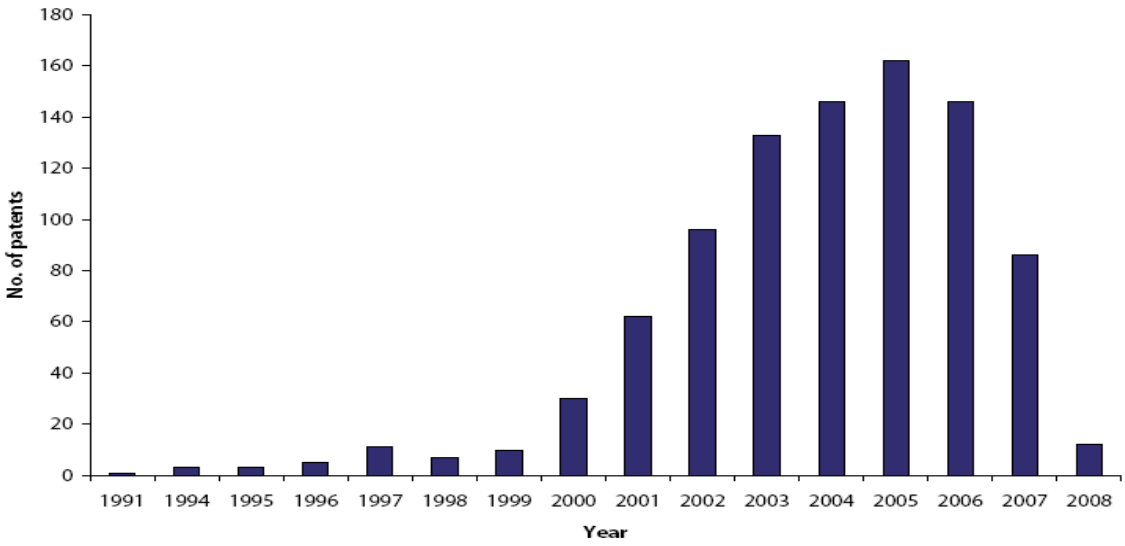


(b)

*Figure 1.10: (a) Number of research publications published about development in DMFC and membranes for DMFC, (b) Number of Patents after 1991 [19].*

Although the development and application of DMFC were in progress before 1959 by the prominent laboratories of Shell, Exxon and Hitachi and they used 1 – 2 M sulphuric acid as an electrolyte and un-supported platinum black as catalysts. But a breakthrough happened after 1959 when the sulphuric acid was replaced by solid state proton conducting membranes. For a

desired power output for any particular application; individual fuels cells are combined to produce appreciable voltage levels and so are joined by interconnect (DMFC stack design) and are used as application for transportation, laptops, cellular phones and personnel organizers etc. Some of the prominent research institutions around the world have become actively engaged in developing the desired stacks for the desired applications [18]. Table 1.3 and 1.4 represent the DMFC stack developers and on-wards DMFC potential applications respectively.

*Table 1.3: DMFC Stack developers*

| **Stack Developers** | **Rated Power / (W)** | **Maximum Power Density/ (mW $cm^{-2}$)** | **Power Density @ 0.5V (mW $cm^{-2}$)** | **Operating temperature/ (°C)** | **Methanol (M)/ P atm** | **Number of Cell/surface area $cm^2$** |
|---|---|---|---|---|---|---|
| Siemens Johnson & Matthey | 850 | 100 | 42 | 104 | - | 16/550 |
| Loss Alamos | 17 | 75 | 50 | 60 | - | 5/45 |
| Loss Alamos | 47 | 220 | 175 | 100 | 1 | 5/45 |
| KIER | 40 | 90 | 20 | 90 | 2.5/1 | 3/150 |
| Sodeteg-Nuvera-CNR- TAE Thomson | 150 | 150 | 75 | 110 | 1/1.5 | 5/225 |

*Table 1.4: Potential applications of DMFC*

| **Potential applications** | **Fields** | **Rated Power** | **Over-all Efficiency requirements (%)** | **Specific Power / W $kg^{-1}$** | **Power Density / W $Lit^{-1}$** | **Operating temp / °C** |
|---|---|---|---|---|---|---|
| **Transportation** | Electromotive | 20 – 50 kW | 35 – 45 | 350 – 500 | 350 – 500 | 130 – 150 |
| | APU | 3 – 5 kW | 35 - 45 | 350 – 500 | 350 – 500 | 130 – 150 |
| **Portable** | Laptop Microcomputer | 50 – 100 W | 20 | 50 | 50 | 0 – 45 |
| | Cellular Phones | 1 – 3 W | 20 | 30 | 30 | 0 – 45 |
| **Stationaries** | Residential | 5 – 10 kW | 35 - 45 | 200 | 200 | 90 – 150 |
| | Remote Power generation | 10 – 100 kW | 35 – 45 | 200 | 200 | 90 – 150 |

In all these DMFC stacks, Nafion was the membranes and the catalysts used for electro-oxidation was the Pt black as cathode while Pt-Ru was used as the anode with varying concentration [17]. Now according to the US Department of Energy (US-DOE) the market for mobile fuel cell with DMFC technology is expected to reach US$ 2.6 billion by 2012. But still the cost is a big obstacle and the price for Nafion based MEA with DMFC technology is expected between US$ 600 – 1200 $m^{-2}$. *But if the membrane Nafion is replaced with sulfonated poly (etheretherketon) (SPEEK) then it will reduce the cost to US$ 350 $m^{-2}$ [20].*


(a)

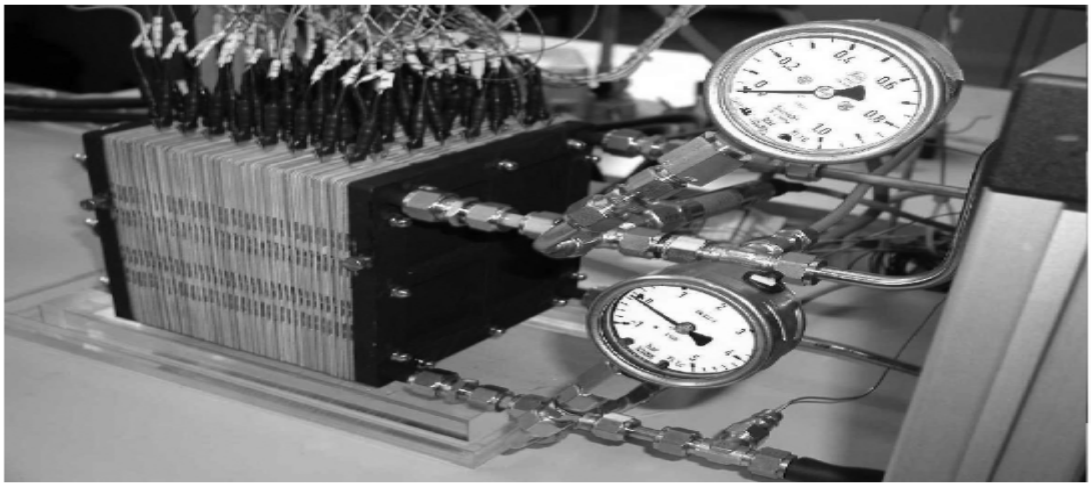

(b)

*Figure 1.11: (a) DMFC Stacks developed by Smart Fuel Cell (SFC) EFOY (Energy for You) for Motor Bike (presented at Hannover Messe April 2008) and (b) 500 W DMFC Stack developed by Forschunzentrum Julich GmbH.*

The American Methanol Institute (AMI) reported the ongoing advancements in methanol use with the emerging fuel cell technology for the successful marketing and introduction of methanol fuel cell vehicles (MFCV). The world major automakers are racing to introduce fuel cell vehicles (FCV) in the markets because many demonstrations, advancements and breakthroughs have been made with methanol fuel cells. Ballard Power Systems and DaimlerChrysler presented a direct methanol fuel cell (DMFC) prototype in Stuttgart Germany. Methanol was used as fuel to empower a one parson vehicle. The cars making industries conclude that within two decades; between 7 and 20 percent of the new cars sold in the markets will be powered by fuel cell technology making the possibility of some 40 millions fuel cell cars on the roads by 2020. But according to an other estimation made by the US-DOE, the total number of cars world wide will increase from present 600 millions to around 1 billions between years 2015 and 2020. It is estimated that the FCV will account 1.3 % of the new cars in market by the year 2015 and 8.33 % by the year 2020. According to Japan Institute of Energy estimation, the share of the FCV only in Japan will increase from 0.1 % in 2010 to 33.5 % in 2020. And definitely this will help reducing the amount of green gases to minimum values. The following table 1.5 shows the kind and quantities of green house gases (grams per mile) coming out from gasoline cars run by internal combustion engine ICE, and from the cars run by fuel cell hydrogen and methanol [21] while figure 1.11 shows the potential applications of DMFC in vehicles and future sale of FCV after 2010 expectedly [22] and gradual increase per anum. In addition to this, now a day DMFC is particularly considered only for portable applications like laptops, cell phones and etc.

*Table 1.5: What's coming out of Cars.*

| **Engine Types** | **Water Vapours** | **$CO_2$** | **CO** | **$NO_x$** | **Hydrocarbons** |
|---|---|---|---|---|---|
| *Gasoline ICE Passenger Cars* | 177 | 415 | 21 | 1.4 | 3 |
| *Gasoline ICE Light Trucks* | N.A | 522 | 28 | 2 | 4 |
| *Methanol FCV* | 113 | 68 | 0.016 | 0.0025 | 0.0034 |
| *Hydrogen FCV* | 113 | 0 | 0 | 0 | 0 |


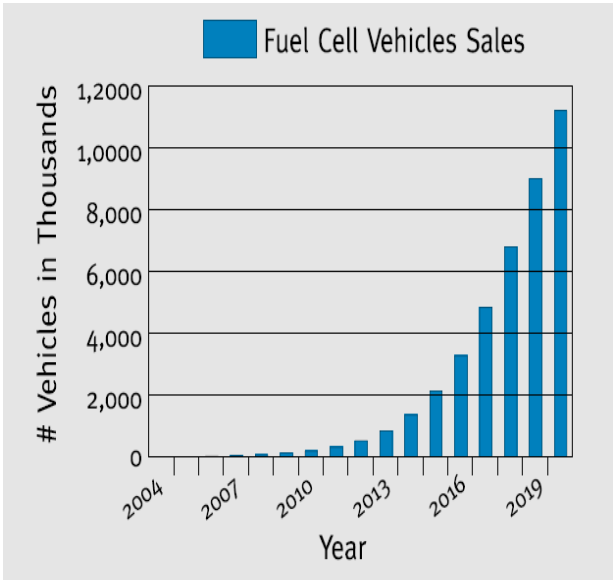


*Figure1.12: (a) DMFC Potential Uses and (b) Estimated sales of FCV each year [22].*

## 1.3 **Membranes for Fuel Cells**

Polymer electrolyte membranes (PEM) have the ability to be use in fuel cell at low temperature and can produce high power densities even at low temperature. Its one of the attractions that they can be made smaller which in turn will reduce the over all weight, cost and specific volume. The PEM is also called now as solid-state exchange membranes that separate electrodes in the fuel cells. William Grubbs and Leonard Niedrach of General Electric (GE) invented and developed the first polymer electrolyte membranes; *sulfonated polystyrene for fuel cells*. William Grubbs discovered in 1959 that without the presence of strong acids in membranes, transportation of protons from the anode side towards the cathode was possible. This discovery was capitalized by NASA and the GE PEM fuel cells were used to provide auxiliary power onboard its Gemini spacecraft (an Apollo mission to Moon).

The PEM is just a hydrated membrane that promotes the conduction of protons. Also the PEM is an immobilised electrolyte and it offers a simplification in the production process that in turn reduces the chances of corrosion and this provides a long life for the stack. So far many kinds of membranes were developed and used for the fuel cell application but still Nafion which was discovered in 1970 by Du-Pont still is considered as an industry standard and therefore all other membranes are compared with it [12, 15]. The Dow Chemical Company and Asahi Chemical Company made one step more advancement by synthesizing perflourosulfonic acid membranes with shorter side chain and with high ratio of sulfonic ($SO_3H$) to $CF_2$.

According to the US department of energy (DOE) the commercialization of fuel cells with DMFC technology will be possible by the year 2010 if the following targets are achieved:

- Power density, 100 W $Lit^{-1}$
- Energy density, 1000 W h $Lit^{-1}$
- Life time 5000 hours
- Cost, \$ 3 $W^{-1}$

Still there are some technology gaps between the recent DMFC technology and DOE targets. In recent years significant developments have been achieved to develop polymer electrolyte membranes for DMFC in term of cost reduction and an improvement in functionality. New membranes materials were developed and test and it was found that these can be substitutes to costly membranes with even better performances [20, 23 – 27].

### 1.3.1 **Types of membrane materials for fuel cells**

There are different ion exchange membranes materials used for fuel cell application and all these can be classified in to some different system;

1. Perflourinated ionomers
2. Partially fluorinated ionomers
3. Non-fluorinated membranes with aromatic backbone
4. Non-fluorinated hydrocarbons
5. Acid-base blends

Each membrane system was described in the following Figure 1.13 and Table 1.6 which were reproduced from ref [23]. Table 1.6 compares the structure and physical properties of different membrane systems to their in-situ performances and it can be easily noticed that new membranes materials are in competition with per fluorinated membranes but still need some more improvements in the relevant properties.

An other type of classification of ion exchange membranes is based on the type of ionic group attached to membrane matrix. They are of two types; anionic exchange membranes and cationic exchange membranes. Cationic exchange membrane contains negatively charged groups like $–SO_3^-$, $-COO^-$, $-PO_3^-$, $-PO_3H^-$, $-C_6H_4O^-$, etc fixed to the membrane backbone and allows the passage of cations but rejects anions. While anionic exchange membranes contain positively charged groups such as $–NH_3^+$, $-NRH_2^+$, $-NR_2H^+$, $-NR_3^+$, $-PR_3^+$, $-SR_2^+$ fixed to membrane backbone allowing anions to pass but reject the cations [24].

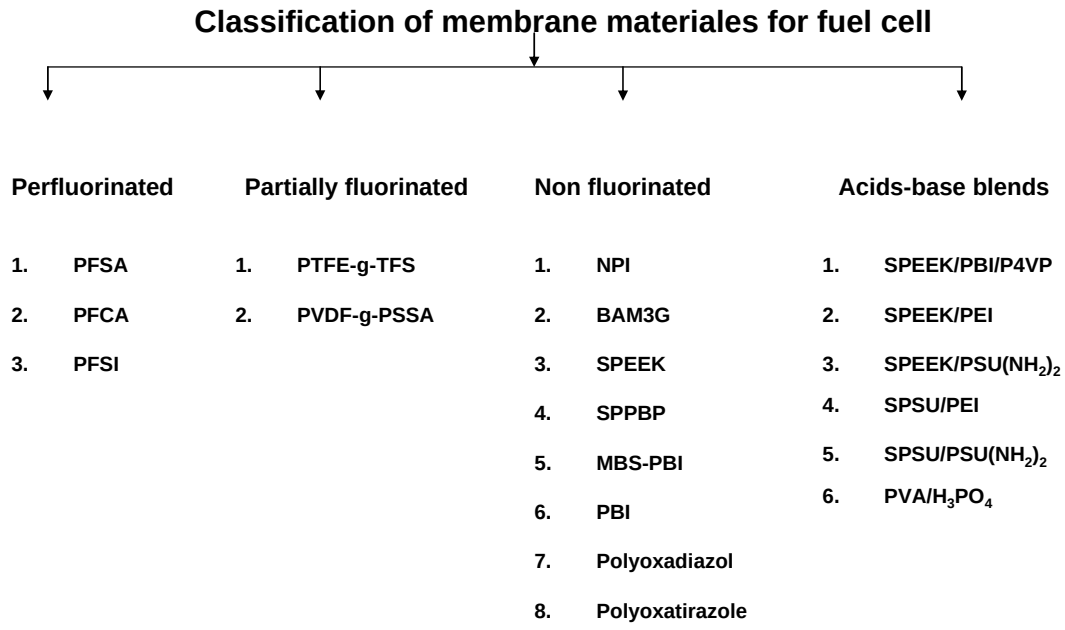


*Figure 1.13: Classification of membranes materials for fuel cell.*

*Table 1.6: Structure properties relation and in-situ performance of polymeric membranes.*

| Category | Structure | Physical properties | *In situ* performance |
|---|---|---|---|
| **Perfluorinated membranes** | 1. Fluorinated backbone like PTFE<br>2. Fluorocarbons side chain<br>3. Ionic clusters consisting of sulfonic acid ions attached to side chain | Membranes are stable in both oxidative and reductive environment | 1. Membranes are durable upto 60,000 h<br>2. Proton conductivities in well humidified membranes are 0.2 S/cm at PEMFC operating temp.<br>3. Cell resistance of 0.05 Ω $cm^2$ for 100 µm thick membranes with voltage loss of only 50 mV at 1 A/cm2 is achieveable |
| **Partially fluorinated mambranes** | 1. Fluororcarbon base<br>2. Hydrocarbon or aromatic side chain grafted onto the backbone, which can be modified | Membranes are relatively stable in comparasion to pf, but degrad fast | 1. Less durable than perfluorinated ones<br>2. Low performance<br>3. Suitable modification yields membranes with comparable proton conductivity |
| **Non-fluorinated membranes** | Hydrocarbon base typically modified with polar groups | 1. Membranes with good mechanical strength<br>2. Poor chemical and thermal stability (linear) | 1. Poor proton conductors<br>2. Shows low durability on swelling by incorporation of polar groups |
| **Non-fluorinated aromatic membranes** | Aromatic base typically modified with polar sulfonic groups | 1. Good mechanical strength<br>2. Chemically and thermally stable even at elevated temperature (aromatic) | 1. Good water absorption<br>2. Broad range of proton conductivity |
| **Acids-base membranes** | Incorporation of components into polymer base | Stable in oxidizing, reducing and acid environments and also thermaly stable | 1.Good dimentional stability<br>2.Proton conductivity comparable to nafion |

### 1.3.2 **Membranes characteristic for DMFC applications.**

A membrane is considered to be the heart of a fuel cell. The following characteristics properties are required for membranes materials to be used in DMFC;

(i) High proton conductivity (> 80 m S $cm^{-1}$) to support current with minimal resistive loses and to electronic conductivity.

(ii) Extremely low fuel (methanol) and Oxygen cross-over.

(iii) Adequate mechanical strength and stability.

(iv) Chemical and electro-chemical stability under operating conditions especially at temperature (60 – 130 °C) and for increase CO tolerance.

(v) Moisture control in stacks.

(vi) Low Ruthenium migration when Ru-alloy is used as anode catalyst.

(vii) Low cost (< $ 10 $kW^{-1}$) [25]

In order to ensure the satisfactory performances of the new materials for the membranes, a scientific approach to the following properties must be considered;

- Structure-property relationship prevailing in the polymers
- the application of thermodynamics (mass transfer kinetics) and
- Surface science (controlling complex morphologies).

However hydration and thickness are the two important parameters that might influence the performance of the membranes during application in the fuel cell.

### 1.3.3 Factors affecting the performance of the membranes

*1.3.3.1 Hydration:* Proton conductivity decides the performance of any membrane and for that membrane must absorb certain amount of water. For higher proton conductivity the hydration level of a membrane must be high. But during the operation of a membrane with wet environment, the over flooding of a cathode slow down the electro-oxidation which in turn lead to decrease the efficiency of a cell. The electro-osmotic drag co-efficient (EODC), a quantitative measure of hydration is defined *as the number of water molecules transported per proton.* Zadowzinski et al. [28] studies indicate that for Nafion 117 (175 um) equilibrated with water vapours the EODC is about 1, while for that immersed in water is about 2.5 water molecule per proton. Their studies also showed that the drag is mainly a function of water and is independent of kind of Nafion membrane used.

*1.3.3.2 Thickness:* Fuel cross over drag is directly dependent on the thickness of membrane and by reducing the thickness it can be minimized to a certain level with an improvement in fuel cell performance. This reduction of the membrane thickness also has some other advantages including lower membrane resistance, high proton conductivity, low cost and rapid hydration. However there is a limit to the extent to which membrane thickness can be reduced because of difficulties with disabilities and fuel cross-over. An ideal way to balance this will be to control the acidic region or increase the charge densities in the chemical micro-structure of the PEM to obtain high conductive materials. Charge densities can be enhanced by synthesizing the membranes in asymmetric or thin film composite or an other way of special control of the acidic region can be brought about by the surface modification of the membranes as discussed in [23]. These techniques not only reduce the thickness but also enhance the proton conductivity of the membranes. Thinner membrane may promote the back diffusion and produce greater concentration gradients of water, on account of enhanced rate of

dehydration at higher temperature. An other advantage is that fuel cell with thinner membrane may be operated at lower humidity.

### 1.4 Sulfonated Poly (etheretherketon) SPEEK membranes:

Poly ether ether ketone (PEEK) is an aromatic, semi-crystalline polymer which shows mild solubility in organic solvents due to its crystalline nature. In order words it's a class of polymers consisting of sequences of ether and carbonyl linkage between phenyl rings. The most common materials have an ether/carbonyl linkage sequence EEK, like in poly (ether ether ketone) (PEEK) which is commercially available under the name Victrex ® PEEK ™ from ICI manufacturer.

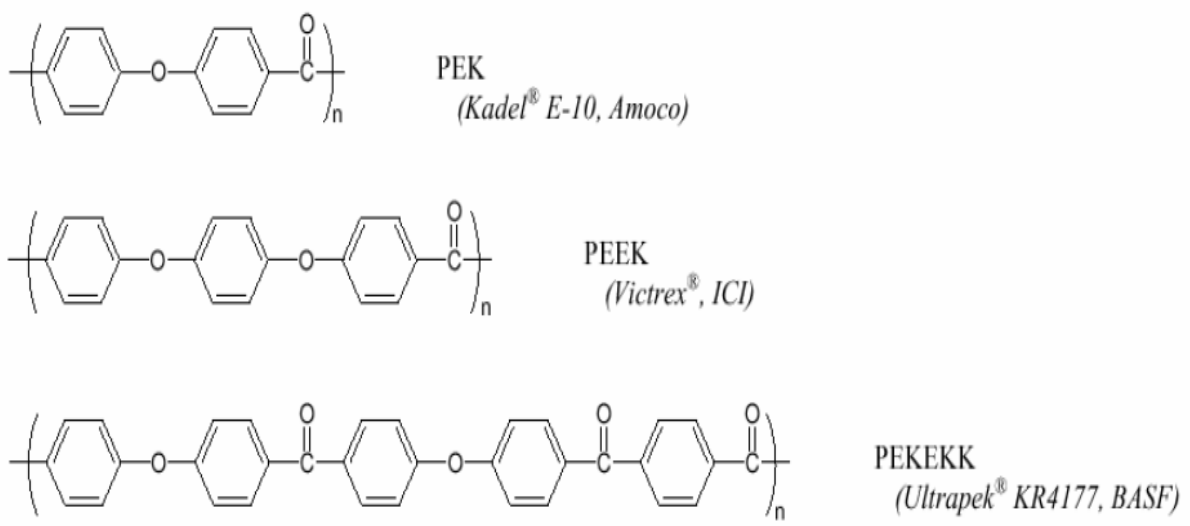


*Figure 1.14: Some of the typical representative of poly (aryl ether ketone)* [29]

Bishop et al [30] were the first to study the solubility and other properties of PEEK in concentrated sulphuric acids. Despite their thermo hydrolytic stability, the proton conductivity of these polymers is insufficient, even in a water-saturated environment. Therefore, the materials are sulfonated to convert them into ionomers and enhance their protonic conduction properties. The sulfonation of a thermo-stable polymer leads to a marked improvement of the

protonic conduction properties. This is possible because of the enhancement of the density of mobile protons, and also due to the increased water uptake possible by this sulfonation and which in turn allows and enhances the proton mobility.

The level of sulfonation in this class of materials is dependent on the number of aromatic rings bridged by Oxygen atom and only O-phenyl-O units are sulfonated while O-phenyl-CO groups remain unsulfonated. Hence, increasing the properties of ether groups relative to carbonyl groups leads to an increase in number of sites available for sulfonation on the poly (aryl ether ketone) back bone. Direct sulfonation of PEEK to form sulfonated poly (etheretherketon) (SPEEK) can give materials with a wide range of equivalent weights [29]. The sulfonation reaction involving PEEK can be well-controlled by the reaction time, temperature and concentration of sulphuric acid. The polymer after sulfonation can be dissolved in organic solvents like dimethyl acetamide (DMAc), dimethyl formamide (DMF), dimethyl sulfo-oxide (DMSO). It has been observed that after casting of these solution polymers for making membranes, the membrane possess amorphous structure and chemical and physical properties were similar to those of sulfonated polymers [27 - 31]. A sulfonation level of around 56 – 60 % was found to be a good compromise between the conductivity and mechanical properties of membranes. But if the sulfonation degree (DS) is higher than 70% then it is soluble in methanol and exhibits poor mechanical properties in hot water also. The conductivity of this material was found to be temperature dependent.

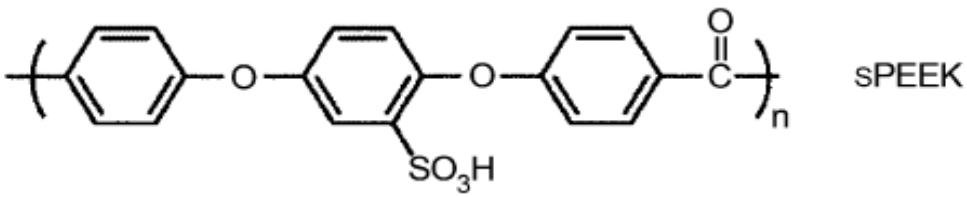


*Figure 1.15: Sulfonated poly ether ether ketone (SPEEK) [29].*

In particular, SPEEK was shown to have a life time of more than 3000 hours, indicating that these polymeric membranes are suitable for commercial production. So far a lot of research

works were carried out on the improvement of SPEEK membranes for its applications in fuel cell technology. The main trends of all research were to develop a membrane with low fuel cross-over with maximum proton conductivities.

The German company Fuma-tech GmbH has now developed cost effective sulfonated poly (arylethere ketone) membrane with trade mark (FKE ® Series 50 um thick) having higher mechanical stability with increased efficiency and high power density due to low methanol permeability than Nafion membranes. FKE membranes operate from 100 °C to 160 °C temperature range. It is concluded that by incorporation of inorganic materials or blending with some polymers will improve its stability [32].

At GKSS during the previous works the main approach chosen by the fuel cell group to reduce methanol crossover in polymeric membranes has been the development of different forms of nanocomposites using functionalized layered silicates, silica and polysilsesquioxanes, zirconium oxides and phosphates as fillers [33-37]. But in case of adverse effect on the proton conductivity due to modification, additional proton conductive materials such as zirconium phosphate were added to the composite system to achieve the lost proton conductivity with low methanol permeability.

## 1.5 Main objective of the present research works.

As can be seen from the above introduction, the SPEEK membrane possesses properties for future development of hydrogen fuel cell technologies however improvements are necessary if DMFC is aimed. For this purpose many research groups around the world are now focussing to make it free from any kind of disadvantages; the most important one is the methanol cross-over. Therefore, the target is to modify the SPEEK membranes by other substance with reduced methanol cross-over but in any case the proton conductivity must not be lower than 10 mS/cm at working temperatures as well as the requirement of high mechanical, thermal stability and chemical stability at the applied conditions.

The over all aim of the present work is the development of proton conducting membranes by using SPEEK polymers for DMFC and hydrogen fuel cell technologies but with reduced methanol cross-over. The specific modifications made to SPEEK polymeric membranes can be summarized as follows;

### *1.5.1 CMS coated SPEEK bilayer membranes:*

- Preparation of a thin layer of carbon molecular sieve (CMS) from the Pyrolysis of polyimide (Matrimid 5218) thin films at high temperature under inert ($N_2$ gas) atmosphere. Based on thickness of CMS layer, two types of bilayer membranes (CMS/SPEEK) were prepared.
    i. SPEEK coated with 180 nm CMS thick layer and
    ii. SPEEK coated with 400 nm CMS thick layer.

  The idea was to take advantage of molecular sieving effects for the rejection of bigger molecules in mixture system during pervaporation and DMFC tests.

- Incorporation of platinum as catalyst into this CMS layer so as to take two advantages of CMS functioning as fuel barrier and catalyst support for platinum at the same time.

1.5.2. *SPEEK/PI Blends membranes:*

Three types of homogeneous SPEEK/PI blends were prepared at high temperatures based on the amount of polyimide (Matrimid 5218) added to blend solution. The blends prepared at different temperature and based on different amount of polyimide in the blend solution can be summarized as follow;

- SPEEK/PI (90/10) blend
- SPEEK/PI (80/20) blend
- SPEEK/PI (70/30) blend

The idea was to take advantage of hydrophobic property of polyimide by incorporating it into SPEEK matrix for rejection of methanol/water mixture during pervaporation and DMFC performances. Blend membranes were prepared for the above mentioned compositions of SPEEK/PI at different temperature like 80 °C, 90 °C, 100 °C, 110 °C, 120 °C and 130 °C. It was observed that homogeneous blend membranes were obtained at temperature (>110 °C) with any amount of polyimide added to the blend solution while non-homogeneous blend membranes were obtained below this temperature. For further characterization the homogeneous SPEEK/PI blend membranes were prepared by casting the solution at 130 °C while one non-homogeneous SPEEK/PI blend prepared at 80 °C was also selected.

Characterization techniques used for these membranes included water uptake, pervaporation, impedance, direct methanol fuel cell (DMFC) and direct ethanol fuel cell (DEFC) tests to observe the behaviour of the membranes during the fuel cell performance. Beside these some other characterization techniques like atomic force microscopy (AFM) and scanning electron microscopy (SEM) were also carried out to observe the morphology of the CMS coated

SPEEK and SPEEK/PI blend membranes (both homogeneous and non-homogeneous). While dynamic mechanical thermal analysis (DMTA), thermogravimetric analysis (TGA), differential scanning calometry (DSC), and attenuated total reflectance (ATR-FTIR) were performed for the SPEEK/PI blend membranes to have an idea for homogeneous blend formation and any change in glass transition temperature as compared to constituents (polyimide and SPEEK).

**1.6 References:**


[1] International Energy Agency (IEA); Key World Energy Statistics 2008.

[2] United Nation (The World at Six Billions).

[3] IPCC (Intergovernmental Panel on Climate Change) (2007c). Climate change 2007: Climate Change Impacts, Adaptation and vulnerability. Contribution of working Group II to the Forth Assessment Report of the IPCC. Online at the IPCC site.

[4] Christian Science Monitor, Aug 15, 2007.

[5] Energy Watch Group October 2007 (EWG-Series No 3/2007).

[6] Renewables 2007 Global Status Report (www.REN21.net).

[7] U.S. Department of Defense (DoD) Fuel Cell Test and Evaluation Center (FC*Tec*) Fuel Cell Basics.

[8] N.J. Cherepy, R. Kruegar, J.F. Cooper, Battery Conference on Applications and Advances, 1999. The Fourteenth Annual, Volume , Issue , 1999.

[9] D.J. Brodrecht, J.J. Rusek, Applied Energy, Volume 74, Number 1, January 2003.

[10] J. Yeoma, R S. Jayashree, C. Rastogi, M.A. Shannon, P.J.A. Kenis, University. Journal of Power Sources, 2006.

[11] Science News, May 10, 2006.

[12] Introduction to fuel cell technology by Chris Rayment and Scott Sherwin; Department of Aerospace & Mechanical Engineering University of Notre, IN 46556 U.S.A. May 2, 2003.

[13] Fuel Cell Handbook ($7^{th}$ Edition) by EG & G Technology Service Inc. Under contract No.DE-AM26-99FT40575, US DOE.

[14] Fuel Cell Handbook ($5^{th}$ Edition) by EG & G Services Parsons Inc. Science application International cooperation under contract No. DE-AM26-99FT 40575 US DOE.

[15] An Introduction to fuel cell and hydrogen technology by Brian Cook; Heliocentris 3652 West 5th Avenue Vancouver, BC V6R-1S2 Canada.

[16] Ulf Bossel; The Physics of Hydrogen economy, European Fuel Cell News, Vol.10, No.2 July, 2003.

[17] Deluca & A. Elabd, Polymer electrolyte membranes for direct methanol fuel cell; A Review, Journal of Polymer Science Part B: Polymer Physics, Vol 44, 2201 – 2225 (2006).

[18] A.S.Arico, DMFC from fundamentals aspects to technology developments; Fuel Cells, 2001, 1, No.2

[19] Fuel Cell today; 2008 Patents Review Q3 by Dr. Jonathan. www.fuelcelltoday.com

[20] H.Wang, A review of polymer electrolyte membranes for direct methanol fuel cell (DMFC), Journal of Power Sources 169 (2007) 221 – 238.

[21] Fuel cells in transportation 7th Edition (www.fuelcells.org)

[22] Beyond the internal combustion; the promise of methanol fuel cell vehicles: American Methanol Institute (AMI) (www.methanol.org)

[23] B.Smitha, S. Sridhar, A.A Khan, Solid polymer electrolyte membranes for fuel cell application - a review. Journal of Membranes Science 259 (2005) 10 – 26.

[24] Tongwen Xu, Ino exchange membranes: State of their development and perspective (Review), Journal of Membranes Science 263 (2005) 1 – 29.

[25] V. Neburchilov, J. Marten, H.Wang, J. Zhang; A review of polymer electrolyte membranes for direct methanol fuel cells, Journal of Power Sources 169 (2007) 221 – 238.

[26] Joseph Jagur-Grodzinski, Polymeric material for fuel cells; a concise review of recent studies, Polym. Adv. Technol. 2007; 18: 785 – 799.

[27] K.V.Peinemann, S.P.Nunes; Membranes for energy technology volume 2.

[28] T. Zadowzinski, J. Davy, J. Valerio, S. Gottesfeld, the water content dependence of electro-osmotic drag in proton conducting polymers electrolyte, Electrochem. Acta 40 (1995) 297 – 302.

[29] Organic-inorganic hybrid membranes with heteropoplyacids (HPA) for DMFC application, Ph.D thesis by Maraila Ponce.

[30] Satheesh Sambandam & Vijay Ramani, SPEEK/functionalized silica composite membranes for polymer electrolyte fuel cells, Journal of Power Sources 170 (2007) 259 – 267.

[31] M.T. Bishop, F.E. Karasz, P.S.Russo, K.H. Langley; Solubility and properties of poly (aryl ether ketone) in strong acids, Macromolecules, 1985, 18 (1) 86 – 93.

[32] Fuma-tech GmbH website (www.fumatech.com)

[33] S. P. Nunes, B. Ruffmann, E. Rikowski, S. Vetter, K. Richau. Inorganic modification of conductive polymer membranes for direct methanol fuel cell. *J. Membrane Sci.* 203 (2002) 215-225.

[34] C.S. Karthikeyan, S.P. Nunes, L.A.S.A. Prado, M.L. Ponce, H. Silva, B. Ruffmann and K. Schulte. Polymer nanocomposite membranes for DMFC application. *J. Membrane Sci.,* 254 (2005) 139–146

[35] V.S. Silva, B. Ruffmann, S. Vetter , A. Mendes, L.M. Madeira b, S.P. Nunes, Characterization and application of composite membranes in DMFC, *Catalysis Today* 104, 205 (2005)

[36] V. S. Silva, B. Ruffmann, H. Silva, V. B. Silva, A. Mendes, L. M. Madeira, S. Nunes, Zirconium oxide hybrid membranes for direct methanol fuel cells - Evaluation of transport properties. J. Membrane Sci. 284(1+2) (2006) 137-144.

[37] V. Antonucci, A. S. Arico, V. Baglio, J. Brunea, I. Buder, N. Cabello, M. Hogarth, R. Martin, S. Nunes, Membranes for portable direct alcohol fuel cells. Desalination 200 (1-3) (2006) 653-655.

# Chapter 2. Theoretical background

### 2.0 Proton transportation

So far proton transportation in a solid electrolyte membrane can be explained by two mechanisms; Grothus and vehicle mechanism. According to Grothus mechanism the protons move through an infinite network of hydrogen bonds. This process consists of two steps; first the translation of a proton from an oxonium ion to a water molecule by tunnelling in hydrogen bond and secondly the subsequent re-orientation (rotation) of water molecule thus formed in order to be able to take up the next proton and in this way the transportation of protons takes place in between relatively stationary anions. This phenomenon is also known as free-proton mechanism. The rate of proton transfer and reorientation of water molecule directly affect this mechanism. Usually Grothus mechanism is preferred in that media where strong hydrogen bonding exists.

*Figure 2.1: Simple schematic of proton transportation along with hydrogen bonding [1]*

But according to vehicle mechanism the proton does not migrate as $H^+$ ion but as $OH_3^+$, $NH_4^+$ and $CH_3OH_2^+$ depending upon the nature of the vehicle like $H_2O$, $NH_3$ and $CH_3OH$ respectively. The vehicle shows a diffusion coefficient corresponding to the proton conduction and behaves like Bronsted base (Proton acceptor). Therefore the presence of dissolved water in membranes upto a certain extent improves the proton conductivity. Vehicle mechanism is the characteristics of that media where weak forces exist. Consequently, Grothus mechanisms are progressively dominated over vehicle mechanism when the temperature is increasing [1].

*Figure 2.2: Simple schematic of vehicle mechanism for transportation of protons [1].*

High level of hydration in PEM promotes excellent proton conductivity but at the same time it creates some problems like operation at high temperature and expensive water management in fuel cells. Therefore the target for operating at high temperature is such a membrane exhibiting good proton conductivity with minimal water tightly bound to a stable host. Hydrated sulfonic acid groups fixed on a stable polymer host donate their protons to the aqueous domain. Membranes with high degree of sulfonation shows good proton mobility rationalized on the basis of Grothus mechanism or structural diffusion mechanism. Such a proton–relay mechanism comprises a sequence of forward and backward transformation between an Eigen-ion ($H_9O_4^+$) and Zundel-ion ($H_5O_3^+$). The sulfonate head groups, which bind the surface of surrounding water molecules, inhibit proton mobility [3].

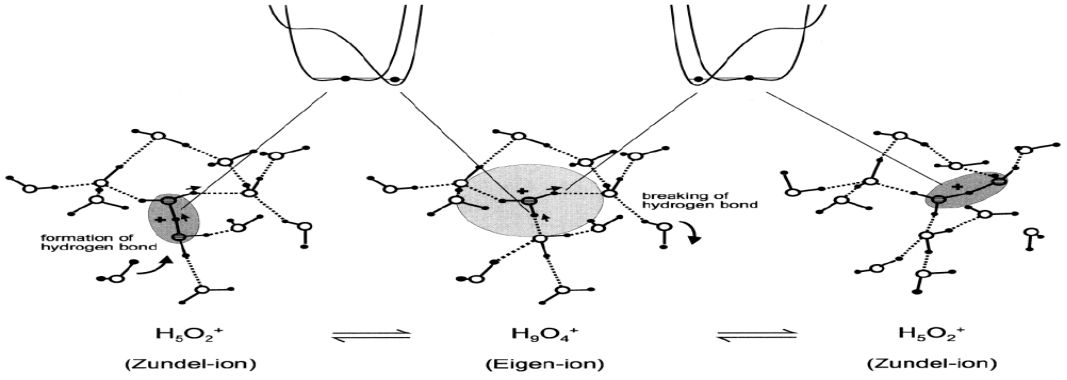


*Figure 2.3: Proton conduction through hydrogen-bond pattern, which diffuses by hydrogen bond breaking and forming process (reproduced from [4]).*

So far sulfonated poly(etheretherketon) (SPEEK), sulfonated poly(etherketon) (SPEK) and Nafion are trade mark off membranes in the industries. The structural view of these membranes show the phase separated domains consisting of an extremely hydrophobic back-bone (morphological stability) and extremely hydrophilic functional groups which aggregate to form hydrophilic nano-domains acting as water reservoir. A comparasion of the important parameters is presented in the below figure 2.4 for Nafion and SPEEK membranes.

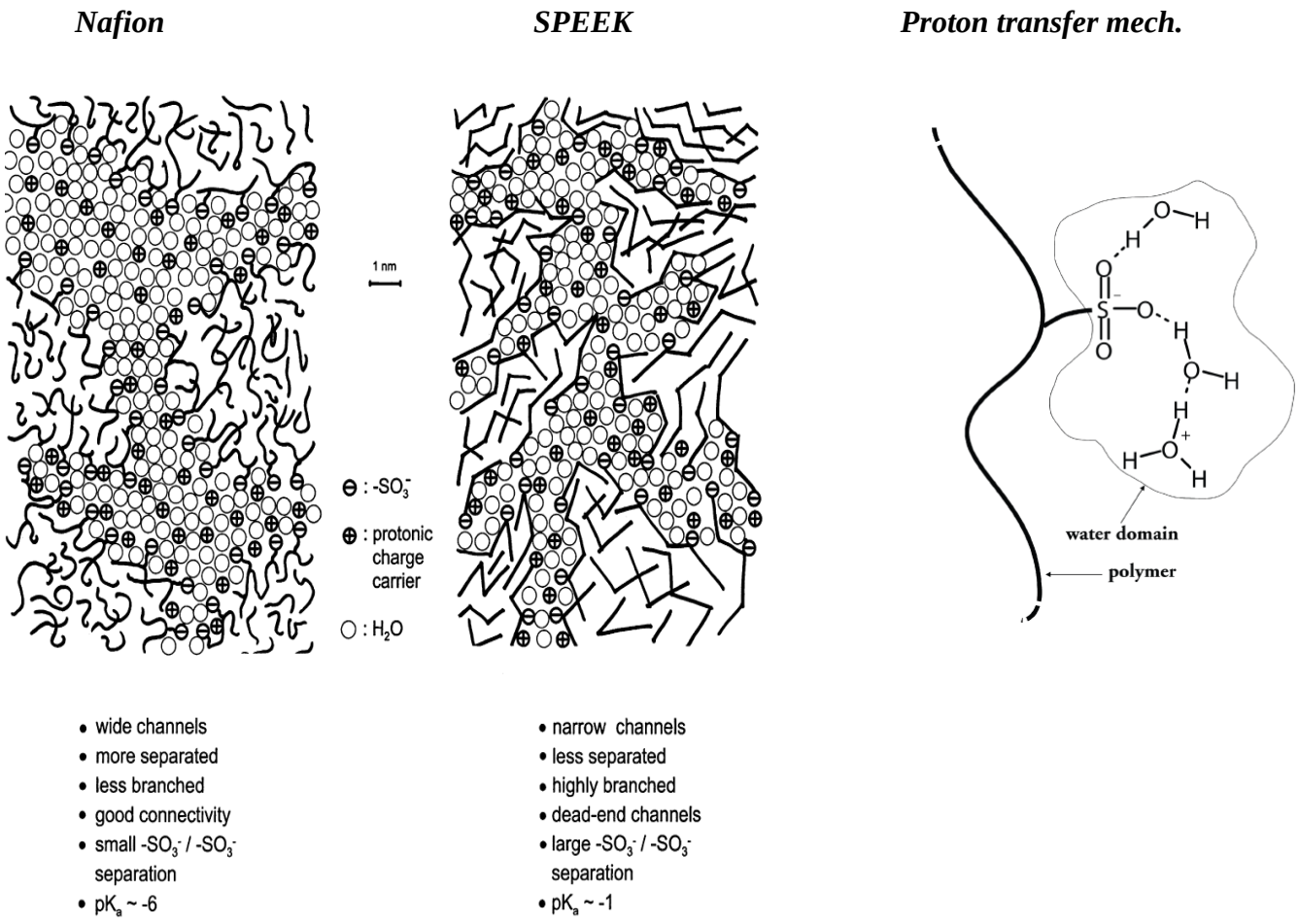


*Figure 2.4: Comparasion of structure of Nafion and Sulfonated poly(etheretherketon) SPEEK (Reproduced from [4]) and proton transfer mechanism*

Unfortunately at lower level of hydration the diffusion coefficient for the sulfonated aromatic polymer are lower than Nafion and due to which low proton conductivity is observed for such membranes. The main reason for this is the association of proton with the $(SO_3)^-$ groups and

greater electro-static potential differences due to space charges surrounding the sulfonic groups which cause a reduced phase separation and higher activation energy when compared with the Nafion®. In Nafion® membrane, because of its high hydrophobic perflourinated backbone and its high hydrophilicity of the sulfonic acid groups, it would give rise to formation of hydrophobic/hydrophilic domains, especially in the presence of water. As indicated in the figure 2.4, the sulfonic acid groups aggregate to form a hydrophilic domain. These hydrophilic domains are interconnected in Nafion® membrane. Not only proton and water can be transported through these domains but a smaller polar molecule such as methanol can also permeate through these domains. However, the micro-structure of SPEEK membrane was found to be distinctly different from Nafion membranes. By modifying the model proposed by Kreuer [5], the membrane is less separated due to smaller hydrophobic/hydrophilic differences i.e the backbone is less hydrophobic and the sulfonic acid groups is less acidic than in Nafion; and more branched with more dead-end "pockets" as shown in figure 2.4. Owing to this smaller difference and the lesser flexibility of the polymer backbone, the separation into a hydrophobic and hydrophilic domain is less pronounced. This has one of the advantages that methanol permeability is much lower than Nafion® membrane, which in turn makes the SPEEK membrane very attractive for future development of DMFC technology [6].

The study of dynamics of proton conduction is also complicated because of the complex structure of ionomer membranes and for investigations different types of techniques like quasi-elastic neutron scattering, field-cycling nuclear magnetic relaxation and pulsed field gradient NMR must be used together with the modelling of proton transport [7 – 9]. Many bulk properties of polymeric membranes are due to ionic interaction in the sub molecular regions of the polymeric materials and the macromolecular properties of the system are therefore characteristics. The polymeric architecture may be different by the position, type and concentration of the ionic groups on the backbone. These encourage a lot of research

works to be carried out on this topic. It is worth mentioning that conditions (acidification and humidity exposure) for making membranes also influence the nature of the network of the nano-pores, and that in turn also affect the macroscopic membrane properties [10 – 12].

## 2.1 Electrical work, Potential and Efficiency of fuel cell

*2.1.1 Theoretical electrical work*

The enthalpy or higher heating value (HHV) of hydrogen combustion is 286 kJ $mole^{-1}$. It is the amount that may be generated by combusting one mole of hydrogen. If one mole of hydrogen is enclosed in calorimetric bomb with ½ mole of $O_2$ , ignited, fully combusted and then allow to cool to room temperature (25 °C) at atmospheric pressure, there will be left only water in the calorimetric bomb. The amount of heat released during this process should be 286 kJ $mole^{-1}$ and this value is known as *higher heating value (HHV)*.

$$H_2 + ½\ O_2 \longrightarrow H_2O_{(Liquid)} + 286\ kJ\ mole^{-1}$$

But usually this value is not equal to above theoretical value (286 kJ $mole^{-1}$) because of the combustion of hydrogen with excess amount of oxygen; the product water will be left with un-burnt oxygen or nitrogen in air mixed in the form of vapours in the system. Therefore, the observed value (241 kJ $mole^{-1}$) is less than the above calculated one. This value is called as *lower heating values (LHV)* of hydrogen combustion.

$$H_2 + ½\ O2 \longrightarrow H_2O_{(liquid)} + 241\ kJ\ mole^{-1}$$

The difference between the higher heating value (HHV) and lower heating value (LHV) is the heat of evaporation of water at 25 °C.

$$H_{fg} = 286 - 241 = 45\ kJ\ mole^{-1}$$

But as we know there in no combustions of fuel inside the fuel cell then what is relevance of HHV and LHV of hydrogen to a fuel cell. These values are used as a measure of energy input in a fuel cell [13, 14]. This is the maximum amount of thermal energy that may be extracted

from hydrogen but instead of heat, electricity is produced in a fuel cell and the question arises is that is it possible to convert all the input energy into electricity. The answer is definitely not. Because in every chemical reaction some entropy is produce due to which some parts of the HHV are not converted into useful work (Electricity). The portion of enthalpy reaction of HHV of hydrogen that can be converted into electricity in fuel cell corresponds to Gibb's free energy (ΔG) and is represented by the following relationship.

$$\Delta G = \Delta H - T\Delta S \qquad \text{Eq. 2.1}$$

Where ΔH is the difference between heat of formation of products ($H_2O$) and reactants ($H_2$ & $O_2$), ΔS is the difference between the entropies of products and reactants and T is the temperature. ΔH and ΔS can be further explained by the following relationships

$$\Delta H = (H_f)_{H2O} - (H_f)_{H2} - \tfrac{1}{2}(H_f)_{O2} \qquad \text{Eq. 2.2}$$

$$\Delta S = (S_f)_{H2O} - (S_f)_{H2} - \tfrac{1}{2}(S_f)_{O2} \qquad \text{Eq. 2.3}$$

The values of ($H_f$) and ($S_f$) for reaction reactants and products at ambient pressure and at 25 °C are listed in following table 2.1.

*Table 2.1: Enthalpies and entropies of formation of fuel cell reactants and products.*

| **Reactants / Products** | **(Hf) kJ mole$^{-1}$** | **(Sf) kJ mole$^{-1}$ k$^{-1}$** |
|---|---|---|
| Hydrogen ($H_2$) | 0 | 0.13066 |
| Oxygen ($O_2$) | 0 | 0.20517 |
| Water ($H_2O$) Liquid | -286.02 | 0.06996 |
| Water ($H_2O$) Vapours | -241.98 | 0.18884 |

Therefore, at 25 °C out of the available energy (286 kJ mole$^{-1}$), the amount of energy that can be converted into useful work-electricity is (237 kJ mole$^{-1}$) and the remaining (48 kJ mole$^{-1}$) is converted into heat [15 – 17].

*2.1.2 Theoretical potential of fuel cell*

Generally the electrical work can be defined as the product of charge and potential.

$$W_{el} = q * E \qquad \text{Eq. 2.4}$$

Where

$W_{el}$ = Electrical work (J $mole^{-1}$)

q = Charge (Coulomb $mole^{-1}$)

E = Potential (Volts)

The electrochemical reactions in a fuel cell happen on both sides of the membranes at the same time on the anode and cathode. The basic fuel cell reactions can be given as;

Anodic Oxidation reaction

$$H_2 \longrightarrow 2\,H^+ + 2\,e^-$$

Cathodic reduction reaction

$$\tfrac{1}{2}\,O_2 + 2\,e^- + 2H^+ \longrightarrow H_2O$$

Over-all reaction

$$H_2 + \tfrac{1}{2}\,O_2 \longrightarrow H_2O$$

In a fuel cell these reactions are not so simple and may have some several steps up to completion but for now these reactions accurately describe the reactions in a fuel cell. The total charge transferred in a fuel cell according to these reactions per mole of hydrogen consumed can be expressed as below;

$$q = n\,N_{avg} * q_{el} \qquad \text{Eq. 2.5}$$

Where

n = No of electrons per molecule of $H_2$ (2 electrons for $H_2$ molecule).

$N_{avg}$ = No of molecules per mole (Avogadro's number = $6.023 * 10^{23}$ molecules per mole)

$q_{el}$ = Charge on 1 electron ( $1.602 * 10^{-19}$ C)

By putting the value of (q) in the above Eq 2.25 then the electrical work can be expressed in the following Eq 2.26.

$$W_{el} = (n\ N_{avg} * q_{el}) * E \qquad \text{Eq. 2.6}$$

The product of Avogadro's No ($N_{avg}$) and charge of one electron ($q_{el}$) is known as Faraday constant (F=96,485 C/electron-mole) and it can be presented as;

$$F = (N_{avg} * q_{el}) = (96{,}485\ C\ /\text{electron-mole}) \qquad \text{Eq. 2.7}$$

And finally the electrical work ($W_{el}$) can be expressed by the following Eq 2.8 by putting the values from the above Eq 2.7.

$$W_{el} = n\ F\ E \qquad \text{Eq. 2.8}$$

As mentioned before, the maximum amount of electrical energy generated in a fuel cell corresponds to Gibb's free energy (ΔG),

$$W_{el} = -\ \Delta G \qquad \text{Eq. 2.9}$$

And by comparasion of equations 2.8 and 2.9, the relationship for the theoretical potential of a fuel cell can be found as bellow;

$$n\ F\ E = -\ \Delta G \qquad \text{Eq. 2.10}$$

Or

$$E = \frac{-\Delta G}{nF} \qquad \text{Eq. 2.11}$$

As ΔG, n and F all are known therefore, the theoretical potential of fuel cell for hydrogen/oxygen can be given as,

$$E = \frac{-\Delta G}{nF} = \frac{237{,}340\ J\ /\ mole}{2 * 96{,}485\ A\ s\ /mole} = 1.23\ \text{Volt (LHV)} \qquad \text{Eq. 2.12}$$

$$E = \frac{\Delta H}{nF} = \frac{286{,}000}{2 * 96{,}485} = 1.48\ \text{Volts} \quad \text{(HHV)} \qquad \text{Eq. 2.13}$$

*From the above Eq 2.12 it is clear that at 25 °C the theoretical potential for $H_2/O_2$ fuel cell is 1.23 Volt.*

*2.1.3 Theoretical fuel cell efficiency*

The efficiency of a fuel cell is defined as the ratio between the electrical power output and fuel input. Assuming that all of the Gibb's free energy can be converted into useful electrical work, the maximum possible theoretical efficiency of a fuel cell at 25 °C by using the hydrogen HHV can be given by;

$$\text{Efficiency } (\eta) = \frac{\Delta G}{\Delta H} = \frac{237\ kJ/mole}{286\ kJ/mole} = 83\ \% \qquad \text{Eq. 2.14}$$

If both ΔG and ΔH are divided by (n F) then the fuel cell efficiency may be expressed as the ratio of two potentials as can be derived from Equations 2.12 and 2.13 already discussed before.

$$\text{Efficiency } (\eta) = \frac{\Delta G/nF}{\Delta H/nF} = \frac{1.23}{1.48} = 83\ \% \qquad \text{Eq. 2.15}$$

Where 1.23V is the cell theoretical efficiency and 1.48V is the potential corresponding to HHV of hydrogen combustion, or the thermo neutral efficiency. The theoretical efficiency is some time also known as the thermodynamics efficiency or maximum efficiency limit. The theoretical efficiency at different temperature and standard pressure can be observed in the following figure 2.5. It is also evident there is a connection between the reversible open current voltage (OCV) and its theoretical efficiency (or maximum efficiency) based on the above equations 2.14 & 2.15 [16 – 18].

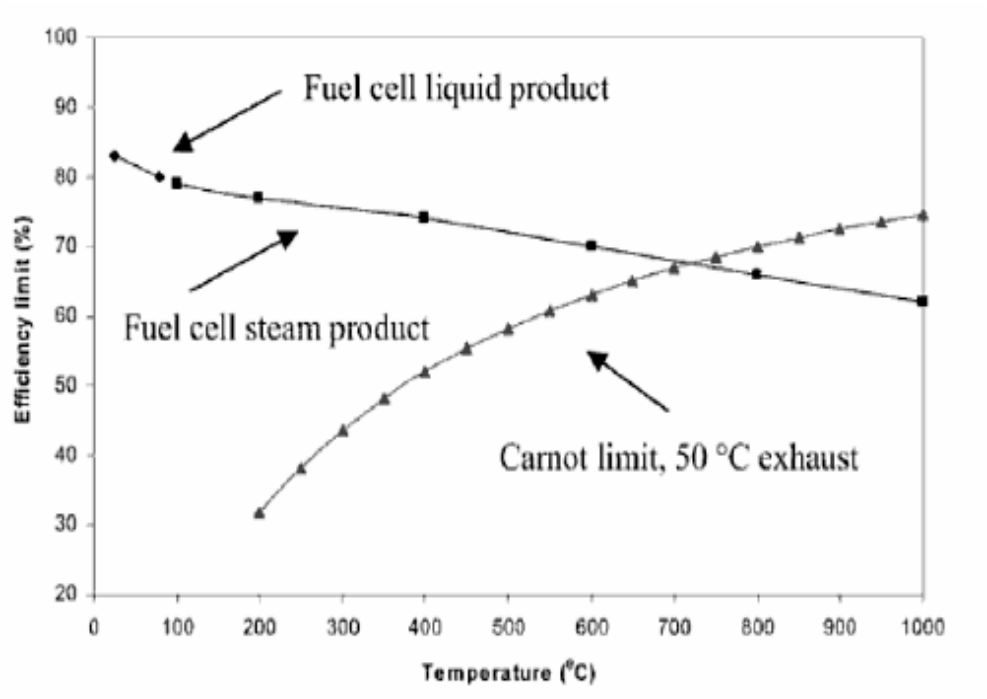


*Figure 2.5: Theoretical Hydrogen fuel cell efficiency at standard pressure based on HHV [17].*

*2.1.4 Actual efficiency of fuel cell*

The actual efficiency of a fuel cell is defined as the actual voltage divided by the thermo neutral potential e.g.

$$\text{Cell efficiency} = \frac{Vcell}{1.48} * 100 \quad \text{based on (HHV)} \qquad \text{Eq. 2.16}$$

Or $$\text{Cell efficiency} = \frac{Vcell}{1.23} * 100 \quad \text{based on (LHV)} \qquad \text{Eq. 2.17}$$

In practice the fuel cell is normally operated under condition such that not all of the fuel fed is utilized during the process but some fuel has to pass though unreacted. Therefore to calculate the cell efficiency, another parameter needs to be taken into account and that parameter is known as the fuel utilization coefficient. By definition it's the ratio of reacted fuel in the cell to the input of fuel.

$$\mu f = \frac{Mass\ of\ \ fuel\ reacted\ in\ cell}{Mass\ of\ \ fuel\ input\ \ \text{to}\ cell}$$

Therefore equations 2.16 and 2.17 can be modified as by putting this parameter as follow.

Cell efficiency = $\mu f \frac{Vcell}{1.48} * 100$ based on (HHV) Eq. 2.18

Or Cell efficiency = $\mu f \frac{Vcell}{1.23} * 100$ based on (LHV) Eq. 2.19

Now from any of the above equations; one can calculate the actual efficiency of fuel cell during PEM test performances. Because of polarization losses at the electrodes interface the maximum voltage observed for polymer electrolyte membrane (PEM) fuel cell is between 0.95 V to 1.00 V. Under operating condition the voltage is further reduced by *Ohmic resistance* within the cell. A common fuel cell design voltage is 0.70 V but the values may change between 0.6 V and 0.8 V depending on the electrical current drawn from the electrochemical reaction. A fuel cell operating at 0.70 V corresponds to its voltage efficiency equal to (0.70/1.48 = 50%) or about 50 %.

*2.1.5 Comparasion of Carnot and fuel cell efficiencies*

An ideal reversible cycle where heat is taken in at constant upper temperature ($T_H$) and then rejected at a constant lower temperature (Tc) is called as Carnot cycle. The efficiency at maximum power of a Carnot engine may be given by the following equation 2.20.

Carnot efficiency ($\eta$) = 1 - $\sqrt{T_c} / \sqrt{T_H}$ Eq. 2.20

Where

Tc = the absolute temperature of cold reservoir

$T_H$ = the absolute temperature of hot reservoir

The Carnot efficiency does not apply to fuel cell efficiency because of the fact that fuel cell is not a heat engine but it is an electrochemical energy converter. For this reason a fuel cell operating at low temperature (60 °C) and discarding heat outside to the environment at 25 °C may have efficiency significantly higher than any heat engine operating between the same two temperatures. The theoretical efficiency of a fuel cell operating at higher temperature may be lower than the theoretical Carnot efficiency of a heat engine operating between the same

temperatures. One of the arguments that for any *hydrogen/oxygen or hydrogen/air system*, the high temperature source is the temperature of hydrogen/oxygen flame and therefore, the efficiency of fuel cell can not exceed the Carnot efficiency of an engine using this flame as source of heat. This might be true but this has no relation to the fuel cell because in fuel cell there is no flame and the theoretical efficiency is determined from the ratio between the Gibb's free energy and enthalpy of hydrogen/oxygen reaction regardless of hydrogen/oxygen flame temperature [16, 19].

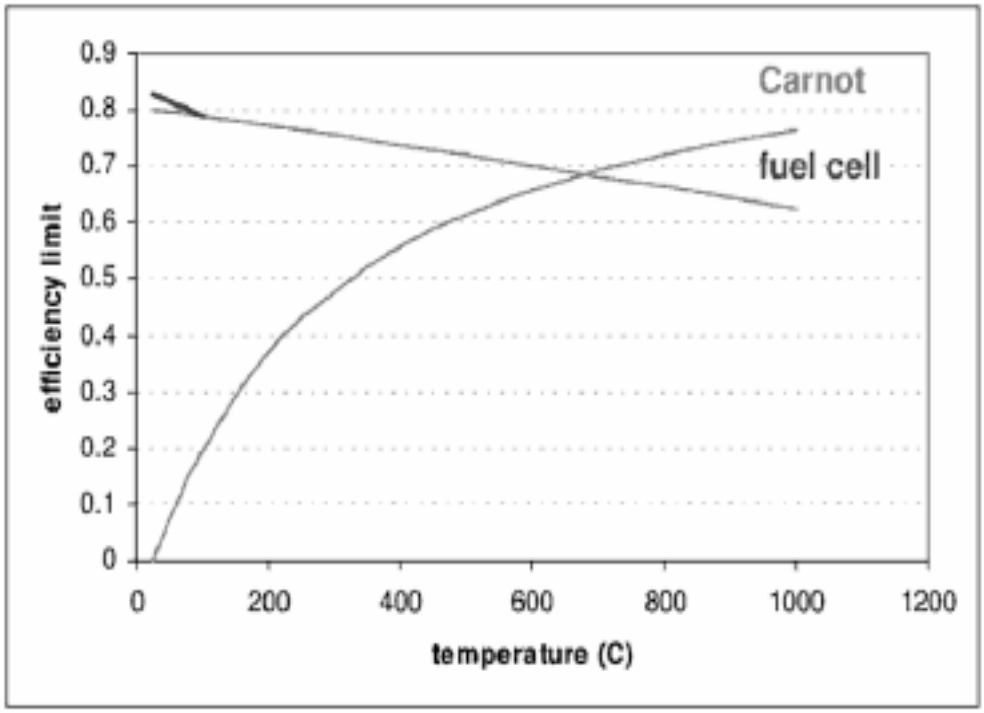


*Figure 2.6: Theoretical efficiencies of Carnot engine and fuel cell as a function of temperature [16].*

## 2.2 References


[1] Angew. Chem. Int. Ed. Engl. 21 (1982) No. 3

[2] Kaus-Dieter Kreuer, Transport in proton conductors for fuel cell applications: Simulations, Elementary Reactions, and Phenomenology; Chemical review 2004, 104, 4637 – 4678.

[3] Stephen J. Paddison, Defect structure for proton transport in a triflic acid monohydrate solid, Chemical Physics Letter 368, (2003) 108 – 114.

[4] W.H.J. Hogarth, Solid acid membranes for high temperature (> 140 °C) proton exchange membrane fuel cells, Journal of Power Sources 142 (2005) 223 – 237.

[5] K.D. Kreuer, On the development of proton conducting polymer membranes for hydrogen and methanol fuel cells, Journal of Membrane Science 185 (2001) 29 – 39.

[6] A.F. Ismail et al Physico-chemical study of sulfonated poly (ether ether keton) membranes for DMFC applications, Malaysian Polymer Journal (MPJ), Vol.2, p 10 – 28 (2007).

[7] G.Gebel, O. Diat; Neutron & X-Ray scattering: Suitable tools for studying ionomers membranes, Fuel cell 5, 267 – 276 (2005).

[8] J.C.Perrin; Water dynamics in Ionomers membranes by field-cycling NMR relaxometry, Fuel Cell 6, 5 – 9 (2006).

[9] A.Z. Weber; Modelling transport in polymer-electrolyte fuel cell, Chemical reviews 104, 4679 – 4726 (2004).

[10] Robertson G.P et al, Casting solvent interaction during with sulfonated poly (etheretherketon) during proton exchange membrane fabrication; Journal of Membrane Science 219, 113 – 121 (2003).

[11] Y.S.Kim et al, Effect of acidification treatment and morphological stability of sulfonated poly (arylene ether sulfon) copolymer proton exchange membranes for fuel

cell use above 100 °C; Journal of Polymer Science Part B-polymer physics 41, 2816 – 2828 (2003).

[12] S. P. Nunes and K. V. Peinemann, Membrane Materials and Membrane Preparations (Part I). In S. P. Nunes and K. V. Peinemann, editors, "Membrane Technology in the Chemical Industry", Wiley-VCH, Weinheim, Germany, 2001, 2nd edition 2006.

[13] Fuel Cell Handbook (7th Edition) by EG & G Technology Service Inc. Under contract No.DE-AM26-99FT40575, US DOE.

[14] Fuel Cell Handbook (5th Edition) by EG & G Services Parsons Inc. Science application International cooperation under contract No. DE-AM26-99FT 40575 US DOE.

[15] An Introduction to fuel cell and hydrogen technology by Brian Cook; Heliocentris 3652 West 5th Avenue Vancouver, BC V6R-1S2 Canada.

[16] Frano Barbir, PEM Fuel Cell: Theory and Practice.

[17] PEM Fuel cell, Electrocatalysts and catalysts layers, Fundamentals and applications by Jiujun Zhang (Editor).

[18] B. Sljukic et al, An overview of electrochemical reduction of oxygen at carbon based modified electrodes; Journal of Iranian Chem.Soc (2005) 2: 1- 25.

[19] C. Van den Broeck, thermodynamic efficiency at maximum power, PRL 95, 190602 (2005).

# Chapter 3. Characterization methods

### 3.0: Impedance measurements

The proton conductivity of a membrane can be measured by AC Impedance spectroscopy or (Electrochemical impedance spectroscopy, EIS). The main advantage of EIS is to use a purely electronic model to represent an electrochemical cell. An electrode interface undergoing an electrochemical reaction is typically analogous to an electronic circuit consisting of a specific combination of resistors and capacitors. This analogy offers the advantage by using established ac circuit theory to characterize the electrochemical system in term of its equivalent circuit. Once a particular model being selected, it can be correlated physical or chemical properties with circuit elements and exact numerical values by fitting the data to the circuit model. EIS theory is a well- developed branch of a.c. theory that describes the response of a circuit to an alternating current or voltage as a function of frequency. According to Ohm's Law resistance is defined in term of ratio of voltage to the current

$$R = \frac{V}{I} \qquad \text{Eq. 3.1}$$

This is a well known relationship and its application is limited to only one circuit element – the ideal resistor. An ideal resistor has several simplifying properties like (a) it follow Ohm's law at all current and voltage level (b) its resistance value is independent of frequency and (c) AC current and voltage signals through a resistor are in phase with each others. But the real world contains circuit elements with much more complex behaviour. These elements force us to abandon the simple concept of resistors and to use a more generalised word "Impedance". Like resistance, impedance is the measure of the ability of a circuit to resist the flow of electrical current. Unlike resistance, impedance is not limited to above mentioned simplifying properties.

EIS is normally measured by applying an AC potential (sinusoidal potential excitation) to an electrochemical cell and then measuring the AC current signal through the cell as a result of

the applied AC potential. This current signal can be analyzed as a sum of sinusoidal functions (a Fourier series). EIS is normally measured using a small excitation signal and this is done so that the cell response is Pseudo-linear. In Pseudo-linear system the current response to a sinusoidal potential will be a sinusoid at the same frequency but shifted in phase and this behaviour can be seen clearly in the following figure 3.1.

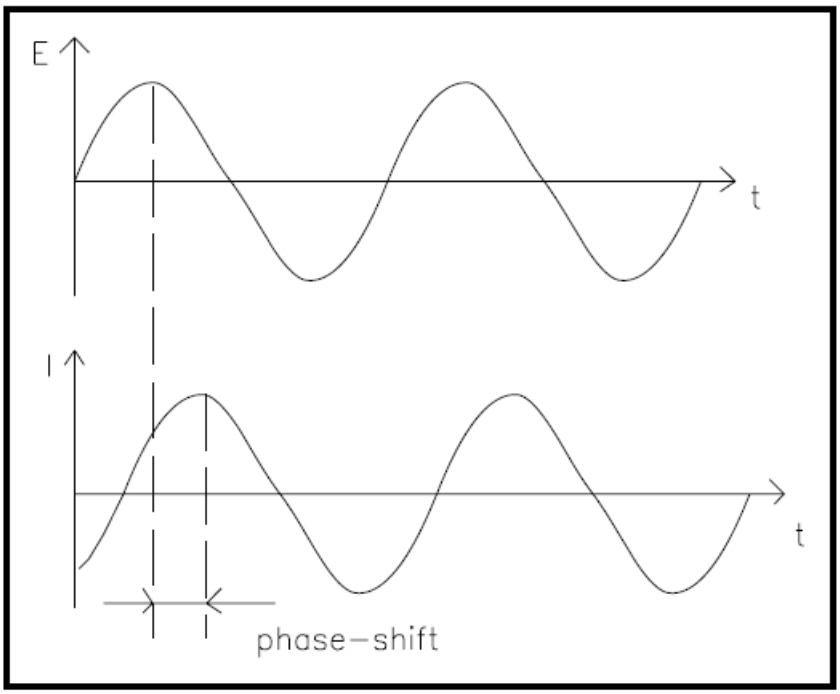


*Figure 3.1: Sinusoidal current response in linear system [12]*

The excitation signal expressed as function of time can be written as;

$$E_t = E_0 \sin(\omega t) \qquad \text{Eq. 3.2}$$

Where

*$E_t$ is the potential at time (t)*

*$E_0$ is the amplitude of signal*

*$\omega$ is the radial frequency.*

The relationship between the radial frequency ω (expressed in radian / second) and frequency *f* (expressed in Hertz) can be given in the following equation 3.3.

$$\omega = 2\pi f \qquad \text{Eq. 3.3}$$

In linear systems the response signal (It) is shifted in phase ($\phi$) and has a different amplitude ($I_0$) therefore;

$$I_t = I_0 \sin(\omega t + \phi) \qquad \text{Eq. 3.4}$$

An expression analogous Ohm's law, allows us to calculate the Impedance of the system in the following equation 3.5.

$$Z = \frac{E_t}{I_t} = \frac{E_o \sin(\omega t)}{I_o \sin(\omega t + \phi)} = Zo \frac{\sin(\omega t)}{\sin(\omega t + \phi)} \qquad \text{Eq. 3.5}$$

The impedance is therefore expressed in terms of magnitude, $Z_0$, and phase shift ($\phi$). A plot of applied sinusoidal signal $E_t$ on the X-axis against the sinusoidal response signal $I_t$ on the Y-axis will give rise to an Oval; known as Lissajous figure. Analysis of Lissajous figure on the oscilloscope screen was the accepted method of impedance measurement before the availability of the present day modern EIS instrumentation.

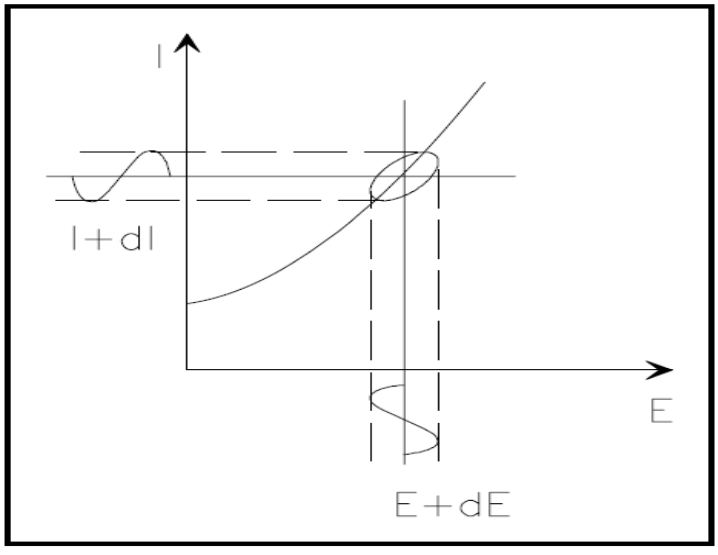


*Figure 3.2: Origin of Lissajous Figure*

With Euler relationship,

$$\exp(j\,\phi) = \cos\,\phi + j\sin\,\phi \qquad \text{Eq. 3.6}$$

It is possible to express the impedance as a complex function. The potential is described as;

$$Et = E_0 \exp(j\omega t) \qquad \text{Eq. 3.7}$$

And the current response as,

$$I_t = I_0 \exp(j\omega t - \phi) \qquad \text{Eq. 3.8}$$

The impedance is then represented as a complex number,

$$Z(\omega) = \frac{E}{I} = Z_0 \exp(j\phi) = Z_0(\cos\,\phi + j\sin\phi) \qquad \text{Eq. 3.9}$$

A close view on the above equation 3.9 shows that the expression for Z (ω) is composed of a Real [$Z_0(\cos\,\phi)$] and Imaginary [$Z_0(j\sin\phi)$] part [12,13]. If the real part is plotted on the X-axis against imaginary part on the Y-axis then the graph resulted will be called as *"Nyquist plot"*. In this plot the Y-axis is negative and each point of the Nyquist plot corresponds to the impedance at one frequency. Higher frequency data are on the right side while low frequency data are on the left side of this plot. In the Nyquist plot the impedance can be represented as vector (arrow) of length (Z). The angle between this vector and X-axis commonly called the "phase angle" is $\phi$ (= arg Z). Below figure 3.3 (a) shows the Nyquist plot which results from electrical circuit as shown in the following figure 3.3 (b). The semicircle is the characteristics of a single "time constant". The EIS plot contains many semicircles but only a portion of a semi-circle can be seen.

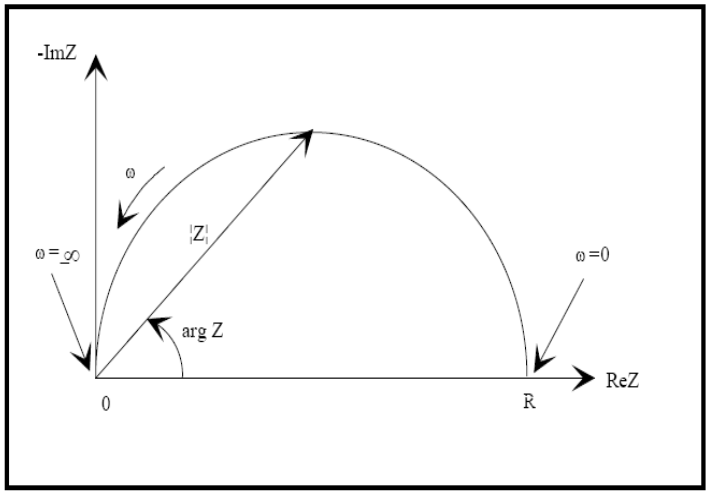


(a)

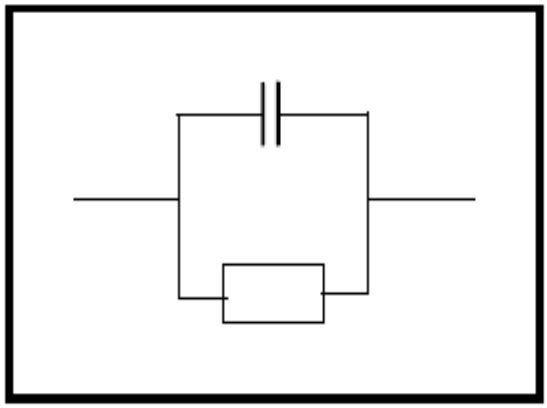

(b)

*Figure 3.3: (a) Nyquist plot with impedance vector and (b) simple equivalent circuit with one time constant [12]*

One major shortcoming of the Nyquist plot is that looking to any point on the plot; one can not tell what frequency was used at the time of recording this point.

Another popular presentation method is the *Bode Plot* in which the impedance is plotted with log frequencies on the X-axis and both absolute values of the impedance ($Z = Z_0$) & the phase shift on the Y-axis. From the Bode plot one can know about the frequency information at the time of recording the point. A Bode Plot for the electrical circuit from Fig 3.3 (b) can be observed in figure 3.4.

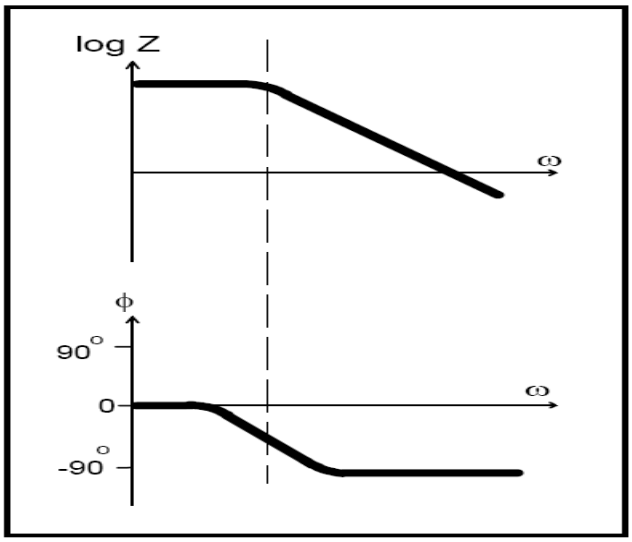


*Figure 3.4: Bode Plot with one time constant.*

In normal EIS measurement, a small AC signal (1 – 10 mV) is applied to the cell and certainly with such a small potential signal, the system is pseudo-linear. Therefore one can not see the cell's larger non linear response to the DC potential because the cell current is measured only at the excitation frequency. By close view of the cell current vs Voltage curve, it appears to be linear as shown in figure 3.5.

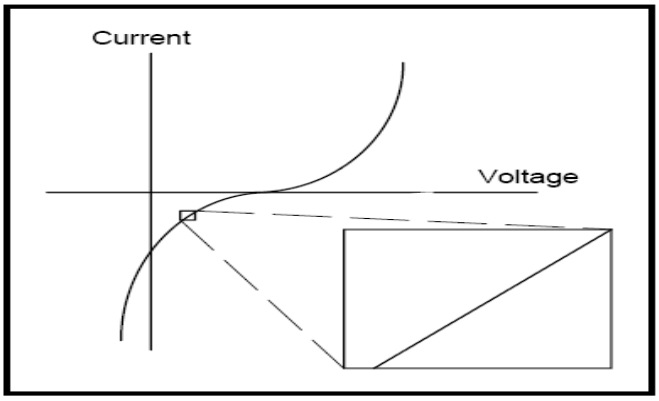


*Figure 3.5: Current vs Voltage curve showing Pseudo-linearity.*

The EIS model consists of a number of elements most commonly electrical elements like *resistors, capacitors and inductors* in a network, both parallel and series combinations. There are simple formulas which describe the impedance of circuit elements both in parallel and series combinations. Figure 3.6 (a) and (b) shows the impedance in series and parallel respectively.

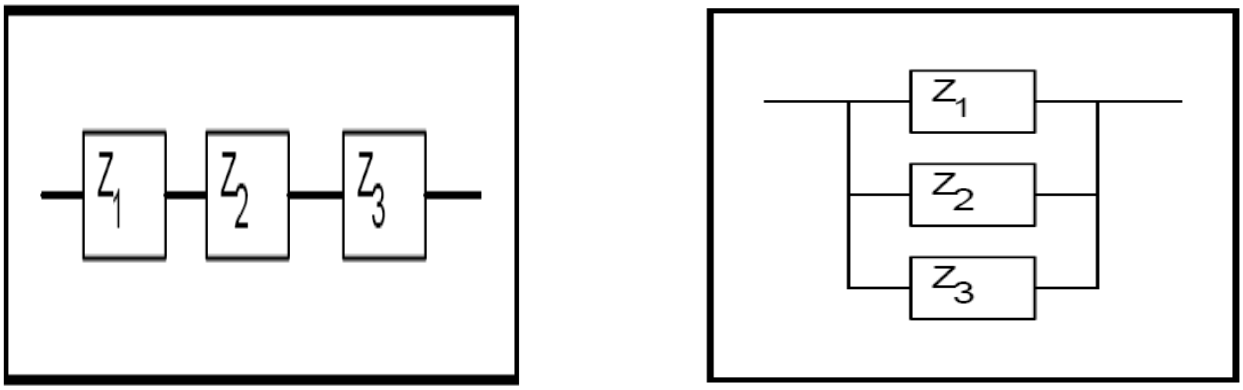


*Figure 3.6: (a) represents impedance in series and (b) impedance in parallel.*

For linear impedance elements in series and parallel, the equivalent impedance can be calculated according to the following equations 3.10 and 3.11 respectively taking in to account the current – voltage relationships from table 3.9.

$$Z_{eqv} = Z_1 + Z_2 + Z_3 \qquad \text{Eq. 3.10}$$

$$\frac{1}{Zeqv} = \frac{1}{Z1} + \frac{1}{Z2} + \frac{1}{Z3} \qquad \text{Eq. 3.11}$$

*Table 3.1: Current voltage relationships of common electrical elements.*

| Component | Current Vs.Voltage | Impedance |
|---|---|---|
| resistor | E= IR | Z = R |
| inductor | E = L di/dt | Z = jωL |
| capacitor | I = C dE/dt | Z = 1/jωC |

Under true fuel cell conditions the protons are supposed to migrate through the thickness of membrane. The proton conductivity of a membrane can be measured in-plane or through-plane. However, through-plane conductivity experiments are difficult to perform due to significant interfacial resistance that may occur during the test. Conversely, it is easier to measure the membrane conductivities by measuring the resistance in the plane of a membrane. This technique allows for higher and more easily measurable resistance in a simplified set-up. The proton conductivity (σ) can be calculated from the impedance data using the following equation 3.12.

$$\sigma = \rho^{-1} = \frac{L}{R * A} \qquad \text{Eq. 3.12}$$

Where

ρ= Resistivity

L = Thickness of the membrane

A = Area of the membranes

R = Bulk resistance of the membrane

The resistance is derived from the low intersect of the high frequency semicircle on a complex impedance plane with the Re (z) axis. Usually *two or four probe cell systems* are used for impedance measurements of a membrane and yet some level of discrepancies arises when the results obtained from both systems are compared.

### 3.1 Pervaporation of alcohols / water mixture

One of the important criteria for a DMFC membrane is that it must act as a barrier to methanol or any other kind of fuel to be used in the system. The selection of a suitable membrane for DMFC application usually is based on:

1. Proton conductivity
2. Electrical resistance
3. Methanol cross-over through the membranes.

The methanol permeability co-efficient is to be preferred since this can be considered as an intrinsic material property. Furthermore, this parameter is concentration or activity and temperature dependent which implies that methanol permeability co-efficient of different polymeric membranes can be compared at any concentration and any temperature. Therefore methanol and water permeability coefficient can be determined by pervaporation process using a known concentration solution of alcohol / water mixture as a feed. In our case we used 5 wt % of methanol solution and then ethanol solution of the same concentration in separate pervaporation process for our polymeric membranes. The pervaporation configuration is a good approximation to show the alcohols and water transport through the DMFC membranes, because both in DMFC and in pervaporation the transport is influenced very much by the swelling of the membrane by the fuel (alcohols) used.

Pervaporation is a process in which a liquid stream of two or more than two components is allowed in contact with one side of the non-porous membranes or molecularly porous membrane (CMS and Zeolite etc.) while a vacuum or gas purged is applied on the other side. The components in the liquid stream then sorbs into/onto the membrane permeate through the membrane and evaporates into a vapour phase (pervaporate). In our case vacuum applied to the permeate side was coupled with the immediate condensation of the permeate components by liquid nitrogen. Figure 3.7 represents pervaporation process and apparatus designed for

pervaporation. Permeation of vapours or liquids through the non-porous membranes is driven by chemical potential gradient across the membrane and that is maintained by ensuring immediate sorption and rapid desorption of the permeated species at the downstream side of the membrane.

The properties of the membrane materials also dictate the separation achieved during pervaporation measurements. For example a hydrophobic membrane will preferentially permeate the organic compounds relative to water and therefore the permeate will contain a high concentration of organic compounds. On the other hand, a hydrophilic membrane will allow a high amount of water to permeate side and the organic compound in the feed mixture will be enriched and dehydrated. This shows that the general procedure of the pervaporation is the same but as the membrane materials are changed therefore the permeate obtained from the feed solution is also changed [14].

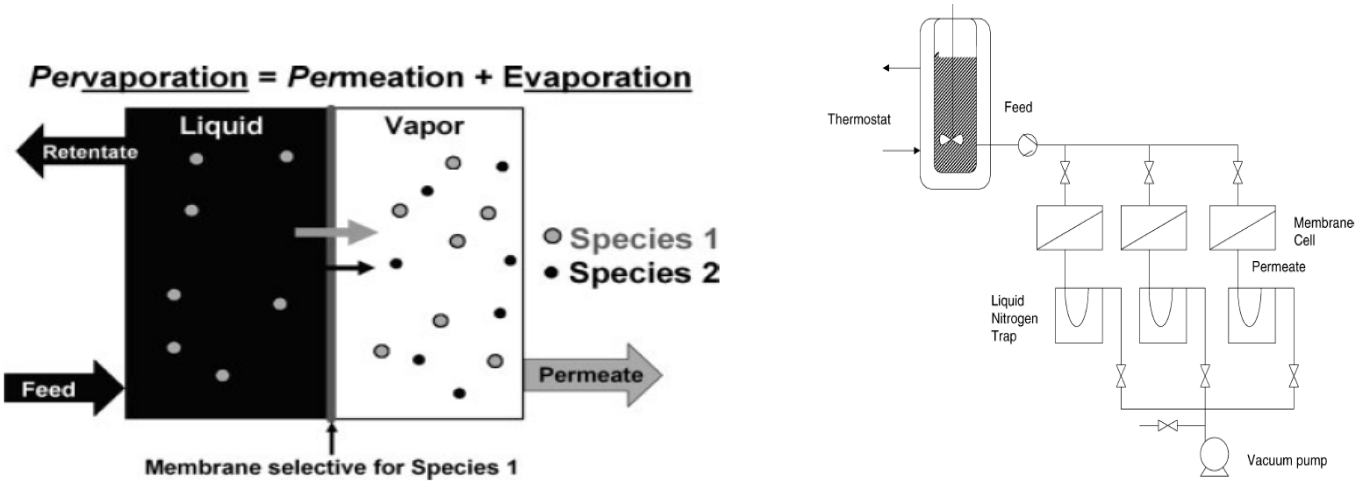


(a) (b)

*Figure 3.7: (a) Pervaporation process and (b) pervaporation apparatus.*

Pervaporation is typically suitable for the separation of a minor component present in the mixture and for this purpose a membrane with high selectivity is required. Pervaporation can be useful for breaking azeotropes, dehydration of solvents and other organics, organic /

organic separation such as ethanol or methanol removal; and waste water purification. Characteristics of pervaporation include:

- Low energy consumption
- No entrainer required, no contamination
- Permeate must be volatile at operating conditions
- Functions independent of vapour / liquid equilibrium

*3.1.1 Diffusion through polymeric membranes.*

Liquid transport in pervaporation is described by various solution-diffusion models; one is known as the *solution-diffusion theory* and the other is known as *modified solution-diffusion theory*. The later one also takes into account the behaviour of polymer swelling due to mixture of components used. The steps included are the (i) sorption of permeate at the interface of the solution feed onto the membrane, (ii) diffusion across the membrane due to concentration gradients (rate determining steps), and (iii) finally desorption into a vapour phase on the permeate side of the membranes. The first two steps are mainly responsible for permselectivity. As the permeate passes through the membrane it makes the membrane more permeable (because of swelling effects) with the passage of time and due to this the membrane becomes less selective. The other driving force for separation is the difference in partial pressures across the membrane and it can be created by reducing the pressure on the permeate side of the membrane which is usually done by application of vacuum on this side.

*3.1.2 Permeability, flux and selectivity*

For the permeation of permeante gases through the membranes, the permeability co-efficient (P) is usually estimated from the gas flux and the driving force gradient for mass transfer.

$$P = \frac{Flux}{Driving\ force\ gradient} = \frac{Flux}{\Delta p / \delta} \qquad \text{Eq. 3.13}$$

Also according to the solution-diffusion model, the permeability co-efficient is a product of diffusion and solubility co-efficient.

*Permeability = Diffusion * Solubility* Eq 3.14

Many units are found in the literature for reporting the permeability coefficients, however the most unit certainly remains the Barrers {$10^{-10}$ $cm^3$ (STP) cm/ ($cm^2$ s cm Hg)} when gases are the feed and permeate.

Permeation of liquid or vapours through the polymeric membranes usually involves much higher sorption coefficient than for permeante gases and that in turn leads to much more complex system for which plasticizing effects generally occur. For these particular systems the permeability co-efficient is no more a characteristics for the penetrant-polymer system because it varies strongly with different parameters such as penetrant concentration in the feed solution. Therefore in all such cases, it is common practice to characterize mass transfer by the permeation flux defined as; *the amount of a component permeated per unit area per unit time for a given membrane.*

$$\text{Flux} = \frac{amount\ of\ \ permeant}{(membrane\ area)(time)} = \frac{Kg}{h * m^2} \qquad \text{Eq. 3.15}$$

But as we know that the permeation flux is dependent on the membrane thickness and the relation is inverse to the thickness of film, therefore to allow a comparasion of the properties of membranes film with close but not constant thickness, a normalized flux can be calculated for a reference thickness of the dense film and such calculations are termed as thickness corrected flux.

$$\text{Flux} = \frac{(amount\ of\ \ permeant)\ (film\ thickness)}{(membranes\ area)\ (time)} = \frac{Kg * \mu m}{h * m^2} \qquad \text{Eq. 3.16}$$

To characterize the permeation of binary feed mixtures, the total flux is calculated as for the permeation of pure species. Mass transfer through the polymeric membrane is usually selective, and that means that the composition of the permeated mixture usually is different from that of feed mixture. Therefore, the normalized partial permeation fluxes are also

estimated from the composition of the permeated mixture according to the following equation 3.17.

$$J_i \text{ (Flux)} = \frac{(amount\ of\ species, i)(film\ thickness)}{(membranes\ area)\,(time)} = C_i J \qquad \text{Eq. 3.17}$$

Where Ci is the mass fraction of species (i) in the permeate mixture [15, 16].

In our case, we used the equations (3.16 and 3.17) but with little change or modifications relevant to time and membrane thickness as can be seen in the following equation 3.18.

$$\text{Flux} = \frac{(amount\ of\ permeant)(film\ thickness)}{(membranes\ area)(time)} = \frac{Kg * m}{\sec * m^2} \qquad \text{Eq. 3.18}$$

Where

*Kg = the weight of permeante*

*m = membrane thickness*

*Sec = the time of permeation*

*$m^2$ = the effective membrane area used during pervaporation process*

When characterizing membranes for pervaporation a commonly used parameter is the separation factor [17], which can be estimated according to equation 3.19.

$$Water/Alcohol\ Separation\ Factor = \frac{C_F/(1-C_F)}{C_P/(1-C_P)} \qquad \text{Eq. 3.19}$$

where $C_F$ and $C_P$ are the wt % fractions of alcohol in the feed and permeate, respectively.

When characterizing membranes for gases and vapours the selectivity is defined by the ratio between the permeabilities of two permeant molecules [18], according to equation 3.20:

$$Water/Alcohol\ Selectivity = P_{water}/P_{alcohol} \qquad \text{Eq. 3.20}$$

In our case the selectivity was calculated according to equation 3.20, which is more helpful to understand the processes taking place in the fuel cell experiments.

### 3.2 References


[1] K.D. Kreuner, W.Weppner, Angew. Chem. Int. Ed. Engl. 21 (1982) No. 3

[2] Kaus-Dieter Kreuer, Transport in proton conductors for fuel cell applications: Simulations, Elementary Reactions, and Phenomenology; Chemical review 2004, 104, 4637 – 4678.

[3] S. J. Paddison, Defect structure for proton transport in a triflic acid monohydrate solid, Chemical Physics Letter 368, (2003) 108 – 114.

[4] W.H.J. Hogarth, Solid acid membranes for high temperature (> 140 °C) proton exchange membrane fuel cells, Journal of Power Sources 142 (2005) 223 – 237.

[5] K.D. Kreuer, On the development of proton conducting polymer membranes for hydrogen and methanol fuel cells, Journal of Membrane Science 185 (2001) 29 – 39.

[6] A.F. Ismail et al Physico-chemical study of sulfonated poly (ether ether keton) membranes for DMFC applications, Malaysian Polymer Journal (MPJ), Vol.2, p 10 – 28 (2007).

[7] G.Gebel, O. Diat; Neutron & X-Ray scattering: Suitable tools for studying ionomers membranes, Fuel cell 5, 267 – 276 (2005).

[8] J.C.Perrin; Water dynamics in Ionomers membranes by field-cycling NMR relaxometry, Fuel Cell 6, 5 – 9 (2006).

[9] A.Z. Weber; Modelling transport in polymer-electrolyte fuel cell, Chemical reviews 104, 4679 – 4726 (2004).

[10] Robertson G.P et al, Casting solvent interaction during with sulfonated poly (etheretherketon) during proton exchange membrane fabrication; Journal of Membrane Science 219, 113 – 121 (2003).

[11] Y.S.Kim et al, Effect of acidification treatment and morphological stability of sulfonated poly (arylene ether sulfon) copolymer proton exchange membranes for fuel

cell use above 100 °C; Journal of Polymer Science Part B-polymer physics 41, 2816 – 2828 (2003).

[12] Basic of electro-chemical impedance spectroscopy; ApplicationNote, Gamry Instruments (www.gamry.com).

[13] Impedance spectroscopy, theory, experiment and applications; 2nd Edition E.Barsoukov and J.R. Macdonald

[14] Leland M vane, A review of pervaporation for product recovery from bio-mass fermentation process; J. Chem Technol biotechnol 80 : 603 – 629 (2005)

[15] A. Jonquieres et al, Permeability of block copolymers to vapours and liquids; Prog. Polym. Sci. 27 (2002) 1803 – 1877.

[16] P.Shao et al, Polymeric membrane pervaporation, Journal of membrane Scince 287 (2007) 162 – 179.

[17] H. E. A. Brüschke, State-of-art of pervaporation processes in the chemical industry (Part II, Chapter 3). In S. P. Nunes and K. V. Peinemann, editors, "Membrane Technology in the Chemical Industry", Wiley-VCH, Weinheim, Germany, 2001, 2nd edition 2006.

[18] S. P. Nunes and K. V. Peinemann, Membrane Materials and Membrane Preparations (Part I). In S. P. Nunes and K. V. Peinemann, editors, "Membrane Technology in the Chemical Industry", Wiley-VCH, Weinheim, Germany, 2001, 2nd edition 2006.

### 3.3 Electro-oxidation of fuel during fuel cell performance.

*3.3.1 Electro-oxidation of Hydrogen during fuel cell performance*

In PEMFC for the electro-oxidation of pure hydrogen gas, usually platinum based catalysts are used as anodic materials. The process of the electro-oxidation of hydrogen at the anode is not a simple one or single step reaction but it includes many steps like the following.

$$H_2 + Pt \longrightarrow Pt - H_2$$

$$Pt - H_2 \longrightarrow Pt - H_{ads}$$

$$Pt - H_{ads} \longrightarrow Pt + H^+ + e^-$$

The oxidation reaction of hydrogen on platinum electrode has a lower oxidation potential and a higher kinetic rate. The apparent exchange current density of hydrogen oxidation reaction (HOR) has been calculated to be ($i^o_{anode}$ = 0.1 A $cm^{-2}$) which is extremely high when compared with the oxygen reduction reaction (ORR) ($i^o_{cathode}$ = 6 μ A $cm^{-2}$) according to charge transfer of the cathode and anode obtained from EIS measurement done by Wager et al [1]. This proves extremely fast reaction kinetics of HOR. The following table 3.2 shows the exchange current density of hydrogen evolution reactions at different electrode materials in 1M $H_2SO_4$ solution at ambient temperature.

*Table 3.2: Exchange current density of hydrogen evolution reaction at different electrodes materials.*

| Metal | $i^0$ / $Acm^{-2}$ |
|---|---|
| Palladium, Pd | $1.0 \times 10^{-3}$ |
| Platinum, Pt | $8.0 \times 10^{-4}$ |
| Rhodium, Rh | $2.5 \times 10^{-4}$ |
| Iridium, Ir | $2.0 \times 10^{-4}$ |
| Nickel, Ni | $7.0 \times 10^{-6}$ |
| Gold, Au | $4.0 \times 10^{-6}$ |
| Tungsten, W | $1.3 \times 10^{-6}$ |
| Niobium, Nb | $1.5 \times 10^{-7}$ |
| Titanium, Ti | $7.0 \times 10^{-8}$ |
| Cadmium, Cd | $1.5 \times 10^{-11}$ |
| Manganese, Mn | $1.3 \times 10^{-11}$ |
| Thallium, Tl | $1.0 \times 10^{-11}$ |
| Lead, Pb | $1.0 \times 10^{-12}$ |
| Mercury, Hg | $0.5 \times 10^{-13}$ |

*3.3.2 Electro-oxidation of methanol fuel during (DMFC)test*

In recent years, direct alcohols fuel cells (DAFC) have attracted much more attention because of many advantages of the liquid fuel instead of pure hydrogen gas. These advantages are easy handling, safe storage, no need for reforming and favourable power capability for use in portable devices. Methanol is one of those simple structures of alcohols that are still extensively studied in DMFC technology. The over all oxidation reaction of methanol on platinum catalyst as anodic material involves the removal of six electrons which can be presented as:

$$CH_3OH + H_2O \longrightarrow CO_2 + 6\,H^+ + 6e^-$$

That corresponds to the anodic potential ($E_a^o$ = 0.016 V) under STP versus SHE, resulting in the equilibrium standard electromotive force of 1.213 V for a DMFC [1]. The over all reaction can summarized as:

$$CH_3OH + 1.5\,O_2 \longrightarrow CO_2 + 2H_2O$$

As mentioned before, platinum (Pt) is a best catalyst for oxidation of pure hydrogen and therefore attentions were diverted to wards the electro-oxidation of methanol molecule using the same platinum as anodic material in fuel cell. The researches were carried out both in acidic as well as alkaline media. The oxidation of methanol is not a simple or one step process but even more complicated than the pure hydrogen oxidation reaction. It is reported that the dissociative adsorption of methanol on Pt-catalyst occurs through the formation of irreversible adsorbed CO species on the catalyst surface and thus making the catalyst inactive because of its poisoning property. CO bonding on the surface of catalyst may be linearly bonded or bridged but linearly bonding of CO can cover upto 90 % surface area of the catalyst so that most of active areas are blocked. Basically the oxidation of methanol to CO includes six electrons; therefore the reaction process involves several steps with formation of many intermediates products. Analysis from mass spectral measurement, high performance liquid chromatography (HPLC) and gas chromatography have shown that intermediates like H&O,

HCOOH, HCOOCH, and $CO_z$ were all produced during the oxidation of methanol on Pt catalyst in acidic media. These species were then eventually converted to CO. In addition to this some other intermediates such as $(CHO)_{ads,}$ or $(COOH)_{ads}$, were also identified by FTIR spectroscopy. The detailed mechanism of the electro-oxidation of methanol on Pt-catalyst can be observed in the following figure 3.8.

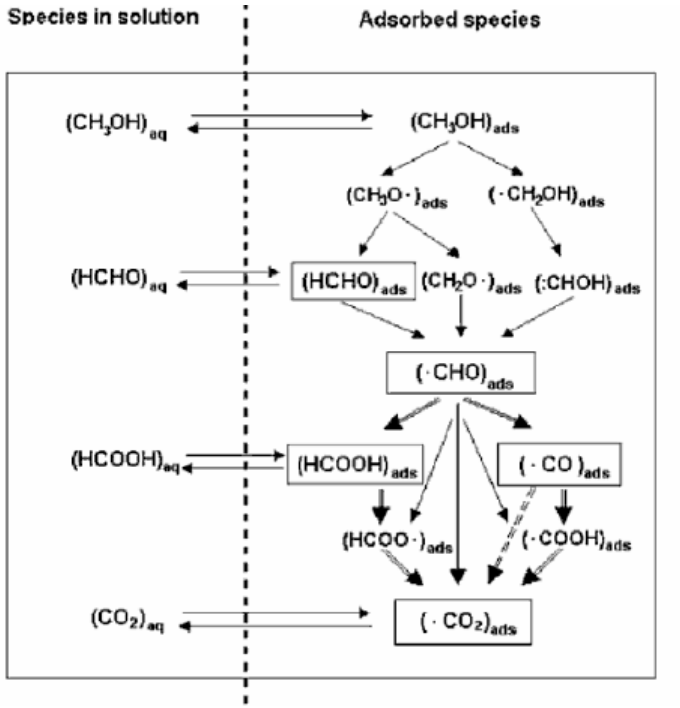


*Figure 3.8: Electro-oxidation mechanism of methanol on Pt-catalyst [1].*

As can be seen that in this mechanism the adsorbed species (CHO) play an important role; further intermediates may be $(CO)_{ads}$ or $(HCOOH)_{ads}$ . Therefore it is necessary to develop such an efficient electrocatalysts that lead to the formation of this adsorbed species and subsequently avoid the formation of CO. To avoid CO poisoning; an alloy of Ru-Pt catalysts are presently the most effective electrocatalysts for oxidation of methanol. It is believed that Ru acts to remove the $(CO)_{ads}$ from system in the form of $CO_2$.

$$Ru\text{-}OH + Pt\text{-}CO \longrightarrow Ru + Pt + CO_2 + H^+ + e^-$$

This role of ruthenium can be a combination of two effects; (a) a bifunctional mechanism in which a partially oxidized Ru surface supplies the oxygenated species necessary for complete oxidation of CO to $CO_2$ and (b) the ligand effect, in which the presence of ruthenium atoms close to platinum changes the electronic structure of platinum surface making the Pt-CO bond more weaker [1 – 3, 13].

*3.3.3 Electro-oxidation of ethanol fuel (DEFC)*

Direct ethanol fuel cell (DEFC) draws much more attention of the researcher groups all over the world because of its non toxic nature and high theoretical energy density of (8 kW h $Kg^{-1}$) to that of methanol (6 kW k $Kg^{-1}$). From the literature survey it is evident that much more work is focused on the development of different kind of catalysts for the complete oxidation of ethanol (Breaking of C-C Bond in addition with C-H and O-H bonds) without producing acetic acid, acetaldehyde etc. with the removal of all 12 electrons [4 -13]. A simple schematic of DEFC can be seen in figure 3.9.

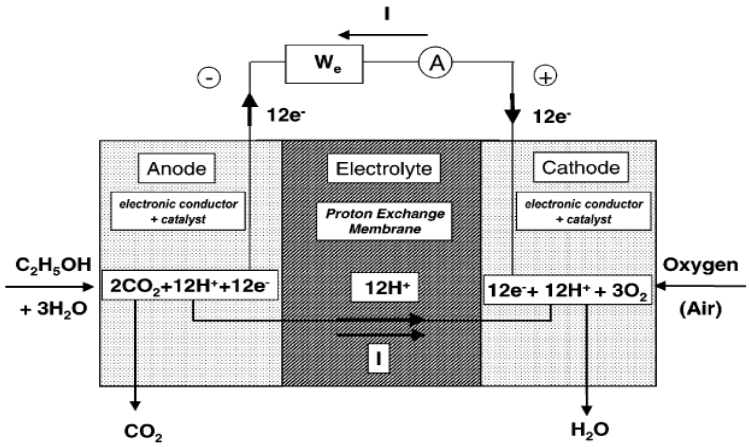


*Figure 3.9: Simple schematic of DEFC.*

The anodic, cathodic and over-all reactions of DEFC can be presented as follows:

Anodic reaction:

$$CH_3CH_2OH + 3H_2O \longrightarrow 2CO_2 + 12\,H^+ + 12\,e^-$$

Cathodic Reaction:

$$3O_2 + 12\,H^+ + 12\,e^- \longrightarrow 6\,H_2O$$

Over-all reaction:

$$CH_3CH_2OH + 3O_2 \longrightarrow 2CO_2 + 3H_2O$$

The corresponding anodic and cathodic potentials and equilibrium standard electromotive force calculated according to [1] at STP against SHE could be ($E_a^o$=0.084 V) and ($E_a^o$=1.229 V) and 1.145 V respectively.

But the electro-oxidation of ethanol is not a simple reaction because the (C – C) bond requires rather higher activation energy. On the Pt anode the electro-oxidation of ethanol is very slow and sluggish at low temperature. Despite of significant studies and works, the mechanism of electro-oxidation of ethanol is still not clear. A lot of works have been done to identify the adsorbed intermediate on the surface of anode catalysts by analysing the reaction species by different techniques such as FTIR, mass spectrometry and electrochemical thermal desorption mass spectrometry. The reaction species identified so far include $CO_2$, acetaldehyde and acetic acid but the identification of methane and ethane is also reported. Like methanol electro-oxidation, the surface-adsorbed CO is still the main leading intermediate during the electro-oxidation of ethanol but with more intermediates and by-products. Other surface intermediates include various $C_1$ and $C_2$ compounds like ethoxy and acetyl [4, 10, and 13]. The net conclusion is that the electro-oxidation of ethanol proceeds through a complex multi-steps mechanism involving a number of adsorbed intermediates and also leads to different by-products for incomplete electro-oxidation of ethanol and that in turn leads to a decrease in fuel cell efficiency in DEFC test.

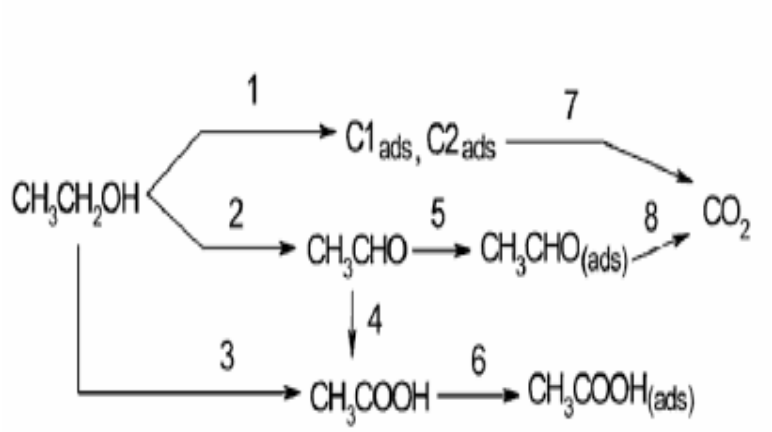


*Figure 3.10: Probable reaction mechanism of electro-oxidation of ethanol [1].*

The presence of both poisoning and intermediate species requires the development of new electrocatalysts for the complete oxidation of ethanol (breaking C – C bonds) to $CO_2$. Platinum or Pt-Ru alloy catalysts are not that much active for ethanol as compared to methanol. Therefore other metals like tin, nickel, gold, rhodium and palladium have been investigated for the electro-oxidation of ethanol. Nice results were reported with an alloy of Pt-Sn-Ni as anodic catalyst [7].

### *3.3.4 Oxygen reduction reaction (ORR)*

No matter what kind of fuel is to be used in fuel cell, the oxidant is the Oxygen either in pure form or in the form of synthetic air. A lot of research is still carrying out on this topic because oxidation is a slow process. Major voltage loss due to high reduction over potential during the performance of PEMFC is one of the major problems that also affect the energy conversion efficiency of a fuel cell. Usually the ORR process on Pt cathode catalyst happens through several individual processes as shown in the figure 3.11. The most examined ones are the TWO processes, with each process containing a few discrete steps. The desired one for a successful ORR catalyst aims the reduction of $O_2$ completely into $H_2O$ via a four-electron

pathway reaction. The other one proceeds through incomplete reduction of $O_2$; first to hydrogen peroxide ($H_2O_2$) and then to water. This leads to a low energy conversion efficiency as well as to the production of some harmful intermediate radical species.

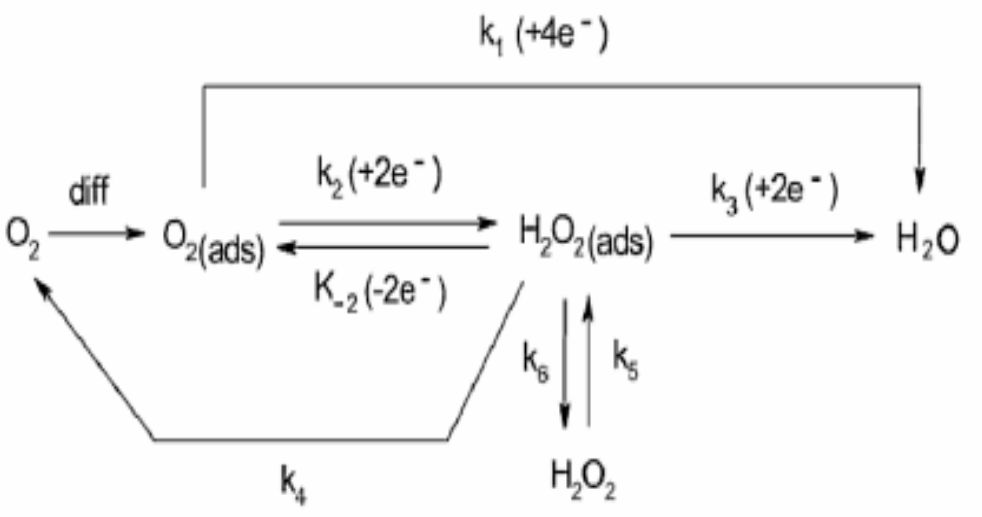


*Figure 3.11: ORR on platinum catalyst [1].*

Apart from platinum, noble metal electrodes, non-noble metal electrodes and organometallic complexes have been studies for the better performace during ORR in fuel cell.

### 3.4 FTIR-ATR Spectroscopy:

This technique provides an important tool for investigating chemical processes and structures. Traditionally attenuated total reflectance (ATR) has extended the applicability of infra-red spectroscopy to those samples that neither reflective nor enough thin for the transmittance examination. They are suitable for studying thick or highly absorbing solid and liquid samples. ATR requires little or no sample preparation for most of the samples and therefore is the most versatile sampling technique.

**Atomic Force Microscopy (AFM):**

The AFM works in the same way as our fingers which ***touch and probe*** the environment when we can not see it. By using a finger to visualize an object and at the same time our brain is able to deduce its shape (topography) while touching it. The resolution by this method is determined by the radius of fingertips and therefore to achieve atomic scale resolution, *a sharp stylus (radius 1- 2 nm)* attached to cantilever is used in this method to scan an object point by point and contouring it while a constant small force is applied to the stylus. With the AFM, the role of brain is taken by a computer while scanning the stylus is accomplished by a piezoelectric tube. In addition to basic AFM, the instrument is capable of producing images in a number of other modes like tapping, magnetic force, electric force and pulsed force.

1. In tapping mode AFM, the tip is oscillated above the sample surface and the data may be collected from the interaction with surface topography, stiffness and adhesion. This result in an expanded number of image contrast methods compared to basic AFM.
2. In magnetic force mode AFM, a magnetic tip is used to enable the visualization of magnetic domains on the sample under study.
3. In electric force mode AFM, a charged tip is used to locate and record variations in the surface charge.
4. In pulsed force mode AFM, the sample is oscillated beneath the tip, and a series of pseudo force-distance curves are generated. This permits the separation of sample topography, stiffness and adhesion values producing three independents images simultaneously.

**3.5 Scanning Electron Microscopy (SEM):**

SEM is a microscope that uses electrons rather than light to form an image. This technique provides topographical and elemental informations at magnification of 10 x to 100,000 x with virtually unlimited depth of fields. In this method a narrow beam of electrons varying in

intensity upto 30 KeV and under high vacuum ($10^{-6}$ Torr) is scanned over the sample surface and in turn that causes the secondary electrons liberation from the atoms of the target sample. These liberated electrons, collected by a detector, provide high resolution images of the morphology of the sample at high or at low magnification. After the bombardment of the electronic beam on the surface of a sample, the following various kinds of radiations are emitted:

- The secondary electrons (SE) give pure image of the surface topography of the sample under study.

- The back scattered electrons (BSE) provides an image that describes the composition of the target samples. Like spatial distribution of elements or compounds within the top micron of the sample. Features as small as 10 nm are resolved and composition variation of as little as 0.2 % can be determined.

- Characteristic X-rays that helps in understanding the chemical composition of the samples.

### *3.7 Thermal properties:*

***3.7.1Dynamic mechanical thermal analysis (DMTA)*:** This technique is usually used to determine the deformation of a sample (dynamic stress-strain behaviour) or (changes in length or thickness) as a function of temperature. The measuring range may be extending from -150 °C to 600 °C. The force (Stress) is applied sinusoidaly with a defined frequency by the motor to the sample and then the response (Strain) is monitored by the actuator. The magnitude of the applied stress and the resultant strain is used to calculate the stiffness of the sample. A storage modulus (E`) is a measure of the energy stored during the cycle and loss modulus

(E``) is a measure of the energy loss. The quantity (tanδ) is the ratio of E`` to E`. Results are usually provided as the graphical plots of E`, E`` & (tanδ) versus temperature. Many types of materials properties that can be measured by this technique include damping, modulus, glass transition and etc.

***3.7.2 Differential scanning calorimetry (DSC):*** This technique is used to detect the difference in heat flow between a sample and a reference crucible that are simultaneously exposed to the same temperature-time protocol during heating and cooling. When a sample undergoes a physical transformation such as phase transition, more or less heat will need to flow to sample than reference in order to maintain both at the same temperature. Whether more or less heat will flow to the sample usually depends on the type of process whether it is endothermic (melting of sample) or exothermic (crystallization of sample). Thus by observing the difference in heat flow between the sample and reference, the differential scanning calorimeters are able to measure the amount of heat absorbed or released during such transitions. Glass transition temperature Tg, crystallization time and temperature, degree of crystallinity and also some more properties can be determined by this technique.

***3.7.3 Thermogravimetric analyses (TGA)*:** This method is used to determine the changes in mass of a sample in relation to changes in temperature (material thermal stability). The changes in mass of sample may be due to evaporation of residual solvent or decomposition. Only mass changes can be observed at different temperatures but no glass transition temperature (Tg) can be determined by this technique. By this technique the material properties that can be determined include compositional analysis, degradation, life time, oxidative stability and many more.

### 3.8 References


[1] PEM Fuel cell, Electrocatalysts and catalysts layers, Fundamentals and applications by Jiujun Zhang (Editor).

[2] H.Wang et al, Progress in preparation of non-noble electrocatalysts for PEM fuel cell reactions, Journal of Power Sources 156 (2006) 171 – 182.

[3] A. Hamnett, Mechanism and electro catalysis in the direct methanol fuel cell; Catalysts Today 38 (1997) 445 – 457.

[4] S.Rousseau , C. Countanceau, C. Lamy , J.-M Leger, Direct ethanol fuel cell (DEFC): performances and reaction products distribution under operating condition with different platinum based anodes *J. Power Sources* 158 (2006) 18–24.

[5] C.B Baretto, R.L.T Parreira, R.R Goncalves, D.C Azevedo, F.Huguenin; Platinum nanoparticles embedded in layer-bi-lyaer films from SnO2/polyallylamine for ethanol oxidation *J. Power Sources* 185 (2008) 6–12.

[6] C. Xu, H. Wang, P.K.Shen, S.P Jiang; Highly orderd Pd nanowire arrays as effective electro catalysts for ethanol oxidation in direct alcohol fuel cell. Adv. Mater. 2007, 19, 4256 – 4259.

[7] E.Ribadeneira, B.A.Hoyos; Evaluation of Pt-Ru-N and Pt-Sn-Ni catalysts as anode in direct ethanol fuel cells J.Power.Sources 180 (2008) 238 – 242.

[8] X.Xue, J.Ge, T.Tian, C, Liu, W. Xiang, T.Lu ; Enhancement of electro-oxidation of ethanol on Pt-Sn-P/C catalyst prepared by chemical deposition process, J. Power sources 172 (2007) 560–569.

[9] Q.Wang, G.Q Sun, L. Cao, L.H. Jiang, G.X. Wang, S.L. Wang, S.H. Yang, Q.Xin ; High performance direct ethanol fuel cell with double-layered anode catalysts layer, *J.Power Sources 17*7 (2008) 142–147

[10] F. Colmati, E.Antolini, E.R. Gonzalez; Effect of temperature on the mechanism of ethanol oxidation on carbon supported Pt, Pt-Ru and $Pt_3Sn$ electrocatalysts, *J. Power Sources* 157 (2006) 98–103.

[11] E.Antolini; Catalysts for dierect ethanol fuel cells; J.Power Sources 170 (2007) 1–12.

[12] A. Ghumman, C. Vink, O. Yepez, P.G. Pickup; Continuous monitoring of CO2 yields from electrochemical oxidation of ethanol: Catalyts, Current density and temperature effects. J.Power Sources 177 (2008) 71–76.

[13] C. Lamy et al, Recent advances in the development of direct alcohol fuel cells (DAFC), Journal of Power Sources, 105 (2002) 283 – 296.

# Chapter 4.

**Preparation and Characterization of Bilayer Carbon Molecular Sieve (CMS)/SPEEK-Polymer Membranes; CMS as fuel barrier in DMFC and as a catalyst support.**

## 4.1 Introduction

Membrane technology has been used for alcohol/water separation at least since the early 80's when the first industrial scale pervaporation plants were installed [1]. For this task composite membranes with a dense selective layer based on hydrophilic (for water removal) or organophilic (for removal of alcohol or other organic chemicals) polymers are used. Such membranes are able to separate via a solution-diffusion mechanism. Inorganic membranes based on zeolites or amorphous silica coatings on an inorganic porous substrate have been also used in large scale for pervaporation. In this case molecular sieving effects determine the separation, eventually in combination with preferential sorption and surface diffusion in the pores.

Over the last decade the importance of membrane technology in the energy sector has substantially increased. A reason for this is the need for new clean alternative energy conversion techniques. Fuel cell technology based on membranes is a very attractive energy conversion system. For portable applications the use of direct alcohol fuel cells (DAFC) is seen as a good option with the fuel delivery infrastructure being much more established than for hydrogen. The main drawback of the DAFC technology currently lies in the available materials. Our group has been investigating materials for DAFC for many years, recently coordinating the development of a 500 W prototype for portable application in the framework of the European project MOREPOWER. As far as the membrane is concerned, besides proton conductivity, alcohol transport is the most important issue. Alcohol crossover should be as low as possible. The water balance in the membrane is also relevant. Most of the currently

available membranes for DAFC are based on sulfonated polymers where proton transport is highly dependent on the water content in the membrane, which helps the protons to diffuse through the membrane by a vehicle mechanism (formation of the $H_3O^+$ or $CH_3OH_2^+$ ions diffusing through the bulk of the proton exchange polymer). Therefore the presence of dissolved water in membranes up to a certain extent improves proton conductivity. Another important issue is the availability of effective catalysts, with high levels of alcohol tolerance, for alcohol conversion to protons and $CO_2$ at the anode and for oxygen reduction at the cathode. These aspects are of course related. For an ideal membrane, which could completely hinder the alcohol transport to the cathode, the requirement for alcohol tolerance cathode catalysts would diminish. At the cathode water is produced by the reaction between oxygen and the protons crossing the membrane. As soon as water is produced, it should leave the catalyst surface, thus avoiding flooding and making the surface free for further reaction. Good catalyst dispersion is essential in any case to ensure a high surface area, thus enhancing the catalytic activity and leading to effective reaction kinetics even with low catalyst levels.

The development of new membranes and catalysts for DAFC is being addressed worldwide by a large number of groups. A recent review of membranes for direct methanol fuel cell (DMFC) has been published by Deluca and Elabd [2]. In previous work the main approach chosen by our group to reduce methanol crossover in polymeric membranes has been the development of different forms of nanocomposites [3-7] using functionalized layered silicates, silica and polysilsesquioxanes, zirconium oxides and phosphates as fillers.

As far as the catalyst is concerned, the development of different Pt alloys and non noble catalysts is under investigation, the aim being high efficiency at reduced cost. The use of carbon supports for catalysts is a well described strategy [8-11]. Carbon black and activated carbon are generally chosen as support for the catalyst nanoparticles due to their high

electrical conductivity, chemical stability and low cost. Recent developments using other types of nanostructured carbon materials such as carbon nanotubes (CNTs) [12-17], carbon nanofibers (CNFs) [13] and ordered mesoporous carbon (OMC) [11] have been reported. The dispersion of catalysts on CNTs has recently been reported with the aim of incorporation into fuel cell membrane-electrode-assemblies [12-17]. CNTs with catalysts have been incorporated into carbon paper or cloth, by dispersion, by growing the CNTs directly on the paper, or alternatively by filtration of a CNT dispersion onto a commercial membrane and subsequent hot pressing with a carbon backing layer. In a recent paper we describe membrane electrode assemblies that were prepared with aligned CNT arrays coated with catalyst and incorporated into sulfonated poly (ether ether ketone) (SPEEK) membranes [18].

A review of ordered mesoporous carbon (OMC) for fuel cells has recently been published [11]. OMC is prepared using templates, which lead to the formation of regular arrays of mesopores. For instance a template could be mesoporous silica, which has been infiltrated by different organic monomers that act as a carbon source. Pyrolysis and later treatment with fluoridric acid lead to the final porous carbon structure.

In this chapter we propose a new multilayer membrane-electrode assembly constituted by a polymer electrolyte membrane and a continuous carbon molecular sieve (CMS) layer. A scheme outlining the proposed system is shown in Figure 4.1. The carbon molecular sieve is prepared by pyrolysis of polymer films, analogous to procedures described in the literature for preparation of CMS membranes [19]. This is much simpler than OMC preparation. The catalyst is introduced during the CMS preparation procedure. The thin CMS layer functions both as a catalyst support and as a barrier for alcohol transport. With this method thin membrane-electrode-assemblies could be prepared for DAFC.

CMSs were initially used for chromatography [20], but in the early 70's they were already being used as supports for catalysts [21-23]. At that time the applications such as propylene hydrogenation were envisaged. Koresh and Soffer [24, 25] were the first to prepare CMS membranes that were tested for gas separation. Since then CMS membranes have been investigated by other membrane groups [26-39], mainly for gas separation. Hidetoshi et al. [39] reported the separation of benzene/cyclohexane and benzene/n-hexane mixtures by pervaporation using CMS membranes. Peng et al. [40] used silicone membranes filled with CMS for the removal of benzene from aqueous solutions by pervaporation. Most CMS membranes are currently prepared from polyimides [19, 26-33], but other polymers such as phenolic resins [38, 39], cellulose [34] and poly (phthalazinone ether sulfone ketone) are also used [37]. Barsema et al. [35] introduced Ag clusters in CMS membranes to improve $O_2/N_2$ separation.

Koros [19] and Wessling [44] investigated the effect of temperature on the formation of CMS membranes (dense or mixed-matrix for gas separation application. Due to brittleness of the CMS, the use of "stand alone carbon membranes" is mostly impossible. Thus researchers have made numerous attempts to prepare CMS membranes deposited onto rigid supports or to disperse CMS in the membrane polymer matrix to such extent that transport properties of the CMS start to prevail.

The aim of our current work was to prepare an extremely thin (and thus flexible) continuous layer of CMS deposited on a proton exchange polymeric membrane to results in a sandwich structure that is able to block fuel cross-over, to be a catalyst support for the anode part of the membrane-electrode assembly and to provide reasonable if not outstanding proton transport properties.

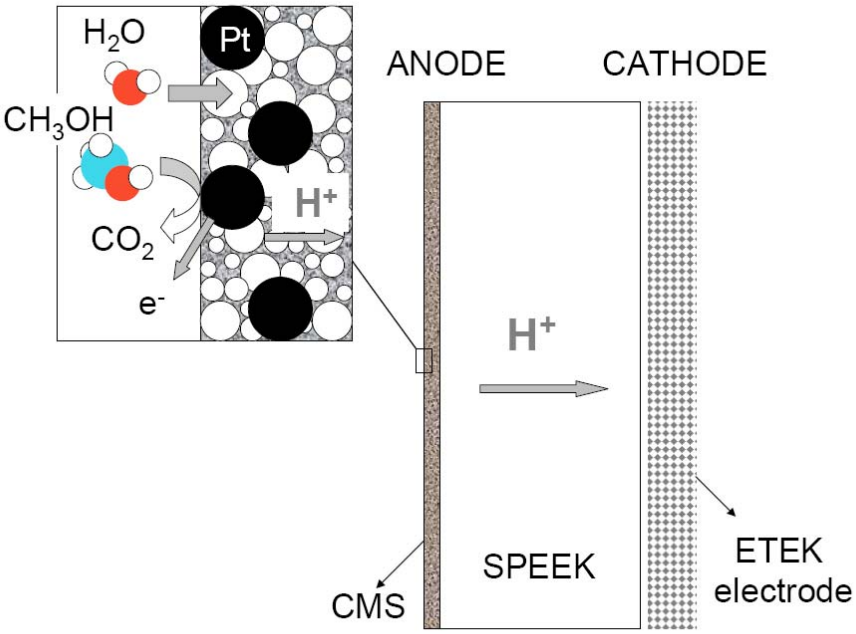


*Figure 4.1: Schemematic diagram showing the membrane electrode assembly for fuel cells based on a bilayer CMS/SPEEK membrane.*

## 4.2 Experimental Work:

### 4.2.1 Materials

The polyimide precursor used for synthesis of the carbon molecular sieve (CMS) in this research was Matrimid® 5218 (the polyimide condensation product of 3,3'4,4'-benzophenone tetracarboxylic dianhydride and diamino-phenylindane) bought from Ciba Geigy (Switzerland). Before dissolution in chloroform, the polymer was heated in an oven at 120 °C for 24 h to remove any residual water. Quartz plates were purchased from GE Quartz Europe GmbH and cut according to the size of the furnace tube used for the pyrolysis of the thin Matrimid® films. Poly (ether ether ketone) (PEEK), purchased from Victrex, was dried at 120$^{o}$C under vacuum and sulfonated according to the procedure described in ref. [3, 41]. Chloroform (99.0 – 99.4 %), dimethyl sulphoxide (DMSO) (99.9%), methanol (99.9%) and ethanol (99.9%) were purchased from Merck and used as received. N-Propanol (99.5%) and iso-propanol (99.5%) were received from Scharlau, n-butanol (99.5%) from Sigma-Aldrich, and dihydrogen hexachloroplatinate(IV) hexahydrate (99.9%) from Alfa Aesar. These were all used as received . Cathode material loaded with 100% Platinum black catalyst (4 mg/cm$^2$), anode material loaded with 60% of Pt:Ru (3mg/cm$^2$) both on Vulcan X-72 paper cloth and the diffusion layers (carbon cloth) were purchased from E-TEK (USA).

### 4.2.2 Preparation of Carbon Molecular Sieve (CMS) layer

The preparation of the CMS was performed based on the procedure published by Steel and Koros [19]. For the CMS, Matrimid® solutions of two different concentrations (1 and 2 wt %) were prepared using chloroform as a solvent. The solutions were stirred for about 3 to 4 h to ensure complete dissolution of the polyimide, filtered through a fine cotton filter and cast on quartz plates at room temperature. The solution was protected from dust contamination and allowed to evaporate for 12 h. Quartz plates with the thin defect-free polymer layer were treated under vacuum at 110$^{o}$C for at least 12 h to remove any residual solvent. A tubular

furnace (FRH-100/520/1250 Linn-High-Therm GmbH) with a 65 mm diameter quartz glass tube was used for the pyrolysis of the thin polyimide films cast on the quartz glass.

The procedure for pyrolysis followed the block-scheme below:

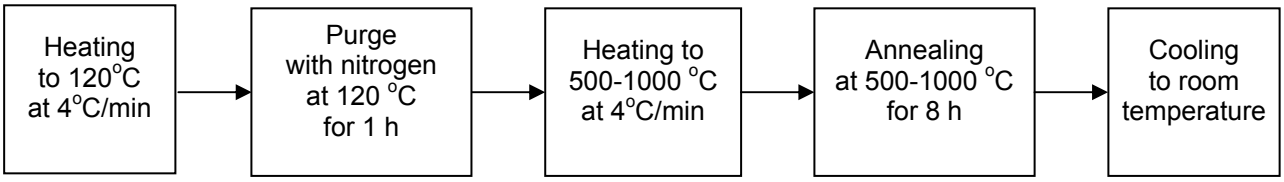


Thin polyimide films were pyrolyzed at different temperatures (500, 600, 700, 800, 900 and 1000 °C) in order to investigate the influence of the pyrolysis conditions on CMS properties. Nitrogen (99.99% purity) was used as an inert atmosphere for pyrolysis. The flow rate of the nitrogen was high in order to ensure the absence of oxygen in the oven after 60 minutes. According to calculations using the ideal mixing reactor model, the atmosphere in the oven was exchanged at least 20 times during 60 minutes, thus ensuring that only traces of oxygen were present in the pyrolysis zone. The flow of nitrogen was kept constant during the whole time of the experiment. Samples were annealed for 8 hours at the pyrolysis temperature, cooled down to room temperature, removed from the furnace and then the quality of the CMS coating was visually checked. Only uniform samples without visible cracks or colour density fluctuations were used for further experiments.

### 4.2.3 Preparation of bilayer membranes

Dried SPEEK (degree of sulfonation 56%) was dissolved in dimethyl sulphoxide leading to a 7 wt % solution. The solution was stirred for 24 hours at 80°C to ensure complete dissolution and uniform mixing.

CMS coated quartz plates were placed on a levelled table and coated with the 7 wt % SPEEK solution, the solvent was evaporated at 80 °C for about 24 h. The quartz plates were then placed into the vacuum oven at 110 °C for about 24 h to remove any residual solvent. After

this step, the bi-layered membranes obtained were easily removed from the quartz surface without damaging the CMS layer.

**4.2.4 FTIR-ATR Spectroscopy:** FTIR-ATR spectra were taken using an EQUINOX 55 (Bruker) FTIR spectrometer, equipped with attenuated total reflectance (ATR). Thin polyimide films and pyrolysed CMS were analysed at room temperature from 4000 to 550 $cm^{-1}$ under a $N_2$ gas environment. The number of scans taken was 128 with a spectral resolution of 2 $cm^{-1}$.

### 4.2.5 Morphology of the bilayer membrane

The morphology of the CMS layer before coating with SPEEK was studied by surface probe (atomic force) microscopy. For this a VEECO NANOSCOPE 4 Surface Probe Microscope was used and the image acquisition was done using the tapping mode.

The surface and cross-section morphology of the CMS coated SPEEK membrane was studied by scanning electron microscopy (SEM) using a LEO 1550 VP field emission microscope. Images were obtained with secondary electrons. Samples for the SEM study were prepared by fracturing the membrane in liquid nitrogen and sputtering under vacuum with a thin layer of Au/Pd prior to analysis.

The CMS layer containing Pt catalyst was also investigated by SEM, but using backscattered electrons to give selective contrast of the metal particles.

### 4.2.6 Pervaporation measurements

Pervaporation experiments were performed by using 5 wt % methanol solution in water at 55 $^{o}C$, a total pressure of 1 bar on the feed side and a vacuum ($10^{-2}$ mbar) on the permeate side. The effective membrane area (the area accessible for the feed mixture after the membrane is sealed in the measurement cell with Viton® O-ring) was 12.5 $cm^2$. The CMS side of the bilayer membrane always faced the feed side. After the establishment of a steady state, the

permeate was collected for 1 hour in cold traps immersed in liquid nitrogen. The compositions of feed and permeate were determined by gas chromatography using a Hewlett Packard 5890 chromatograph equipped with a SUPELCOWAXTM-10 capillary column (30m x 0.53 mm x 1.0 um film thickness) and using an oven temperature of 280$^{o}$C and flame ionization detector at 280$^{o}$C. Prior to the pervaporation experiments, the membranes were conditioned in the corresponding feed solutions over night.

The permeabilities (P) and selectivities were calculated according to equations 3.18 and 3.20 as discussed in chapter 3.

### 4.2.7 Impedance measurement

The proton conductivities for plain SPEEK and bilayer polymeric membranes were measured by impedance spectroscopy using a Zahner IM6 Spectrometer within a frequency range from 10 to $10^6$ Hz and an applied voltage of 5 mV. Before the measurement, the membranes were conditioned in de-ionised water for 24 hours at room temperature. Five pieces of membrane (with total thickness around 500 μm) were placed in-between the two diffusion layers (carbon cloth) in a two specimen system cell. Measurements were carried out at 100% relative humidity and at temperatures varying from 40°C to 100°C. The proton conductivity for plain SPEEK and CMS layer (180 nm 6 400 nm) coated were calculated according to the equation 3.12 discussed in chapter 3.

### 4.2.8 Membrane Electrode Assembly (MEA) preparation

The membrane electrode assemblies (MEA) for plain SPEEK and for bilayer CMS/SPEEK membranes (without Pt dispersed in the CMS layer) were prepared by hot pressing membranes between two E-TEK electrodes. The E-TEK cathode electrode was loaded with 100% pure platinum black catalyst (4 mg/cm$^2$), while the E-TEK anode electrode was loaded with an alloy of 60% Pt Ru (3mg/cm$^2$) on Vulcan XC-72 paper cloth.

Additionally MEAs were prepared with bilayer CMS/SPEEK membranes with Pt dispersed in the CMS layer. 0.2 g of $H_2PtCl_4$ was added to 100 ml of a 3 % Matrimid® solution in chloroform and stirred for one day. A 3 wt% Matrimid solution was used rather than the lower (1 or 2 wt %) concentrations used previously. This was because Matrimid® solution containing Pt gave rise to much thinner CMS layers than those prepared in the absence of Pt. The solution was cast onto quartz plates as described earlier and pyrolyzed at 800°C. After coating with SPEEK, the bilayer membrane was pressed with an E-TEK electrode on the cathode side (4 mg Pt/$cm^2$). The MEA without an additional gas diffusion layer on the anode side was then tested as described above. From the concentration of Pt salt in the polymer solution, the thickness of the polymer film and, later, CMS film it was estimated that 1.2 mg of Pt was distributed on the 1 $cm^2$ area of CMS layer.

### 4.2.9 Fuel cell test

The membrane performances were evaluated in a commercial DMFC test stand with an Electrochem.Inc (Comu Cell-DM) gas flow unit and a Scribner Associate (Model 1890B Fuel-Cell Test System) system controller.

The exact procedure for DMFC experiments is described elsewhere [5]. The MEA (25$cm^2$) was fed with 5% methanol solution in water (30mL/min, 1 bar) on the anode side and synthetic air (0.5L/min at 2 to 3 bar) on the cathode side. The operating temperature was 60°C. The $CO_2$ concentration at the cathode outlet was monitored by a $CO_2$ sensor (EasyLine IR, Advance Optima EM) in order to evaluate the methanol cross over, assuming that all the $CO_2$ resulted from methanol conversion at the cathode.

Additionally hydrogen fuel cell experiments were performed with bilayer membranes containing Pt in the CMS layer.

## 4.3. Results and Discussion

### 4.3.1 CMS preparation by pyrolysis

A number of papers have been published on the preparation and characterization of CMS membranes by pyrolysis of polyimides [19, 26-33, 44]. Matrimid®, a commercial polyimide, available in large quantities, was chosen as a precursor. There are many temperature treatment programs that have been reported to work in the presence of inert gases ($N_2$, Ar) or under vacuum. For practical reasons, the pyrolysis in this work was performed under a $N_2$ atmosphere. The pyrolysis temperature was varied from 500 to 1000$^oC$ to find the optimum conditions. The chemical structure of the resulting CMS was investigated by FTIR and the morphology was observed using atomic force microscopy.

Figure 4.2 shows the FTIR spectra of Matrimid® and the CMS membranes obtained after pyrolysis at 500 and 800$^oC$. The spectrum of Matrimid® has characteristic peaks at 2957-2869, 2363, 1786, 1712, 1679, 1514-1481, 1373, 1093, 820, 713 $cm^{-1}$, which agrees with reports from other work [45]. Taking this previous work into account, the peaks can be assigned to the C-H of methyl group stretch (2957- 2869 $cm^{-1}$), C=O (symmetric stretch) (1786 $cm^{-1}$), C=O (anti-symetric stretch) (1712 $cm^{-1}$), C=O (stretch of benzophenon carbonyl) (1679 $cm^{-1}$), C=C (aromatic stretching) (1514-1481 $cm^{-1}$), CNC (axial stretching) (1373 $cm^{-1}$), CNC (transverse stretching) (1093 $cm^{-1}$) and CNC (out of plain bending) (713 $cm^{-1}$). After pyrolysis at 500$^oC$, the same peaks were detected, but with small differences in relative intensity. Peaks related to C=O (e. g. 1679 $cm^{-1}$) were higher in the pyrolyzed polymer, while the CNC peak (713 $cm^{-1}$) characteristic of imide is higher in the pristine Matrimid®. The possibility of imide ring cleavage during pyrolysis at 425$^oC$ has been suggested [45]. When pyrolysis is performed at a temperature of 800$^oC$ or higher, the membrane is completely carbonized as confirmed by the IR spectrum. The major products evolved from the nonoxidative thermal degradation of aromatic polyimides are hydrocarbon, CO, $CO_2$ and $H_2O$ [46].

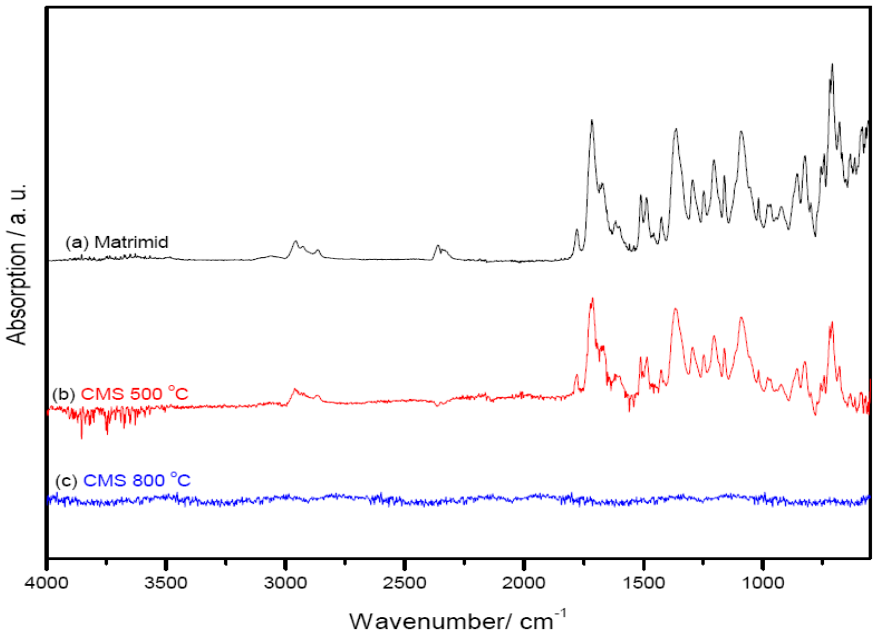


*Figure 4.2: FTIR Spectrum of Matrimid® 5218 film, (a) before, (b) after pyrolysis at 500 and (c) 800 ºC. For the comparison of pyrolyzed specimens spectra to that/those of the pristine Matrimid® the values for the line (b) were multiplied by a factor of 5 and for the line (c) by a factor of 10.*

### 4.3.2 Morphology of CMS layer and bilayer membranes

The morphology of the CMS layer was investigated by atomic force microscopy, using the tapping mode. Figure 4.3 a shows the topographic image, while Figure 4.3 b shows the image obtained using phase contrast. The images did not depend on which side of the membrane was investigated (i.e. exposed to the air or to the quartz plate during pyrolysis). This is an indication that the morphology is uniform without any differences of roughness or pore size across the membrane.

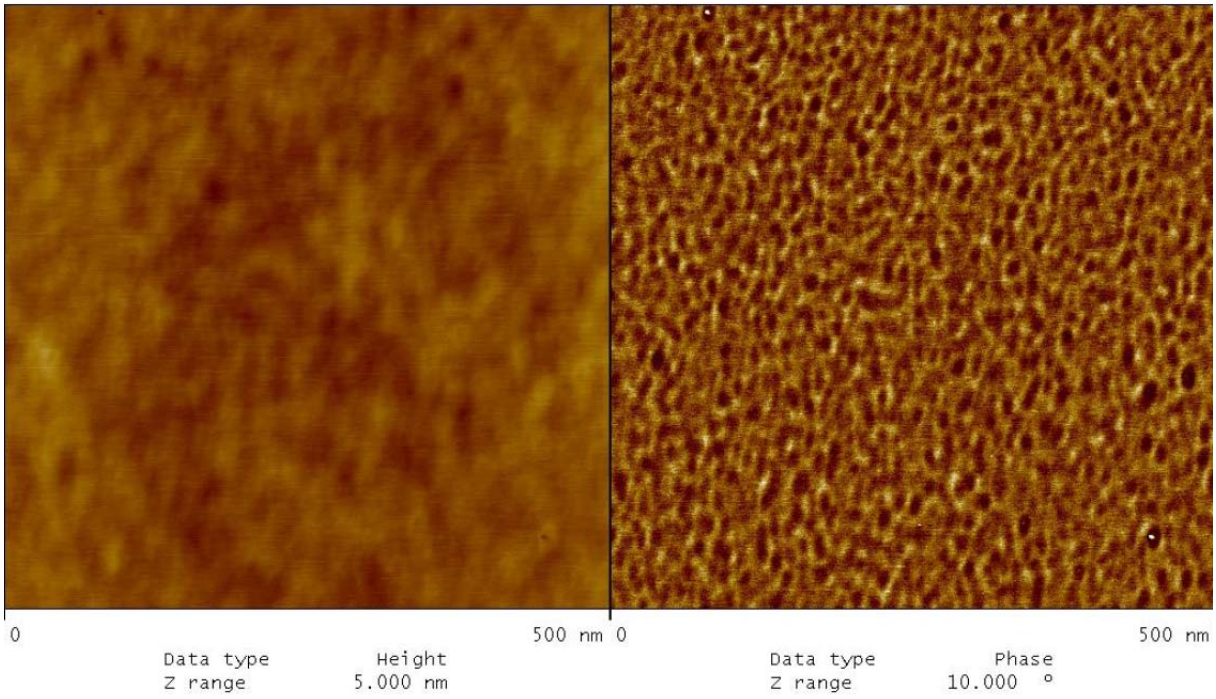


(a) (b)

*Figure 4.3: (a) Height and (b) phase contrast atomic force microscopy of the synthesized carbon molecular sieves prepared at 800 °C pyrolysis temperature.*

In order to better quantify the size distribution of the features observed in these images, a line was drawn from the top-left to the bottom right corner of each image. All protuberances crossed by the line were marked and the distances between them were plotted as a size distribution histogram (Figure 4.4). The histogram shows a monomodal distribution of the CMS material elements with most occurring at a size of 5-7 nm. These elements are an order of magnitude larger than those expected for the molecular sieving pores, as usually observed by sorption method [19]. The pores responsible for the molecular sieving characteristics of the membrane are probably located in the bottom of the "valleys" between the protuberances but they could not be clearly seen using the atomic force microscopy. The quantity of the CMS per prepared sample (about $2 \cdot 10^{-5}$ $cm^3$) was not enough to estimate the porosity using sorption methods.

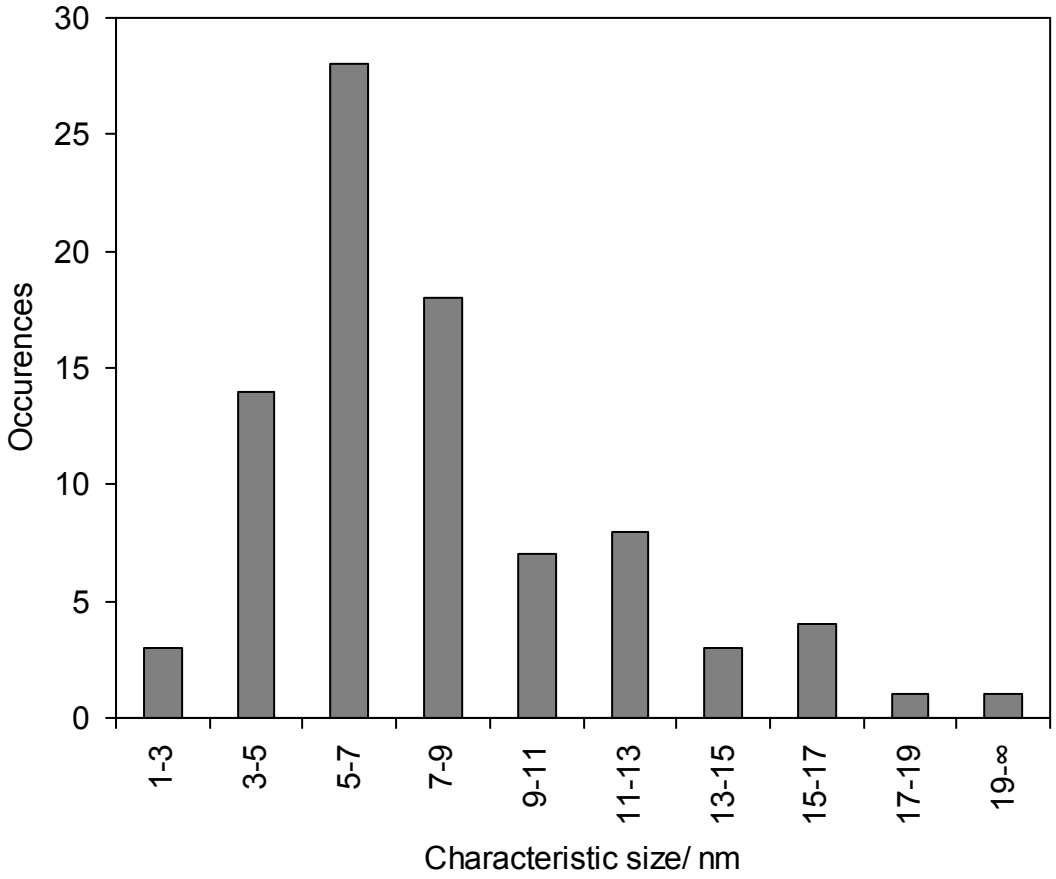


*Figure 4.4. Protuberances (on CMS surface) size distribution determined along the diagonal line in the phase contrast image (Fig 3b).*

The bilayer membrane after coating the CMS with SPEEK was observed by scanning electron microscopy. The image is shown in Figure 4.5. It can be seen that the adhesion between the layers is very good. However, the CMS and SPEEK layers can be easily differentiated. SEM could then be used to determine the thickness of the CMS layers. For the 1 and 2 wt % Matrimid® solutions, CMS with thicknesses of 180 and 400 nm were respectively determined. Taking into account the fact that the highly hydrophilic SPEEK (water uptake about 25 wt% when immersed in liquid water) could shrink upon drying within the microscopes high vacuum conditions; the absence of cracks on the surface of the CMS indicates that it has good mechanical properties and the membrane can withstand swelling/drying conditions such as those experienced in a DAFC application.

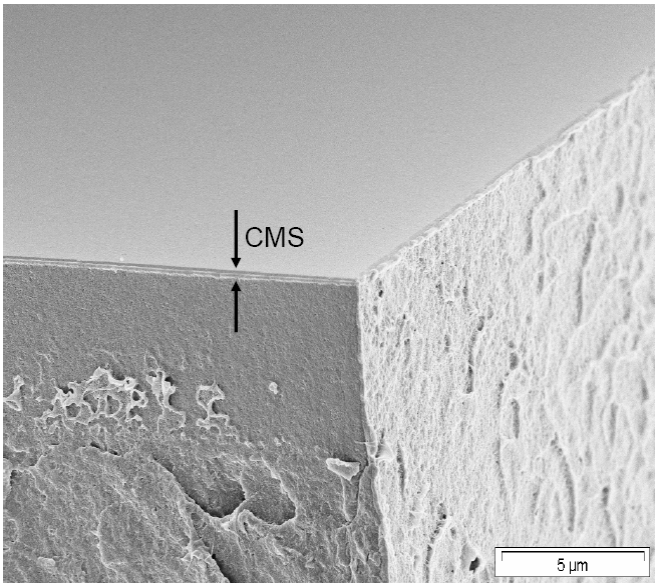


*Figure 4.5: SEM image (secondary electrons) of a bilayer carbon/SPEEK membrane.*

### 4.3.3 Pervaporation of alcohols and water through the bilayer carbon/SPEEK membranes

#### *4.3.3.1 Effect of the pyrolysis temperature on the permeability of bilayer membranes*

Water and methanol permeabilities across the plain SPEEK polymeric membranes and CMS coated SPEEK membranes were measured by pervaporation of water/alcohol mixtures at 55 °C. The total (CMS + SPEEK) membrane thickness was around 73 ± 3 µm. Plain SPEEK membranes have a methanol permeability of 2.8 $10^{-9}$ Kg m $s^{-1}$ $m^{-2}$ and a water permeability of 73.4 $10^{-9}$ Kg m $s^{-1}$ $m^{-2}$. Figure 4.6a shows how the water and methanol permeability across the bilayer membrane with CMS thickness of 180 nm varies as a function of the pyrolysis temperature applied during CMS preparation. It can be seen that the water permeability is more or less constant if the pyrolysis is performed in the temperature range 600 to 800$^{o}$C. Above 800$^{o}$C a considerable decrease is observed. The methanol permeability continuously decreases with an increase of the pyrolysis temperature from 600 $^{o}$C to 1000$^{o}$C. Figure 4.6b shows how the water/methanol selectivity changes with the pyrolysis temperature. Values for

membranes with different CMS thicknesses are presented. As expected the selectivity of membranes with a thicker CMS layer is higher. SPEEK alone has a water/methanol selectivity of 26. In the pyrolysis temperature range 600 to 800°C the water/methanol selectivities in the case of 180 nm CMS increase up to 39, with only 12 % reduction of the water permeability. A water/methanol selectivity of 65 with 57 % reduction of water permeability was measured for 180 nm CMS membranes, obtained by pyrolysis at 500°C as seen by FTIR the pyrolysis is not complete at this temperature. The adhesion of membranes prepared at 500°C to the quartz plates was much stronger than of those obtained at higher temperatures. We chose the membranes prepared by pyrolysis at 800°C for further characterization and membrane electrode assembly and testing in fuel cell experiments, since they had high water/alcohol selectivity and were easy to detach from the quartz substrate, without any damage of the CMS layer.

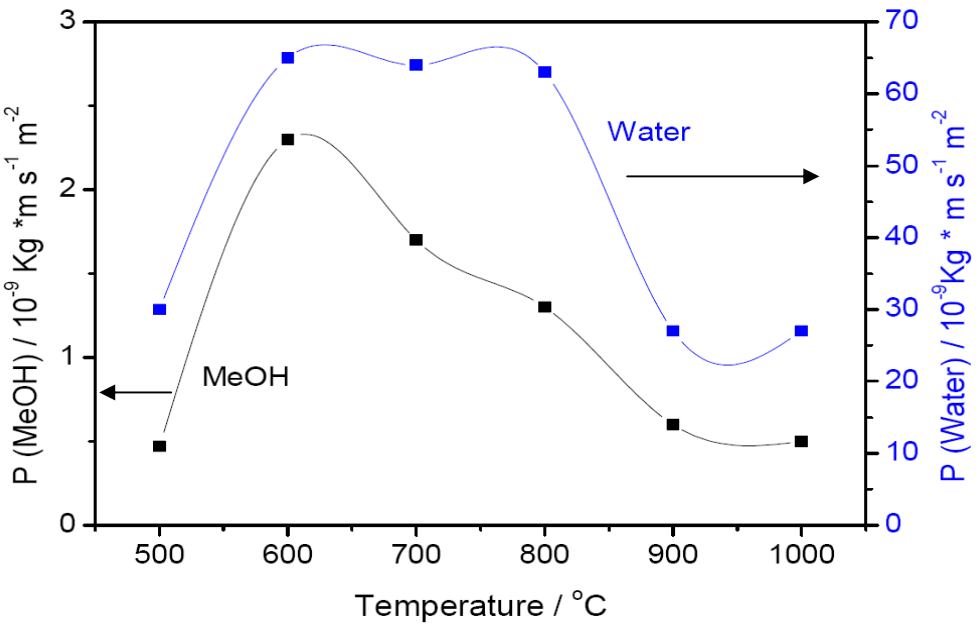


(a)

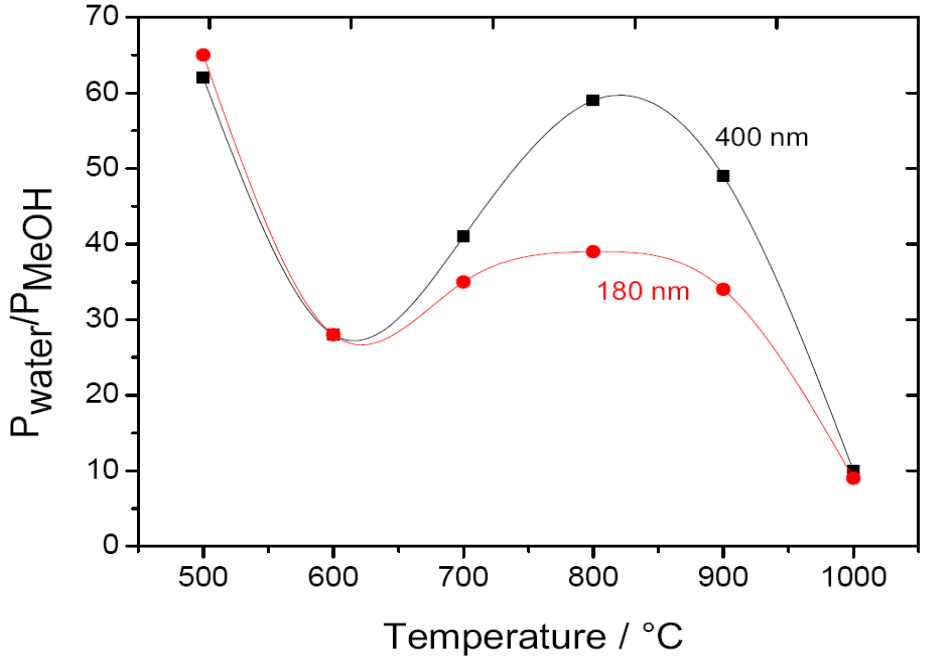


(b)

*Figure 4.6: Effect of pyrolysis temperature on: (a) methanol and water permeability and (b) the water/methanol selectivity.*

#### 4.3.3.2 Effect of alcohol concentration and CMS layer thickness

Methanol solutions of different concentration (5 wt %, 10 wt % and 20 wt % in water) were circulated on the feed side of the measurement cell and the permeate side was evacuated. The difference in permeabilities across the plain SPEEK and bilayer carbon/SPEEK membranes can be seen in Fig 4.7. In pervaporation experiments with 5 wt % methanol solution, the methanol permeation is 36% and 62% reduced when the plain SPEEK membrane is coated with CMS thickness of 180 nm and 400 nm respectively. When the concentration of methanol is increased to 10 wt % or 20 wt % then a substantial reduction of methanol cross over is again observed for carbon/SPEEK as compared to plain SPEEK polymeric membrane. These experiments prove that at least a portion of the CMS pores are smaller than a methanol molecule (0.38 nm) [47]. In the case of 20 wt % methanol pervaporation, a much higher permeability was observed for plain SPEEK as compared to the CMS coated membrane. The

reason for this is the excessive swelling of the hydrophilic SPEEK membrane in water and water/alcohol mixtures. The CMS coating protects the SPEEK layer from direct contact with the concentrated methanol solution during the measurements reducing the excessive swelling. It can be observed from the below figure 7 that in case of 20 wt % methanol pervaporation, the permeation of methanol is quite less from (3 to 4 times) for the CMS coated SPEEK with 180 nm and 400 nm thick layer respectively as compared to plain SPEEK membranes.

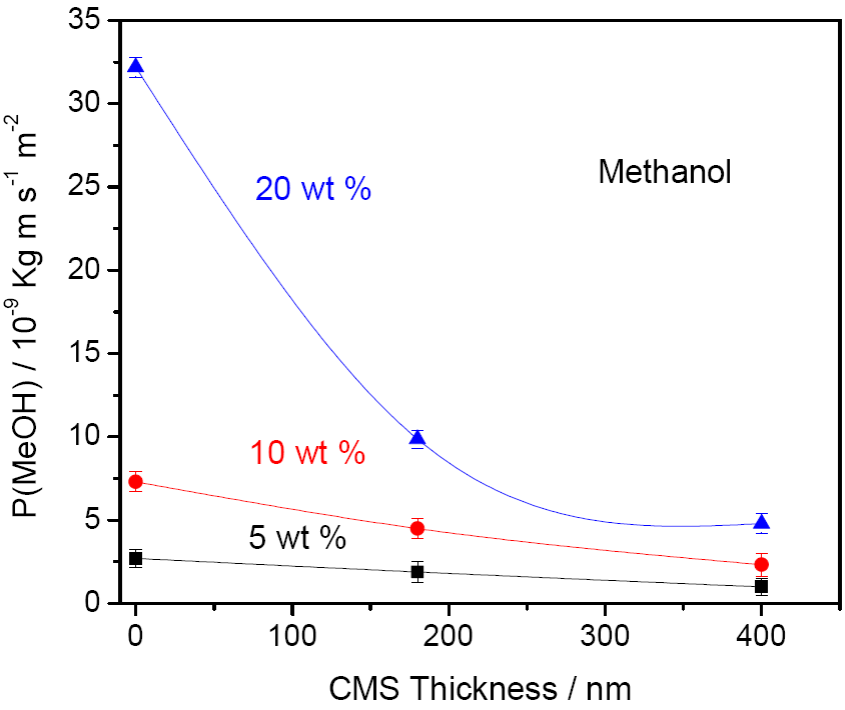


*Figure 4.7: Effect of the CMS thickness on the permeability of bilayer CMS/SPEEK membranes. Feed: 5, 10 and 20 wt % aqueous methanol solutions.*

#### *4.3.3.3 Effect of alcohol molecular size*

After the promising results for water/methanol solutions, experiments with alcohols made up of larger molecules were performed. Besides methanol, ethanol, n-propanol and iso-propanol were used in pervaporation experiments. The results for 5 wt % aqueous solutions of the alcohols used as feed are presented Fig 4.8a. It is clear that selectivity is dependent on the

molecular shape and size of the alcohols [47]. The permeability is higher for methanol as compared to ethanol, while n-propanol and iso-propanol are completely rejected by the bilayer membranes. From this one can conclude that the average pore size of the CMS is in between 0.44 nm and 0.47 nm, corresponding to the kinetic diameter of propanol.

Fig 4.8b shows how the water/alcohol selectivity varies with the CMS thickness and with the size of the permeate molecule. Selectivity as high as 1400 was measured using 5 wt % n-propanol solutions and 180 nm CMS. Using thicker membranes (400 nm) the selectivity was higher than 34000. When methanol or ethanol solutions were used as feed with 180 nm CMS membrane, the selectivity was around 33-36. This again confirms the molecular sieving effect.

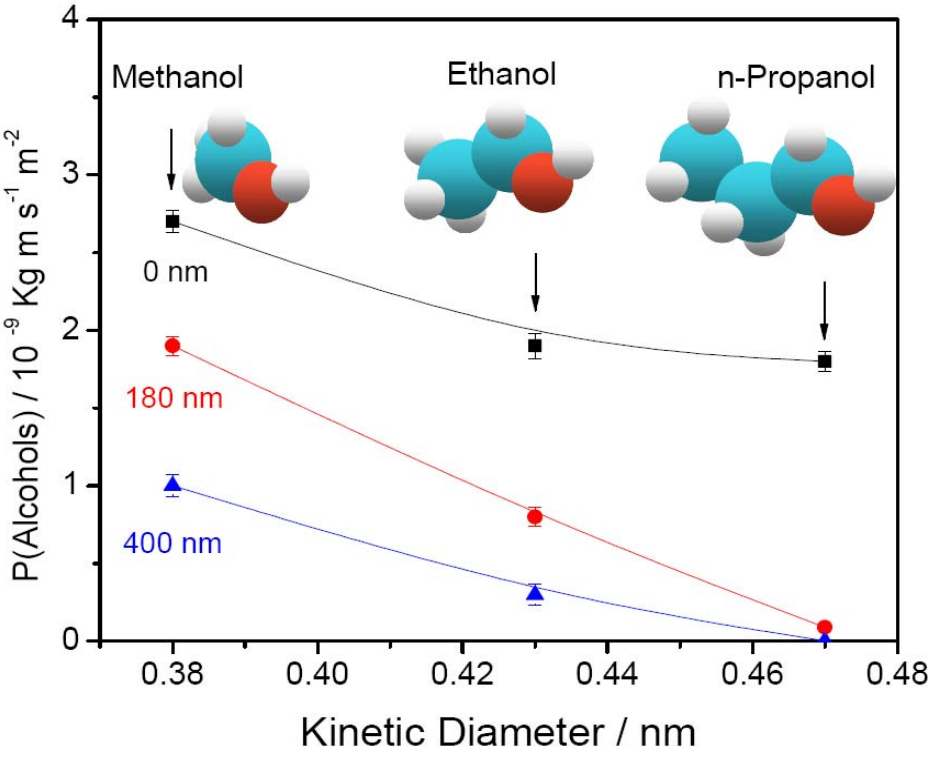


(a)

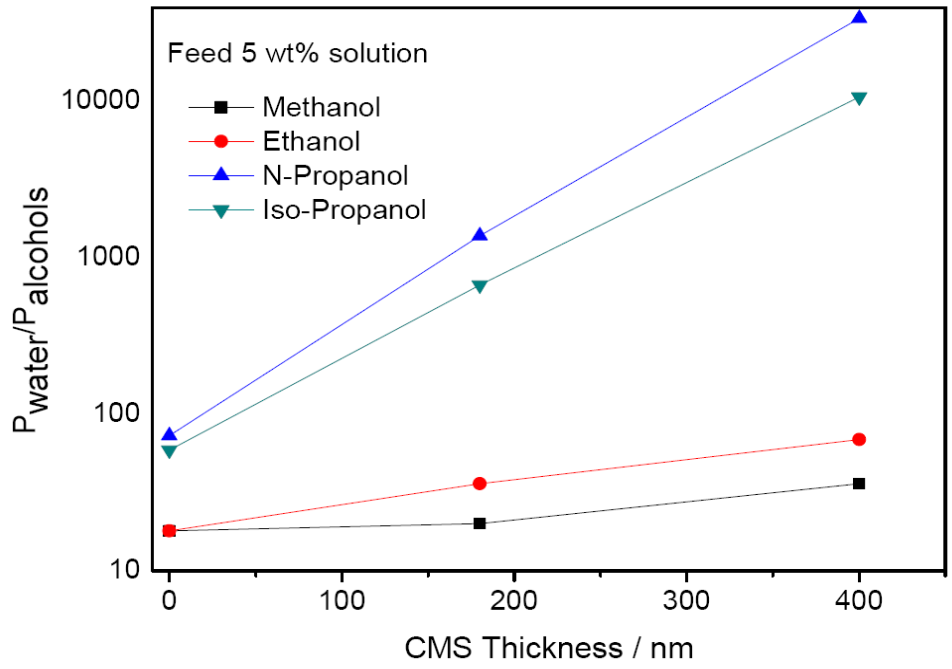


(b)

*Figure 4.8: Effect of penetrant molecule size (kinetic diameter [47]) on (a) the permeability of alcohols and (b) water/alcohol selectivity. Feed: 5 wt % alcohol aqueous solution.*

When 10 wt % propanol solution was used as feed with the plain membrane, significant swelling was observed and both water and propanol permeability were high (260 * $10^{-9}$ kg m $s^{-1}$ $m^{-2}$ and 8 * $10^{-9}$ kg m $s^{-1}$ $m^{-2}$ respectively) with an average selectivity of 31. When bilayer membranes were used for pervaporation of 10 wt % propanol solutions, partial swelling also occurred, leading to a much lower selectivity (75 for 400 nm) than observed for 5 wt % feed solutions, but still more than two times higher than for the plain membrane. When butanol solutions were used as feed, both the plain SPEEK and the polymer layer of the CMS/SPEEK membranes swelled excessively, leading to damage of the CMS layer by the formation of cracks and the selectivity was lost. A Comparasion of permeabilities and selectivity data for the 10 wt % alcohols solutions (methanol, ethanol, iso-propanol and n-propanol) can be observed in the figure 4.9 (a and b). But still the bilayer membranes show better performance

for 10 wt % methanol and ethanol solutions and were not affected by using this concentration of alcohols.

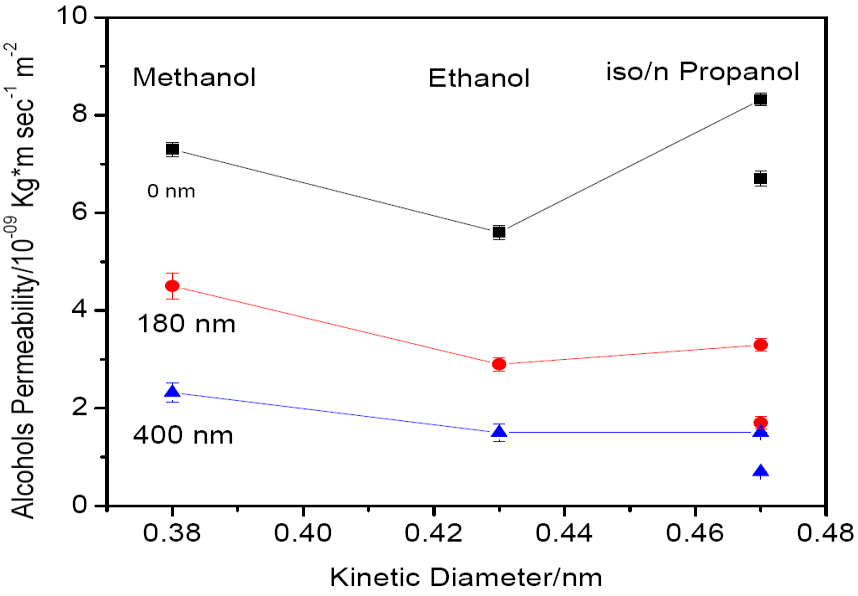


(a)

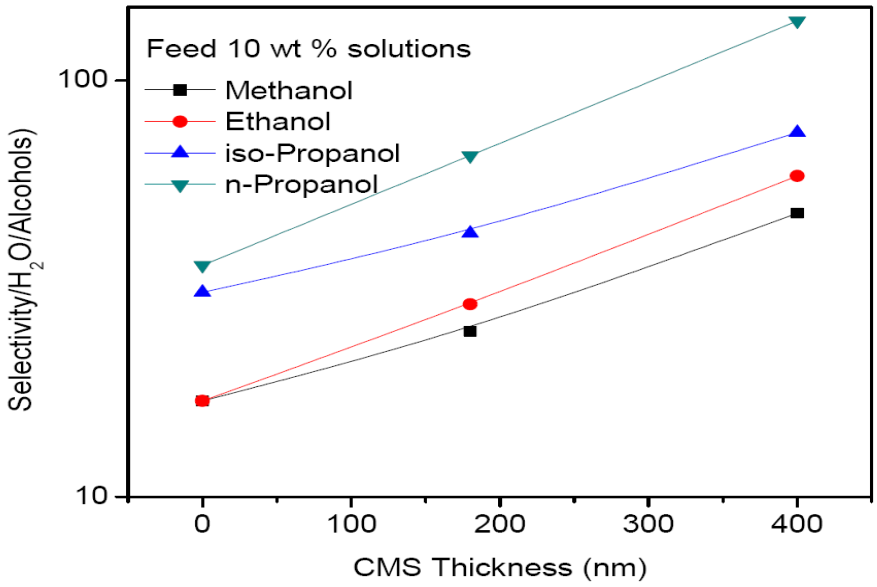


(b)

*Figure 4.9: Effect of penetrant molecule size on (a) the permeability of alcohols and (b) water/alcohol selectivity. Feed: 10 wt % alcohol aqueous solution.*

## 4.4 Characterization of bilayer membranes for fuel cell application

### *4.4.1 Proton conductivity*

The proton conductivities obtained from impedance spectroscopy experiments for plain SPEEK and bilayer CMS/SPEEK at 100% relative humidity were plotted as a function of temperature (Figure 4.10). The results confirm that there is no change in proton conductivity due to the additional CMS layer when compared to the plain SPEEK.

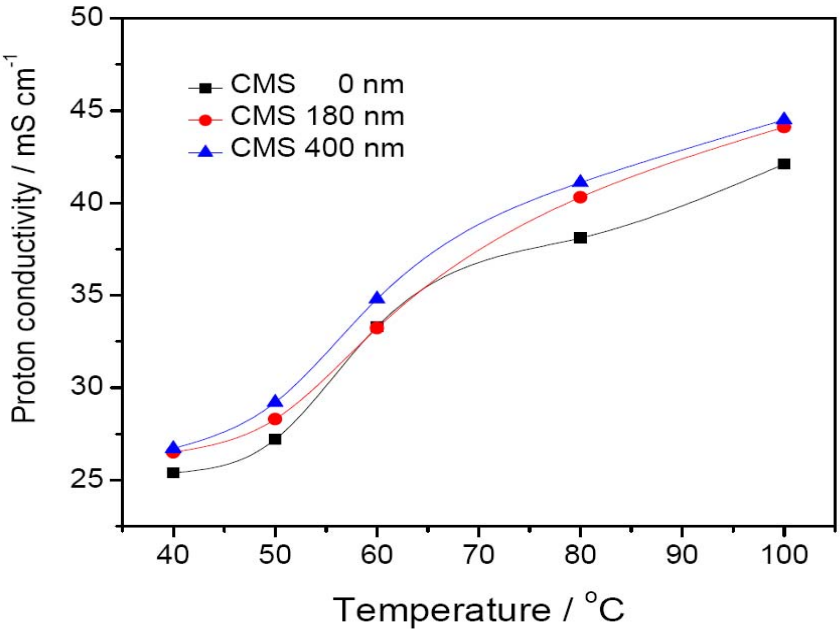


*Figure 4.10: Proton conductivities of SPEEK and CMS/SPEEK membranes as a function of temperature at 100% RH.*

### *4.4.2 DMFC tests with standard electrodes*

The performances of the bilayer membranes were evaluated in a DMFC test stand, after pressing them into anode and cathode commercial electrodes (as specified before). In these experiments the role of the CMS as a barrier for methanol crossover and the effect on the overall DMFC performance were investigated. The polarization curves for plain SPEEK and bilayer CMS/SPEEK membranes with 180 and 400 nm CMS layers were obtained and are

compared in Figure 4.11a. Although the difference between the polarization curves for the membranes was negligible, from the power density curves it is possible to see that the membranes with CMS layer are superior. The membrane with the thicker CMS had the best performance. This results from the reduction in methanol crossover that is promoted by the CMS layer. The methanol crossover observed during the DMFC test with CMS/SPEEK membranes was consistently lower than that of the plain SPEEK. This was measured during a DMFC test by $CO_2$ sensors and can be seen in figure 4.11b. The $CO_2$ concentration at the cathode outlet for the membrane with 180 nm CMS was 60 % of the value measured using a plain SPEEK membrane. With a 400 nm CMS layer the value decreased to 50 %. Assuming that all the $CO_2$ at the cathode outlet resulted from methanol permeation through the membrane and conversion in the presence of the cathode catalyst, these $CO_2$ concentration measurement results give a direct estimation of the methanol crossover.

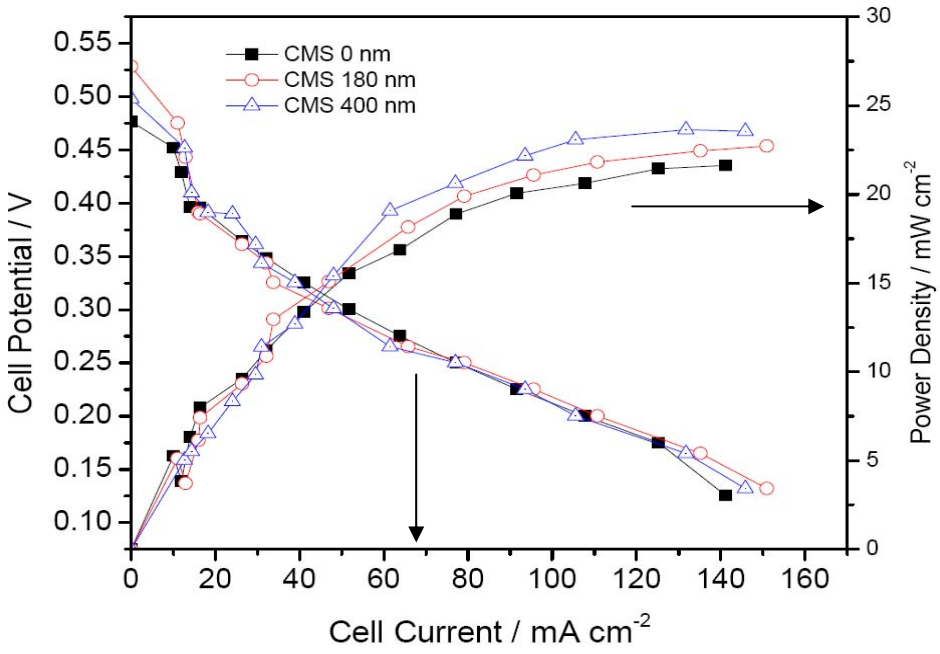


(a)

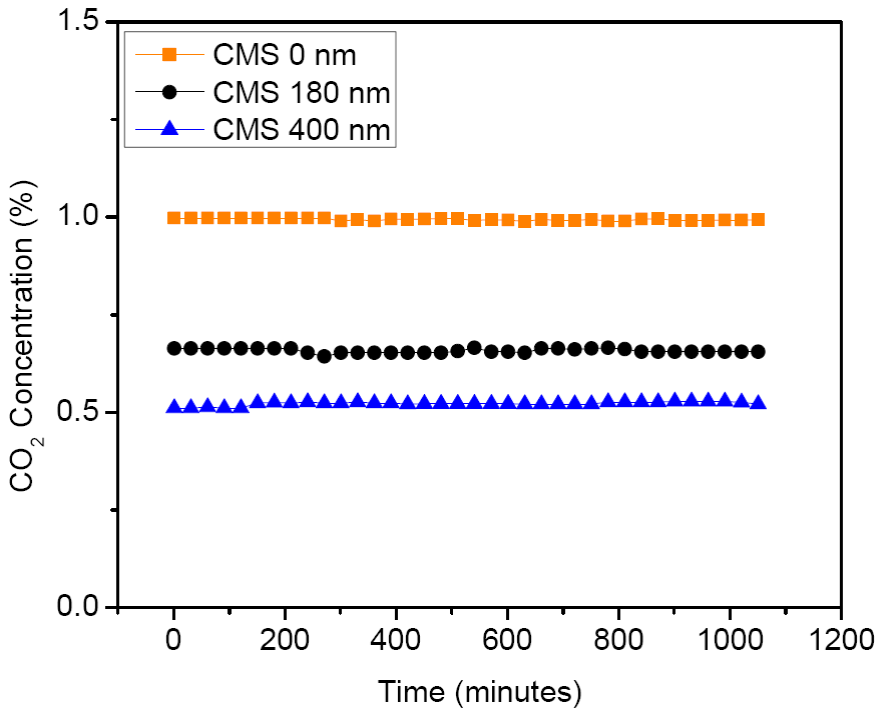


(b)

*Figure 4.11: (a) Polarization and power density curves for plain SPEEK and bilayer CMS/SPEEK membranes and (b) $CO_2$ concentration*

### *4.4.3 Fuel cell results with integrated catalyst in the CMS layer*

The aim of this work was not only to have the CMS functioning as a barrier for alcohol, but also act as a catalyst support. After the DMFC tests confirmed the efficiency of the CMS to reduce the methanol crossover, the next step was to introduce the catalyst into the CMS layer and make preliminary tests in fuel cell experiments.

To incorporate Pt in the CMS layer during the layer preparation, $H_2PtCl_4$ was added to a 3 % Matrimid® solution in chloroform, which was stirred and cast onto quartz plates. The layer with Pt was then pyrolyzed at 800°C under nitrogen. The surface of the resulting layer was then observed using SEM with backscattered electrons. In this mode a very good contrast is obtained for the Pt clusters dispersed in the polymer matrix. Such an image is shown in Figure 4.12. Pt clusters in the range of 30 to 100 nm can be clearly seen. These are much bigger than the optimum size of catalyst particles reported in the literature for fuel cell application, which

is lower than 3 nm [48, 49]. Particles of this size might also be present in the sample without being detected with the resolution of Figure 4.12. An improvement of the Pt dispersion technique will certainly be necessary to decrease the size of the clusters and therefore increase the active surface area. The Pt content in the sample was estimated to be about 1.2 mg/cm$^2$.

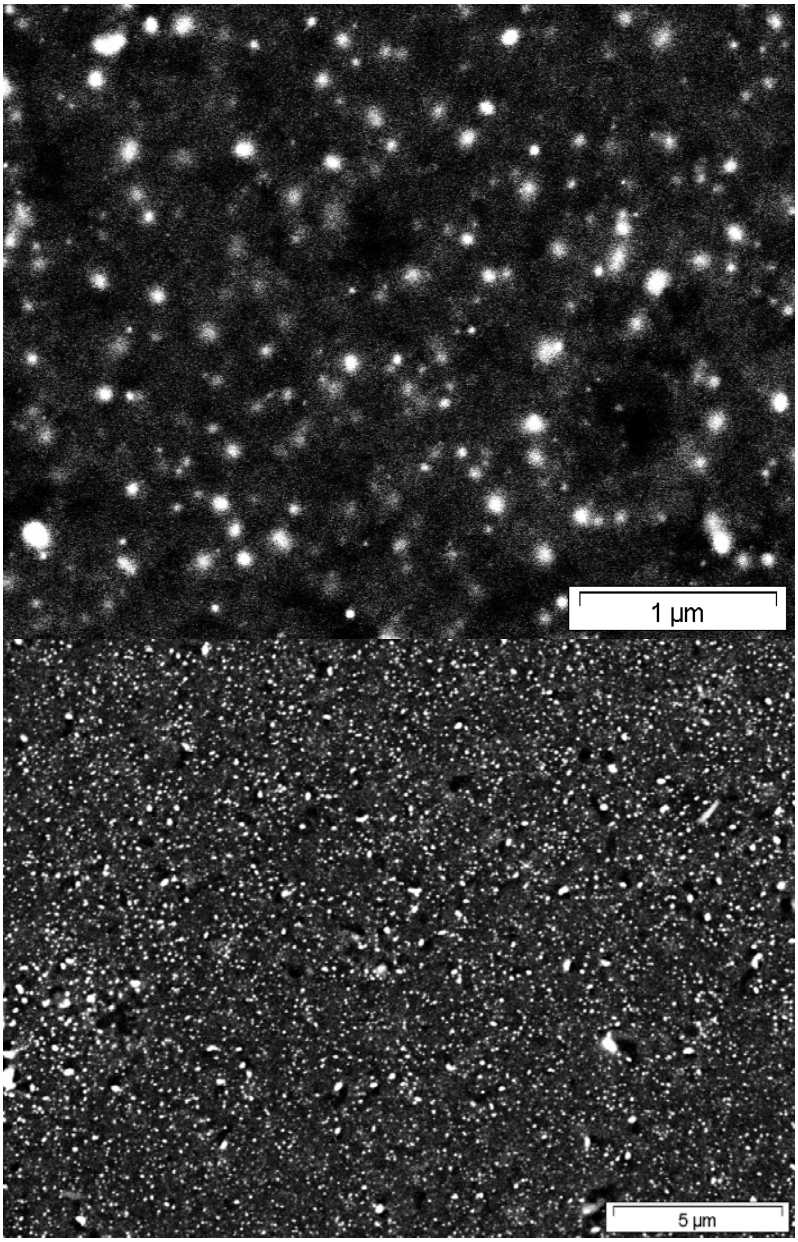


*Figure 4.12: Scanning electron microscopy (backscattered electrons image) of the CMS layer containing dispersed Pt as catalyst.*

The CMS was coated with SPEEK as described earlier and the bilayer membrane obtained was evaluated in fuel cell experiments. For this the SPEEK side of the membrane was pressed against a standard cathode E-Tek electrode with 4 mg Pt/cm$^2$. Not even gas diffusion layer was applied to the CMS side of the membrane exposed to hydrogen during the fuel cell tests. The electric contact was achieved directly with the CMS layer. The resulting assembly was tested in preliminary fuel cell experiments using hydrogen as feed to test the accessibility of the prepared anode catalyst and the feasibility of the assembly. A test was done using the same conditions, with a plain SPEEK membrane, which was pressed against the same commercial cathode catalyst used for the CMS/SPEEK membrane and as anode electrode in this case a commercial one available for the test was used, containing 3mg/cm$^2$ of an alloy of 60% Pt Ru. The results are shown in Figure 4.13. Even if the power density for the CMS/SPEEK membrane was lower than for the SPEEK membrane with standard electrode, it must be taken into consideration that the total amount of catalyst in the CMS was 2.5-fold lower and the size of the metal clusters is still not optimized. In this sense the results are promising and confirm that the assemblies described in Figure 4.1 could be prepared and tested. Optimization of the system is being performed with the aim of obtaining a better catalyst dispersion and smaller CMS pores, as well as further tests for direct methanol and ethanol fuel cell.

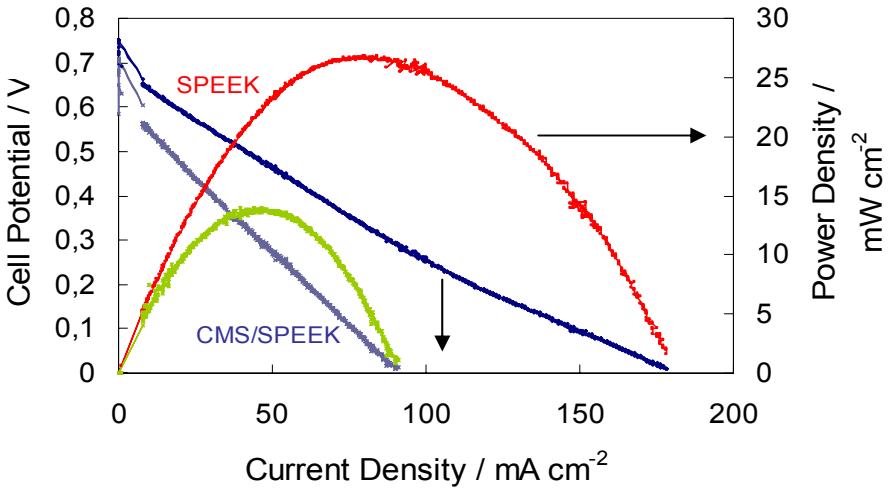


*Figure 4.13: Hydrogen fuel cell (single cell) tests with the membrane-electrode-assembly prepared as depicted in Figure 4.1 and using the CMS layer with dispersed Pt shown in Figure 4.12.*

### 4.5. Conclusions

The concept of a bilayer CMS/SPEEK membrane working with low alcohol crossover and using the CMS as a catalyst support in fuel cell applications has been demonstrated. The membrane has very high water/alcohol selectivity, reaching values as high as 34000 for water/ n-propanol mixtures. It is expected that other molecules with kinetic diameters of approximately 0.47 nm could be separated using such a CMS layer as described in this work. The membranes were tested for DMFC, for which low alcohol cross-over is an important requirement. The assembly is expected to be interesting not only for DMFC but also for direct alcohol fuel cells (DAFC) in general. New effective membranes and catalysts similar to those reported in this study are necessary for the implementation of direct ethanol fuel cell technology. This has advantage over DMFC, since ethanol is less toxic and is already produced on an industrial scale from sugar cane and corn in countries such as USA and Brazil which have an established delivery infrastructure.

## 4.6. References


[1] H. E. A. Brüschke, State-of-art of pervaporation processes in the chemical industry (Part II, Chapter 3). In S. P. Nunes and K. V. Peinemann, editors, "Membrane Technology in the Chemical Industry", Wiley-VCH, Weinheim, Germany, 2001, 2nd edition 2006.

[2] N. W. Deluca and Y. A. Elabd, Polymer Electrolyte Membranes for the Direct Methanol Fuel Cell: A Review, J. Polymer Sci. Part B: Polymer Phys. 44 (2006) 2201–2225.

[3] S. P. Nunes, B. Ruffmann, E. Rikowski, S. Vetter, K. Richau. Inorganic modification of conductive polymer membranes for direct methanol fuel cell. *J. Membrane Sci.* 203 (2002) 215-225.

[4] C.S. Karthikeyan, S.P. Nunes, L.A.S.A. Prado, M.L. Ponce, H. Silva, B. Ruffmann and K. Schulte. Polymer nanocomposite membranes for DMFC application. *J. Membrane Sci.,* 254 (2005) 139–146

[5] V.S. Silva, B. Ruffmann, S. Vetter , A. Mendes, L.M. Madeira b, S.P. Nunes, Characterization and application of composite membranes in DMFC, *Catalysis Today* 104, 205 (2005)

[6] V. S. Silva, B. Ruffmann, H. Silva, V. B. Silva, A. Mendes, L. M. Madeira, S. Nunes, Zirconium oxide hybrid membranes for direct methanol fuel cells - Evaluation of transport properties. J. Membrane Sci. 284(1+2) (2006) 137-144.

[7] V. Antonucci, A. S. Arico, V. Baglio, J. Brunea, I. Buder, N. Cabello, M. Hogarth, R. Martin, S. Nunes, Membranes for portable direct alcohol fuel cells. Desalination 200 (1-3) (2006) 653-655.

[8] A. M. Castro Luna, A. Bonesi, W. E. Triaca, V. Baglio, V. Antonucci, A. S. Arico, Pt-Fe cathode catalysts to improve the oxygen reduction reaction and methanol tolerance in direct methanol fuel cells. J. Solid State Electrochemistry 12(5) (2008) 643-649.

[9] A. Guha, W. Lu, T. A. Zawodzinski, D. A. Schiraldi, Surface-modified carbons as platinum catalyst support for PEM fuel cells, Carbon 45(7) (2007) 1506-1517.

[10] S. K. Natarajan, D. Cossement, J. Hamelin, Synthesis and Characterization of Carbon Nanostructures as Catalyst Support for PEMFCs, J. Electrochem. Soc. 154(3) (2007) B310-B315.

[11] H. Chang, S. H. Joo and C. Pak, Synthesis and characterization of mesoporous carbon for fuel cell applications, J. Mater. Chem. 17 (2007) 3078–3088.

[12] T. Matsumoto, T. Komatsu, H. Nakano, K. Arai, Y. Nagashima, E. Yoo, T. Yamazaki, M. Kijima, H. Shimizu, Y. Takasawa and J. Nakamura, Efficient usage of highly dispersed Pt on carbon nanotubes for electrode catalysts of polymer electrolyte fuel cells, Catalysis Today, 90 (2004) 277–281.

[13] K. Lee, J. Zhang, H. Wang and D. P. Wilkinson, Progress in the synthesis of carbon nanotube- and nanofiber-supported Pt electrocatalysts for PEM fuel cell catalysis, J. Appl. Electrochem., 36 (2006) 507–522

[14] A. Guha, W. Lu, T. A. Zawodzinski Jr. and D. A. Schiraldi, Surface-modified carbons as platinum catalyst support for PEM fuel cells, Carbon, 45 (2007) 1506–1517.

[15] C. Xu, J. Chen, Y. Cui, Q. Han, H. Choo, P.K. Liaw and D. Wu, Influence of the surface treatment on the deposition of platinum nanoparticles on the carbon nanotubes, Adv. Eng. Materials, 8 (2006) 73-76.

[16] J.M. Tang, K. Jensen, M. Waje, W. Li, P. Larsen, K. Pauley, Z. Chen, P. Ramesh, M.E. Itkis, Y. Yan, H. Yushan and R.C. Haddon, High performance hydrogen fuel cells with ultralow Pt loading carbon nanotube thin film catalysts, J. Phys. Chem. – C, 111 (2007), 17901-17904.

[17] C. Wang, M. Waje, X. Wang, J. M. Tang, R. C. Haddon and Y. Yan, Proton exchange membrane fuel cells with carbon nanotube based electrodes, Nano Letters, 4 (2) (2004) 345-348.

[18] K. Prehn, R. Adelung, M. Heinen, S. P. Nunes, K. Schulte, Catalytic active CNT-polymer-membrane assemblies: from synthesis to application, J. Membrane Sci., submitted

[19] K. M. Steel, W. J. Koros, Investigation of porosity of carbon materials and related effects on gas separation properties, Carbon 41 (2003) 253–266.

[20] A. Zlatkis, H. R. Kaufman, D. E. Durbin, Carbon molecular sieve columns for trace analysis in gas chromatography. J. Chromatographic Sci. 8 (1970) 416-17.

[21] J. L. Schmitt Jr., P. L. Walker Jr., Carbon molecular sieve supports for metal catalysts. I. Preparation of the system platinum supported on poly(furfuryl alcohol) carbon. Carbon 9 (1971) 791-6.

[22] D. L. Trimm, B. J. Cooper, Preparation of selective carbon molecular sieve catalysts. J. Chem. Soc., D: Chem. Comm. 8 (1970) 477-8.

[23] D. L. Trimm, B. J. Cooper, Propylene hydrogenation over platinum/ carbon molecular sieve catalysts. J. Catalysis 31 (1973) 287-92.

[24] J.E. Koresh, A. Soffer, Molecular sieve carbon permselective membrane. Part I. Presentation of a new device for gas mixture separation, Sep. Purif. Technol. 18 (1983) 723–734.

[25] J. Koresh, A. Soffer, The carbon molecular sieve membranes. General properties and the permeability of $CH_4/H_2$ mixture, Sep. Sci. Technol. 22 (1987) 973–982.

[26] H. B. Park, Y. K. Kim, J. M. Lee, S. Y. Lee, Y. M. Lee, Relationship between chemical structure of aromatic polyimides and gas permeation properties of their carbon molecular sieve membranes. J. Membrane Sci. 229 (2004) 117-127.

[27] Y. K. Kim, H. B. Park, Lee, Y. M. Lee, Preparation and characterization of carbon molecular sieve membranes derived from BTDA-ODA polyimide and their gas separation properties. J. Membrane Sci. 255 (2005) 265-273.

[28] Y. K. Kim, H. B. Park, Y. M. Lee, Carbon molecular sieve membranes derived from thermally labile polymer containing blend polymers and their gas separation properties. J. Membrane Sci. 243 (2004) 9-17.

[29] Y. K. Kim, J. M. Lee, H. B. Park, Y. M. Lee, The gas separation properties of carbon molecular sieve membranes derived from polyimides having carboxylic acid groups. J. Membrane Sci. 235 (2004) 139-146.

[30] Y. K. Kim, H. B. Park, Y. M. Lee, Gas separation properties of carbon molecular sieve membranes derived from polyimide/polyvinylpyrrolidone blends: effect of the molecular weight of polyvinylpyrrolidone. J. Membrane Sci. 251 (2005) 159-167.

[31] M. N. Islam, K. Tanaka, H. Kita, K. Okamoto, Preparation and gas separation performance of composite carbon molecular sieve membranes derived from NTDA-based polyimides. Transactions of the Materials Research Society of Japan 30 (2005) 401-404.

[32] P. S. Tin, T.-S. Chung, S. Kawi, M. D. Guiver, Novel approaches to fabricate carbon molecular sieve membranes based on chemical modified and solvent treated polyimides. Microporous and Mesoporous Materials 73 (2004) 151-160.

[33] P. S. Tin, T.-S. Chung, Y. Liu, R. Wang, Separation of CO2/CH4 through carbon molecular sieve membranes derived from P84 polyimide. Carbon 42 (2004) 3123-3131.

[34] D. Grainger, M.-B. Hägg, Evaluation of cellulose-derived carbon molecular sieve membranes for hydrogen separation from light hydrocarbons, J. Membrane. Sci. 306 (2007) 307-317.

[35] J. N. Barsema, J. Balster, V. Jordan, N. F. A. van der Vegt, M. Wessling, Functionalized Carbon Molecular Sieve membranes containing Ag-nanoclusters. J. Membrane Sci. 219 (2003) 47-57.

[36] S. Lagorsse, F. D. Magalhaes, A. Mendes, Carbon molecular sieve membranes. Sorption, kinetic and structural characterization. J. Membrane Sci. 241 (2004) 275-287.

[37] S. Liu, T. Wang, Q. Liu, S. Zhang, Z. Zhao, C. Liang, Gas Permeation Properties of Carbon Molecular Sieve Membranes Derived from Novel Poly(phthalazinone ether sulfone ketone). Ind. Eng. Chem. Res. 47 (2008) 876-880.

[38] W. Zhou, M. Yoshino, H. Kita, K. Okamoto, Preparation and gas permeation properties of carbon molecular sieve membranes based on sulfonated phenolic resin. J. Membrane Sci. 217 (2003) 55-67.

[39] H. Kita, K. Nanbu, H. Maeda, K. Okamoto, Gas separation and pervaporation through microporous carbon membranes derived from phenolic resin. ACS

Symposium Series 876 (Advanced Materials for Membrane Separations) (2004) 203-217.

[40] F. Peng, Z. Jiang, C. Hu, Y. Wang, H. Xu, J. Liu, Removing benzene from aqueous solution using CMS-filled PDMS pervaporation membranes. Sep. Purif. Tech. 48 (2006) 229-234.

[41] R. Nolte, K. Ledjeff, M. Bauer, R. Mülhaupt, Partially sulfonated poly (arylene ether sulfone) – a versatile proton conducting membrane material for modern energy conversion technologies, J. Membrane Sci. 83 (1993) 211.

[42] A. Dyck, D. Fritsch, S. P. Nunes, Proton conductive membranes of sulfonated poly phenylsulfone, J.Appl. Polymer Sci. 86 (2002) 2820-2827.

[43] S. P. Nunes and K. V. Peinemann, Membrane Materials and Membrane Preparations (Part I). In S. P. Nunes and K. V. Peinemann, editors, "Membrane Technology in the Chemical Industry", Wiley-VCH, Weinheim, Germany, 2001, 2nd edition 2006.

[44] J.N. Barsema, N.F.A. van der Vegt, G.H. Koops, M. Wessling, Carbon molecular sieve membranes prepared, from porous fiber precursor, J. Membrane Sci. 205 (2002) 239–246.

[45] J.N. Barsema, S.D. Klijnstra, J.H. Balster, N.F.A. van der Vegt, G.H. Koops, M. Wessling, Intermediate polymer to carbon gas separation membranes based on Matrimid PI, J. Membrane Sci. 238 (2004) 93–102.

[46] D. P. Bishop and D. A. Smith, Combined Pyrolysis and Radiochemical Gas Chromatography for Studying the Thermal Degradation of Epoxide Resins and Polyimides. 11. Degradation of Polyimides, J. Appl. Polymer Sci. 14 (1970) 345-354.

[47] T. C. Bowen, S. Li, R. D. Noble, L. Falconer, Driving force for pervaporation through zeolite membranes, J. Membrane Sci. 225 (2003) 165-176.

[48] F. Wen and U. Simon, Loading Pt cathode catalysts for direct methanol fuel cell derived from the particle size effect. Chem. Mat 19 (2007) 3370-3372.

[49] A. M. Castro Luna, A. Bonesi, W. E. Triaca, V. Baglio, V. Antonucci, A. S. Arico, Pt-Fe cathode catalysts to improve the oxygen reduction reaction and methanol tolerance in direct methanol fuel cells, J. Solid State Electrochem. 12 (2008) 643-649.

# Chapter 5.

**Preparation and Characterization of SPEEK/Polyimide blends for proton conductive membranes.**

## 5.1. Introduction

In a proton exchange membrane fuel cell (PEMFC), the proton conducting membrane (PEM) has the important function of transporting protons from anode to cathode, and at the same time it works as a barrier between cathodic and anodic reactant mixtures between the electrodes. In direct methanol fuel cells (DMFCs), the cell performance is reduced by the cross-over of fuel through the membrane towards the cathode [1- 6]. Nafion®, which is the most commonly used material as membrane in PEMFCs, presents both a significant methanol permeability in DMFCs [7], and loss of proton conductivity at high temperature when it is used in hydrogen/oxygen PEMFCs [8]. The sulfonated poly(ether ether ketone) (SPEEK) could be a promising membrane material for DMFC due to its thermal and mechanical stability and easy sulfonation of commercial poly (ether ether ketone) (PEEK). Although SPEEK has high proton conductivity at high sulfonation degree but it also presents high methanol cross-over when is used in DMFCs.

Different attempts have been reported before to reduce the methanol cross-over. A review on these efforts has been published by Deluca and Elabd [9, 10]. Blends of sulfonated poly (ether ether ketones) or poly (etherketone ketones) with different materials, including phenoxy resine, polyamide-imide (PAI), polyphenylsulfone, polyaniline, polyether sufone, polyether-imide (PEI), poly (vinylidene fluoride) and polyvinylpyrrolidone [8, 11- 20] aiming DMFC or other fuel cell related applications. The approach followed by our group to reduce methanol crossover in polymeric membranes has been to develop different forms of nanocomposites using functionalized layered silicates, silica, polysilsesquioxanes, zirconium oxides and

phosphates as fillers [21 - 24]. Recently a bilayer membrane was reported by our group for direct alcohol fuel cell, which was composed by a carbon molecular sieve layer obtained by the controlled pyrolysis of polyimide and an electrolyte layer of SPEEK [25].

In this chapter, polyimide (PI) directly blended to SPEEK to form a membrane with low methanol crossover is described in detail. PI is much less hydrophilic than SPEEK, and at the same time a strong enough interaction between both polymers allows the preparation of low swelling homogeneous membranes. Swier et al. [15] recently proposed the use of poly (ether ketone ketone) (SPEKK) blends with polyetherimide (PEI) as proton conductive membranes. In that case the blends were clearly heterogeneous with domains of about 0.5 μm. By choosing now another polyimide and the right casting conditions quite homogeneous blends are obtained with attractive properties for fuel cell.

## 5.2. Experimental Work

### *5.2.1 Materials*

The used polyimide for blend preparation was Matrimid® 5218, the polyimide resulted from the condensation of 3,3',4,4'-benzophenone tetracarboxylic dianhydride and diamino-phenylindane) commercialized by Ciba Geigy (Switzerland). Before dissolution in dimethyl sulfoxide (DMSO), the polymer was dried in an oven at 120 °C for 24 h to remove any residual water. Poly (ether ether ketone) (PEEK), purchased from Victrex, was dried at 120°C under vacuum and sulfonated according to the procedure described elsewhere [26]. The chemical structures of polyimide (Matrimid 5218) and home made sulfonated poly ether ether ketone (SPEEK) can be seen the following figure 5.1.

DMSO 99.9%, methanol 99.9% and ethanol 99.9% were purchased from Merck and used as received. For the fuel cell tests, electrodes and diffusion layers were purchased from E-TEK (BASF).

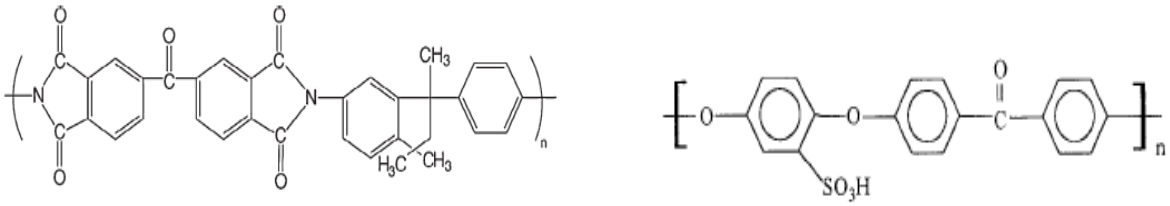

(a) (b)

*Figure 5.1: Chemical structure of (a) polyimide (Matrimid 5218) and (b) home made sulfonated poly ether ether ketone (SPEEK)*

### *5.2.2 Molar mass distribution measurements by GPC*

The apparent molar mass distribution of the polymers sulfonated poly (ether ether ketone) (SPPEK) dissolved in dimethyl acetamide (DMAc) and polyimide (Matrimid 5218) dissolved in chloroform ($CHCl_3$) was determined by the size exclusion chromatography (SEC). For both solvents, polymer solutions of 0.2 wt % in the mobile phase were filtered through a 0.45 μm PTFE- membrane filter.

Analysis in DMAc was performed at 50 °C at a flow rate of 1 mL / min using 0.2 wt % LiCl as an additive. An aliquot of 20 μL was injected on a set of two PSS 10 μ GRAM-Gel columns ($10^3$ and $10^2$ Å, 8 x 300 mm each). A Knauer differential refractometer was used as a concentration detector.

Analysis in chloroform was performed at room temperature at a flow rate of 1 mL / min. An aliquot of 40 μL was injected on a set employing a set of three PSS 5 μ SDV-Gel column ($10^3$, $10^5$ and 50Å, 8 x 300 mm each). A Shodex RI-101 differential refratometer and viscotek VE 3840 UV-detector (operated at a wavelength of λ = 280 nm) were used as concentration detectors.

For both mobile phases apparent molar mass averages *Mn* and *Mw* are based on polystyrene calibration and were calculated using the WinGPC software (PSS GmbH, Mainz Germany).

### *5.2.3 Preparation of SPEEK/Polyimide (PI) blends*

Blends of SPEEK (degree of sulfonation DS 56%) and polyimide (10, 20 and 30 wt. %) were prepared by dissolving both polymers in DMSO and casting as films from solution. Films with each composition were prepared at several different temperature ranges, from 80 $^{o}$C to 130 $^{o}$C with constant stirring for 24 hours. After the mixing step, SPEEK/PI films were prepared by casting the homogeneous polymer solution on clean glass plates which were heated at 100 $^{o}$C for 24 hours, followed by an additional 24 hours at 100 $^{o}$C in vacuum oven in order to eliminate any rest of solvent. The films were easily detached from the glass and were immersed in de-ionised water.

### *5.2.4 Morphology*

The morphology of the SPEEK/PI film cross-section was studied by scanning electron microscopy (SEM) using a LEO 1550 VP field emission microscope. The samples were prepared by fracturing the films in liquid nitrogen and coating it by Au/Pd sputtering.

### *5.2.5 FTIR-ATR Spectroscopy*

FTIR spectra were obtained on a Bruker EQUINOX 55FTIR spectrometer equipped with attenuated total reflectance (ATR) accessory. All spectra were acquired at room temperature from 4000 to 550 $cm^{-1}$ in $N_2$ atmosphere. The number of scans taken was 128 with spectral resolution of 2 $cm^{-1}$.

### *5.2.6 Water and mixture uptake (%)*

Water uptake was measured in de-ionised water and mixture uptake in 5 wt. % methanol solution at room temperature and at 60 $^{o}$C. Before these experiments the pure SPEEK and blends were dried in a vacuum oven at 120 $^{o}$C for 24 hours. 5.0 cm x 2.0 cm films were weighed and then immersed in de-ionised water and methanol solution for 24 hours. After

that, and before weighting again, the excess water was quickly removed with tissue paper. The measurements were repeated three times, the results reported being the average values. The water uptake and mixture uptake of pure SPEEK the blends membranes were calculated according to the following equation

$$Uptake(\%) = \frac{mass(wet) - mass(dry)}{mass(dry)} \text{x}100 \qquad \text{Eq. 5.1}$$

Where mass $_{(wet)}$ and mass $_{(dry)}$ are the masses of the fully hydrated and the dry membrane respectively

### *5.2.7 Thermal properties*

*5.2.7.1 Dynamic mechanical thermal analysis (DMTA)*:

DMTA was performed for SPEEK, PI and 70/30 SPEEK/PI blends cast at 130 $^{o}$C and 80 $^{o}$C to observe thermomechanical behaviour at different temperatures. Storage modulus (E'), loss modulus (E'') and loss tangent (tanδ) were measured in a RSA-II TA-instrument with a film tension mode at a frequency of 1 Hz. The test temperature was increased from 80 °C to 350 °C at a heating rate of 5 °C/min and a constant strain of 0.05 %.

*5.2.7.2 Differential scanning calorimetry (DSC):*

DSC of the SPEEK, PI and 70/30 SPEEK/PI blends cast at 130 $^{o}$C and 80 $^{o}$C blend membrane samples were characterized in the temperature range from 25 to 350 °C on a Netzsch DSC 204 calorimeter equipped with a refrigerated cooling system. Standard aluminium pans of 50 μL were used to encapsulate the blend samples of about 8 – 10 mg. Measurements, including baseline determinations were performed at the scan rate of 10K/min. The experiments were conducted in a nitrogen purge gas stream, and the glass transition (Tg) temperature values were obtained from the first scan thermograms.

*5.2.7.3 Thermogravimetric analyses (TGA)*:

TGA of SPEEK, PI and 70/30 SPEEK/PI blends cast at 130 $^{o}$C and 80 $^{o}$C were performed from 25 $^{o}$C to 600 $^{o}$C, in an argon stream with a Netzsch 209 instrument and a heating rate of 10 K/min.

### *5.2.7 Pervaporation measurements*

Pervaporation experiments were performed by using solutions of 5 wt % methanol solution at 55 $^{o}$C, at a total pressure of 1 bar on the feed side, and vacuum ($10^{-2}$ mbar) on the permeate side. The effective membrane area was 12.5 $cm^2$. After reaching the steady state, the permeated was collected for 1 hour in cold traps immersed in liquid nitrogen and totally 5 permeate samples were collected and then the compositions of feed and permeate were determined by gas chromatography using a Hewlett Packard 5890 chromatograph equipped with a SUPELCO WAXTM-10 capillary column (30m x 0.53 mm x 1.0 um film thickness) with oven temperature of 280$^{o}$C and flame ionization detector. Prior to the pervaporation experiments, the membranes were conditioned in the corresponding feed solutions overnight.

The permeabilities (P) and selectivities were calculated according to equations 3.18 and 3.20 respectively, as discussed in chapter 3 which is more helpful in understanding the processes taking place in the fuel cell experiments.

### *5.2.8 Impedance measurement*

The proton conductivities of plain SPEEK and SPEEK/PI blend membranes prepared with 10, 20 and 30 wt % polyimide were measured by impedance spectroscopy by using a Zahner IM6 Electrochemical workstation. Impedance spectra were scanned in a frequency range from $10^6$ to 10 Hz, with a.c signal amplitude of 5 mV. Before the measurement the membranes were conditioned in de-ionised water for 24 hours at room temperature. Five pieces of membranes (with total thickness around 500 μm) were stacked in between the two diffusion layers

(carbon cloth) in a through-plane conductivity cell. Measurements were carried out at 100% relatively humidity and at temperature varying from 40°C to 100°C. The proton conductivity for plain SPEEK and three SPEEK/PI blends with varying amount of polyimide prepared at 130 °C, were calculated according to the equation 3.12 discussed in chapter 3.

### *5.2.9 Membrane Electrode Assembly (MEA) preparation*

Membrane electrode assemblies (MEA) were prepared with the SPEEK/PI membranes prepared by hot pressing of the membranes between two E-TEK electrodes. The E-TEK cathode electrode was loaded with 100% pure platinum black catalyst (4 mg/cm$^2$), while the E-TEK anode electrode was loaded with an alloy of 60% Pt Ru (3mg/cm$^2$) on Vulcan XC-72.

### *5.2.10 Fuel cell test*

Membrane performances were evaluated in a commercial DMFC test stand (Electrochem Inc. CompuCell GM gas management unit, and Scribner Associates computer-controlled fuel cell test load Series 890B). The DMFC experiments were performed as described before [3]. The cell (25cm$^2$) was fed with a solution of methanol (5 wt %) in water (30mL/min, 1 bar) on the anode side and synthetic air (0.5L/min at 2 to 3 bar) on the cathode side. The operating temperature was 60°C.

## 5.3. Results and Discussion

### *5.3.1 Membrane preparation and morphology*

Fig 5.2 presents some of the SEM pictures of the SPEEK/PI blends prepared at different temperatures. The quality of the films was first visually checked after drying. Blends prepared with different wt. % of polyimide (10, 20 and 30) at 80 $^{o}$C, 90 $^{o}$C and 100 $^{o}$C were turbid. The SEM images of these blends shown in figure 5.2(b, d and f) confirm that they are heterogeneous. On the other hand, the blends prepared with the same wt. % of polyimide (10, 20 and 30) at higher temperatures (110 $^{o}$C, 120 $^{o}$C and 130 $^{o}$C) were transparent and the SEM images can be observed from the figure 5.2(a, c and e) have only a very fine structure in the nanometre scale, confirming the homogeneity. Swier et al. [15] investigated a similar system (SPEKK/PEI). In that case a heterogeneous morphology was observed with large separated domains. A finer phase-separated morphology was observed at higher temperatures but still with domains in the size of 0.5 μm. The obtainment of a finer structure was attributed to the faster evaporation of solvent. Mikhailenko et al. [19] investigated membranes prepared from SPEEK and PEI. They observed phase segregation with domain size around 1 μm and 2-3 μm in blends respectively containing 5 and 25 % PEI. The morphology of SPEEK/PI blends prepared in this work is highly dependent on the casting temperature. A practically homogeneous membrane even at high magnification could be obtained when cast at temperatures higher than 110$^{o}$C.

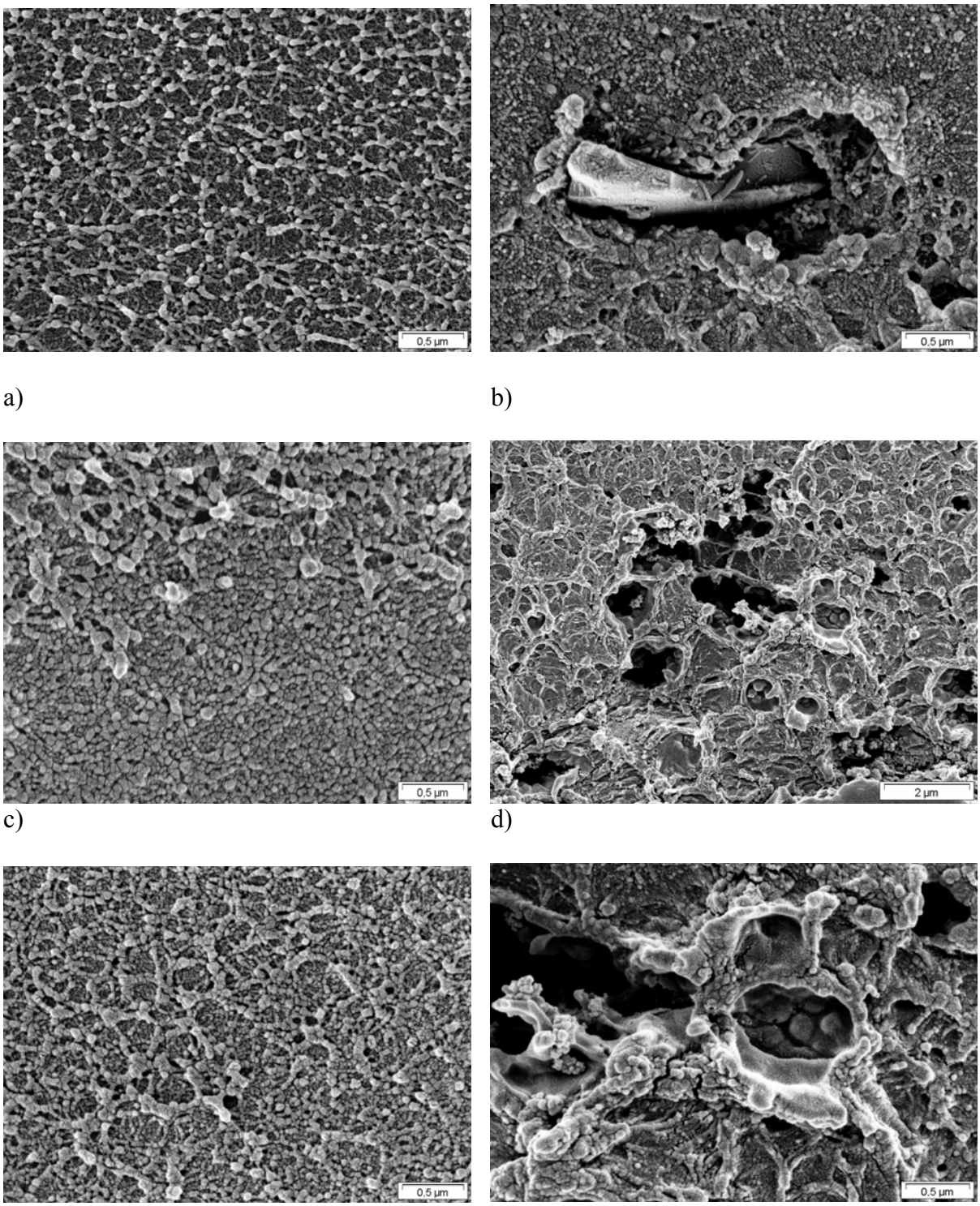


*Figure 5.2: SEM images of SPEEK/PI blend membranes cast at different temperatures: (a, c, e) at 130 °C and (b, d, f) at 80 °C; membranes with different PI content: (a. b) 10 wt. %, (c, d) 20 wt. %, and (e, f) 30 wt. %.*

The blend homogeneity is discussed further below taking into account the glass transition temperatures. For understanding the phase behavior and the resulting morphology, the phase diagram of binary SPEEK/PI blends was theoretically estimated. The phase diagram can be obtained experimentally or by using the Flory-Huggins theory based on the Gibbs energy of mixing [30 – 31]. Here, the phase diagram was estimated by using the Flory-Huggins theory, and the calculation of the binodal curve for the SPEEK/PI blend, was carried out by the mathematical procedure and considerations proposed by Horst and Wolf [31, 32]. A rough estimation of the solubility parameter was done by the group contribution method [33]. For this calculation the SPEEK was considered having one sulfonic group per monomer unit (100 % sulfonation degree).

Fig. 5.3 shows the theoretical phase diagram, as well as the experimental data, mentioning if the blend was transparent or turbid at that preparation condition. The characteristic UCST phase separation behavior could be confirmed. The critical temperature ($T_c$) was estimated as ~260 °C which is far from the casting temperature (80-130 °C). The reasons for the overestimated $T_c$ can be the following: a) the polymer molecular weights ($M_w$) were assumed to be very high to allow mathematical approximations during the calculation. However the real $M_w$ values for SPEEK and PI used in this work were 171 Kg/mol and 72 Kg/mol respectively. For these values, the approximation is not completely valid anymore. It is expected that lower molecular weight entropically favors polymer mixing and would enlarge the one-phase region of the phase diagram, contributing to a $T_c$ shift to lower temperatures; b) The used calculation model was quite simple and the values of Flory-Huggins interaction parameter were roughly estimated without taking into account specific strong interactions between the sulfonic acid groups in SPEEK and the imide groups in PI. The formation of electron donor-acceptor complexes have been reported before [34], for similar blends like SPEEK/poly (amide imide). Preferential strong interaction could considerably increase the homogeneous phase region in the diagram; c) A third important assumption for the rough

estimation of the phase diagram is that the system is practically binary, neglecting the influence of the solvent. In reality the membrane formation starts from a ternary system containing solvent. During the evaporation the composition changes and the binary blend is obtained. A homogeneous solution could be formed in all cases even at temperatures lower than the casting condition. The solvent acts therefore as compatibilizer for SPEEK and PI. Even small amounts of solvent might shift the phase separation curve to lower temperatures.

A last important factor is again related to the presence of solvent and takes in account not only the thermodynamic of the phase separation predicted by the phase diagram but the kinetics of phase separation and membrane formation as well. As mentioned above, during the membrane formation the composition of the solution layer, which will give rise to the final membrane, is changing constantly with the solvent evaporation. Even if a two phase system would be thermodynamically expected for the binary blend at the casting temperature, de-mixing might not occur when the last part of the solvent leaves the film if the mobility of the polymer chains at the final stage of solvent evaporation is low enough. A homogeneous morphology would be frozen leading to a transparent membrane. This frozen state is maintained at room temperature and at the operation temperature.

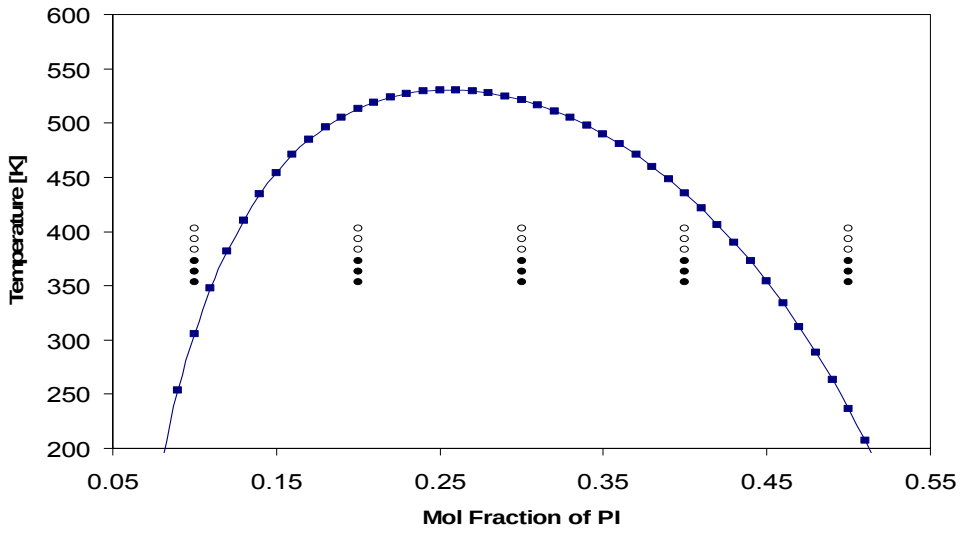


*Figure 5.3: (■) Theoretical phase diagram; Experimental observations: (○) transparent and (●) turbid films after solvent evaporation.*

The following films were chosen for further characterization:

SPEEK, Polyimide (PI) and 70/30 SPEEK/PI blends prepared by solution casting at 130 $^{o}$C (homogeneous membrane) and at 80 $^{o}$C (heterogeneous membrane).

### *5.3.2 FTIR-ATR study*

ATR-FTIR spectra for polyimide, SPEEK and 70/30 SPEEK/PI (130 $^{o}$C) blend were obtained and can be seen in Fig 5.4. The blend contains all the peaks of polyimide and SPEEK. As expected, peaks characteristic of polyimides are diluted in the blend with SPEEK. Peaks that can only be assigned to polyimide in the blend include the methyl group C-H stretching (2957–2863 cm$^{-1}$), C=O (symmetric stretching) (1779 cm$^{-1}$), C=O (anti-symetric stretching) (1721 cm$^{-1}$), CNC ( axial stretching) (1371 cm$^{-1}$) and CNC (out of plane bending) (719 cm$^{-1}$). The peaks corresponding to SPEEK sulfonic group (O=S=O) symmetric and asymmetric vibrations are (1009 cm$^{-1}$), (1075 cm$^{-1}$) and (1216 cm$^{-1}$). In the blend, the first two of these peaks are shifted to lower frequencies (1077 cm$^{-1}$) and (1219 cm$^{-1}$) due to the hydrogen bonding between the hydrogen attached to the sulfonic group of SPEEK and the nitrogen or oxygen atoms of polyimide [35]. This is an evidence of a strong interaction between polymers, thus the assumption of bimodal curve shifted at lower temperatures is possible, and therefore it leads to produce homogeneous blends.

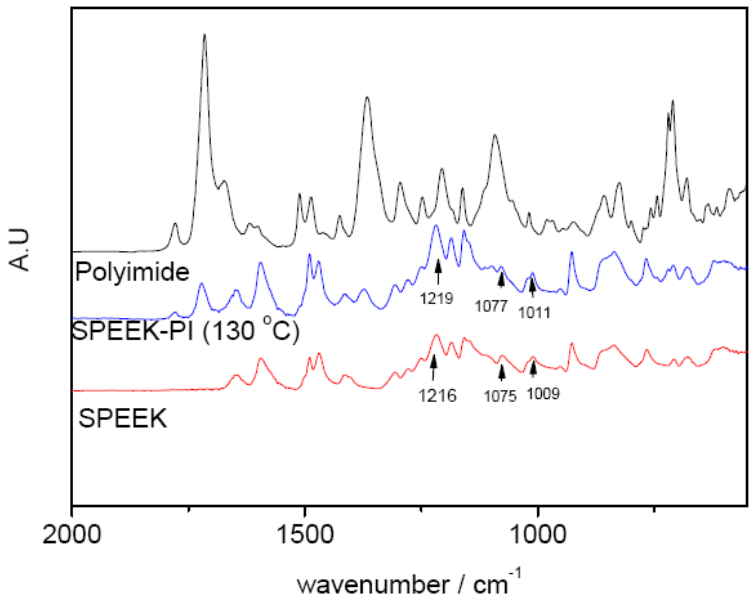


*Figure 5.4: FTIR spectrum of polyimide, SPEEK and a 70/PI SPEEK/PI film cast at 130$^{o}$C.*

### *5.3.3 Water and Mixture Uptake*

Proton conductivity and mechanical properties of membranes are directly affected by water absorption (membrane swelling). Fig 5.5 represents the water and water/methanol solution absorption for SPEEK, and 90/10, 80/20 and 70/30 SPEEK/PI blends cast at 130 $^{o}$C. The blend samples were immersed in de-ionized water and 5 wt% methanol solution at room temperature and then at 60 $^{o}$C. It is evident that SPEEK water uptake capacity depends on temperature and PI content in the blend. By incorporation of more hydrophobic polyimide into the blend, the water uptake capacity decreased prominently, from 24 to 10 wt % at room temperature and from 35 to 11 wt % at 60 $^{o}$C for the 70/30 SPEEK/PI. In the same way the mixture uptake capacity also decreased from 40 to 12 wt % and from 51 to 14 wt % for solution (5 wt % methanol) at room and at 60 $^{o}$C, respectively. The water absorption of 70/30 SPEEK/PI (130 $^{o}$C) blend is lower than that of Nafion 117 [36].

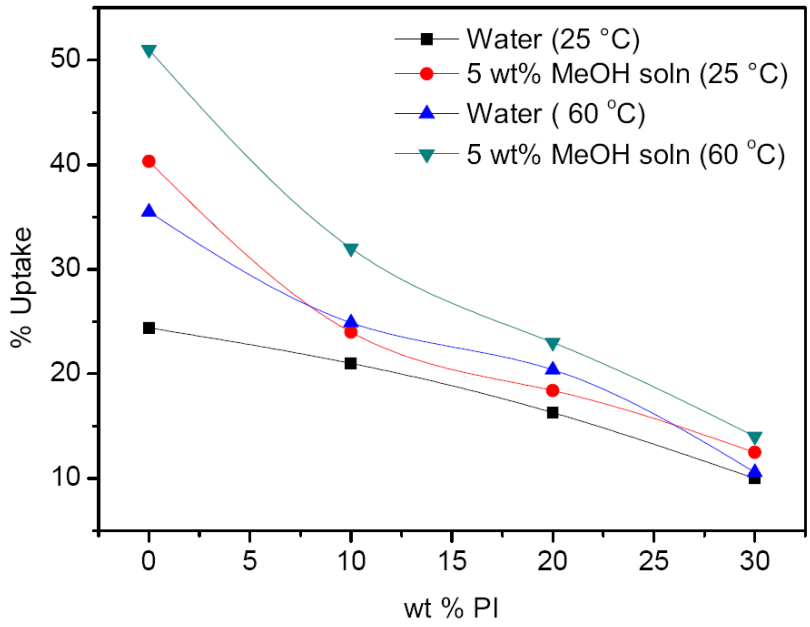


*Figure 5.5: Water and mixture uptake of SPEEK and SPEEK/PI films cast at 130 °C.*

### *5.3.4 Thermal properties*

Fig 5.6 shows the DMTA thermograms of pure polyimide, SPEEK and of two blends obtained with the same composition but different mixing temperatures (70/30 SPEEK/PI cast

at 80 °C and 130 °C). The glass transition temperature (Tg) of the polyimide was around 318 °C. Two Tg values (240 °C and 295 °C) were recorded for the 70/30 SPEEK/PI blend that was cast at 80 °C, confirming that the component polymers are not miscible at 80 °C. The Tg related to the SPEEK chains in the 70/30 SPEEK/PI blend cast at 130 °C is shifted from 224 (for pure SPEEK) to 255 °C, indicating at least a partial miscibility due to strong interaction between SPEEK and PI. The presence of an eventually additional higher Tg could not be confirmed for the blend cast at 130°C, since the sample was mechanically not stable above 290°C to allow the DMTA analysis in this temperature range. For this reason DSC experiments were performed.

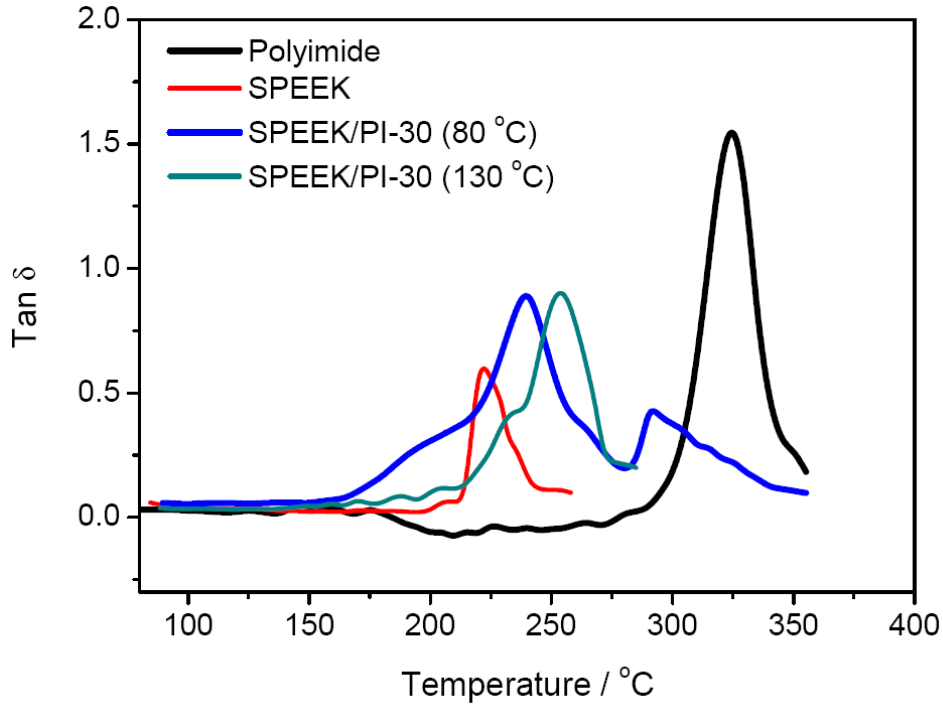


*Figure 5.6: DMTA analysis (Tan δ vs. Temperature/°C) of PI, SPEEK and 70/30 SPEEK/PI cast at 80 and 130°C.*

The Tg for SPEEK, PI and the 70/30 SPEEK/PI blends cast at 80 °C and 130 °C can be estimated from the DSC runs shown in following figure 5.7a while the Tg for with varying amount of polyimide in the blends membranes cast at 130 °C temperature can be observed in

figure 5.7b. Tg values for SPEEK and PI obtained by DSC are 210 $^{o}$C and 305 $^{o}$C respectively. Above 280 $^{o}$C SPEEK starts to loose the sulfonic groups as detected by thermalgravimetric analysis. This degradation might be responsible for the apparent additional transitions above this temperature seen in the SPEEK curve. For the 70/30 SPEEK/PI cast at 80 $^{o}$C 4 transitions can be clearly seen: 210, 305 $^{o}$C, which practically coincides with the Tg of the components polymers and two much less evident additional transitions around 245 and 280 $^{o}$C. An explanation for these additional transitions could be that at the interface between phases of practically pure polymers there is enough interaction between small parts of the chains to shift their Tg. By DMTA the Tgs corresponding to isolated SPEEK and PI could be clearly seen as peaks. The additional transitions appeared as shoulders. For membranes cast at 130 $^{o}$C only one transition can be observed around 250 $^{o}$C by DSC. This confirms the homogeneity of the membrane and the miscibility of SPEEK and PI at 130 $^{o}$C, at least as far as domains as small as 15 nm are concerned.

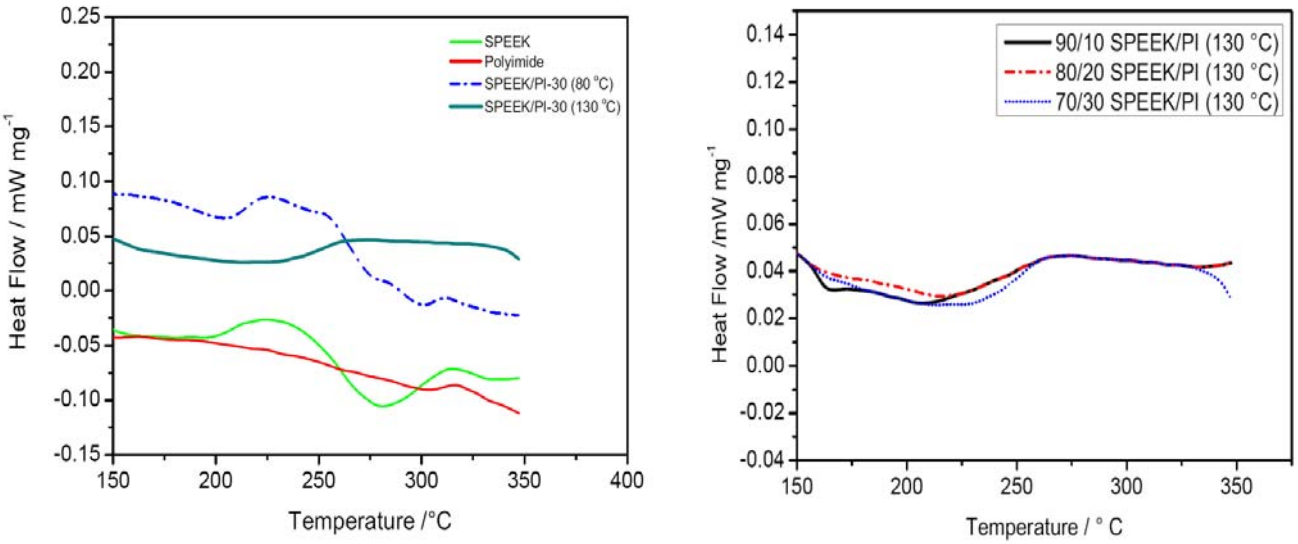


*Figure 5.7: (a)DSC thermograms of PI, SPEEK and 70/30 SPEEK/PI cast at 80 and 130 $^{o}$C & (b) DSC thermograms of three SPEEK/PI blends (90/10, 80/20 and 70/30) SPEEK/PI membranes.*

DSC and DTMA usually are able to detect 2 Tgs in a blend only if different phase domains are larger than this limit [37]. The measured Tg for the SPEEK/PI blend by DSC is not far from the value obtained by DMTA, and that can be estimated by using the Fox equation:

$$1/T_g = w_1/T_{g1} + w_2/T_{g2} \qquad \text{Eq. 5.2}$$

where $T_g$, $T_{g1}$ and $T_{g2}$ are the glass transition temperatures of the blend, polymer 1 and 2; $w_1$ and $w_2$ are the weight fractions of polymer 1 and 2, it is possible to estimate that for a miscible blend with 70 wt % SPEEK and 30 wt % PI the expected Tg would be around 245 $^oC$ which is nearer to the experimental values obtained by DMTA and DSC. However this is just a first approximation. For blends with strongly interacting polymers other equations have been proposed in the literature and reviewed by Utracki [38]. However this is not the focus of this paper. By DMTA a small shoulder below 250 $^oC$ could also be observed, what might indicate the presence of a small amount of another phase richer in SPEEK, but highly dispersed in the predominant SPEEK/PI matrix. DMTA is known to be more sensitive than DSC to differentiate coexistent phases with similar $T_g$'s [39].

To evaluate the thermal stability of the blend, TGA analyses were performed and the results are shown in Fig 5.8. For polyimide most of the mass loss occurs near 500 °C and for the SPEEK membranes two mass losses can be observed; one near 300 °C which is usually assigned to the loss of sulfonic groups and the other at around 500 °C which shows the degradation of the backbone. The thermogravimetric curves for the 70/30 SPEEK/PI blends cast at 80°C and especially for those cast at 130 °C are not as prominent around 300 °C as that for pure SPEEK , due to the presence of polyimide.

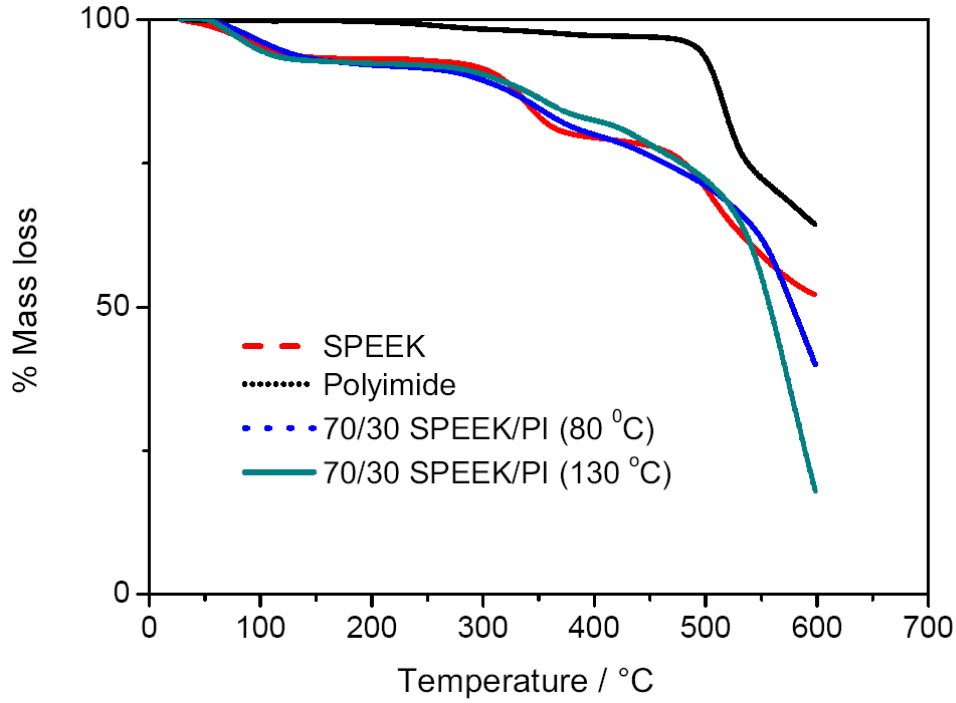


*Figure 5.8: TGA curves of PI, SPEEK and 70/30 SPEEK/PI cast at 80 and 130°C.*

### *5.3.5 Pervaporation of alcohol and water*

Water and methanol permeability through the pure SPEEK and three blend membranes (90/10 SPEEK/PI, 80 /20 SPEEK/PI and 70/30 SPEEK/PI prepared at 130 °C) were measured at 55 °C by pervaporation and they are shown in figure 5.9a. The thicknesses of the membrane samples were 70 ± 5 μm. By addition of PI in the SPEEK, the methanol permeability decrease is possible without sacrificing the proton conductivity. Thus, the 70/30 SPEEK/PI (130 °C) blend has the lowest values of methanol and water permeability: 0.55 x $10^{-10}$ Kg * m $s^{-1}$ $m^{-2}$ and 100 x $10^{-10}$ Kg*m $s^{-1}$ $m^{-2}$ respectively. In both cases a gradual decrease of permeability is observed as the polyimide content in the blend increases since it is much less hydrophilic than SPEEK. The decrease of methanol permeation is, however, much more evident than expected when considering just the dilution of sulfonic groups due to introduction of PI. The strong interaction between polymers reduces the swelling and therefore also the free space for water and methanol transport.

Fig 5.9b shows how the water/alcohol selectivity varies with the amount of polyimide in the blend membranes cast at 130 °C. Selectivities with varying amount of polyimide wt % 10, 20 and 30 were 88, 141 and 182 respectively as compared to that of plain SPEEK 26. These selectivity values are even higher than those obtained with different thickness of carbon molecular sieves (CMS) layers (180 nm & 400 nm) when methanol solutions of the same concentration were used as feed where the selectivity was around 33.

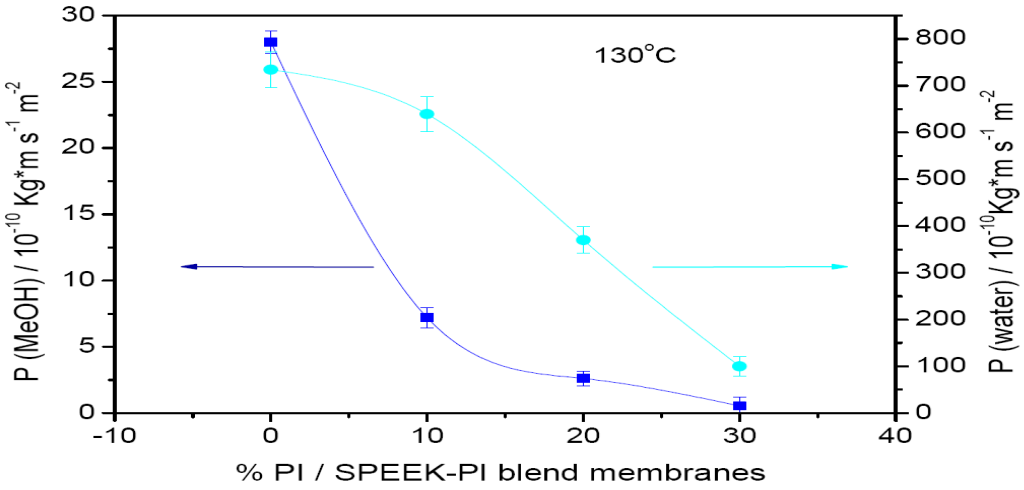


(a)

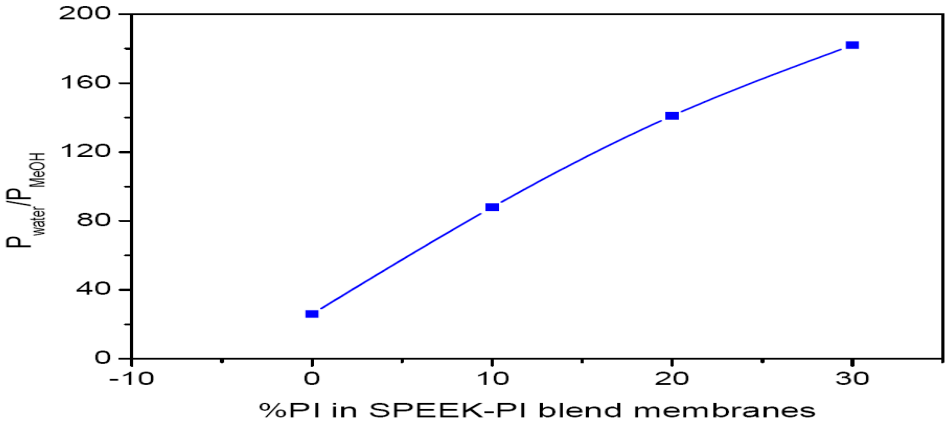


(b)

*Figure 5.9: (a) Effect of polyimide contents (membrane cast at 130 °C) on the methanol and water permeability measured at 55 °C and (b) selectivity of water/alcohol; Feed solution: 5 wt. % methanol aqueous solutions.*

### *5.3.6 Proton conductivity*

The proton conductivities for plain SPEEK and three blend samples at 100% RH were plotted as a function of the temperature in Fig 5.10. The results show a decrease in proton conductivity as an effect of polyimide addition to the SPEEK matrix. For blends with 30 wt.% of PI, the proton conductivity decrease is only around 25% compared to plain SPEEK. While the proton conductivity in blends are lower than SPEEK and Nafion®, the methanol permeability decrease provides membrane with enhanced fuel cell performance. Table 5.1 shows the "relative selectivity" of pure SPEEK, and three of its blends with polyimide, based on their proton conductivity and methanol permeability performed at 60 °C. The relative selectivity defined as the ratio of proton conductivity to the methanol permeability is sometimes used as an indication of the potential performance in DMFC tests. The value for Nafion® and for some other blends reported in the literature [6, 8, 24] are included for comparison. A gradual increasing tendency is observed for the SPEEK/PI blends with increase of polyimide content. The 80/20 SPEEK/PI (130 °C) and 70/30 SPEEK/PI (130 °C) blends have much higher (more than 40-fold) relative selectivity than Nafion®.

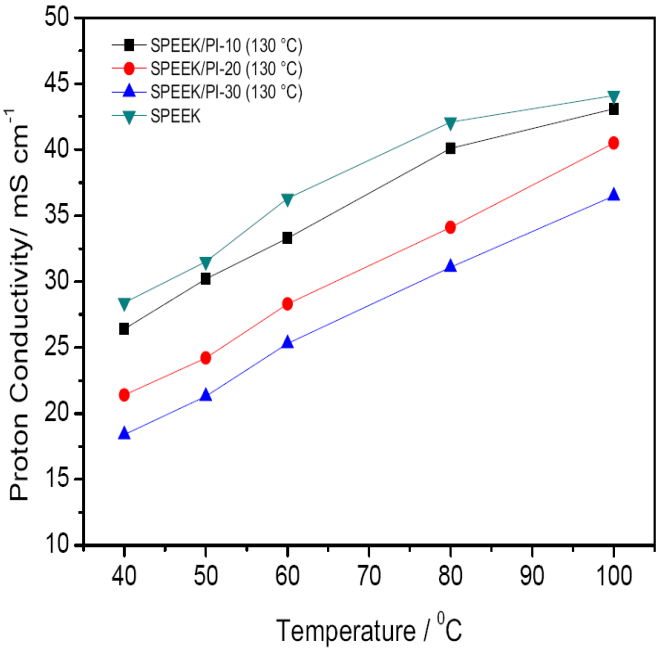


*Figure 5.10: Proton conductivity as a function of temperature for PI, SPEEK and blends measured at 100 % relative humidity.*

*Table 5.1: Proton conductivity, methanol permeability and relative selectivity for the membranes prepared and discussed in this chapter compared to other membranes from the literature.*

| **Membranes** | **T /$^{o}$C** | **Conductivity[a]/ $10^{-3}$ S cm$^{-1}$** | **Methanol permeability/ $10^{-8}$ cm$^{2}$ s$^{-1}$** | **Relative selectivity/ $10^{4}$ S s cm$^{-3}$** | **Refferences.** |
|---|---|---|---|---|---|
| SPEEK (DS 56 %) | 60 | 36 | 3.4 [b] | 106 | This chapter |
| SPEEK (DS 55 %) | 60 | 40 | 3.0 [c] | 133 | 23 |
| 90/10 SPEEK/PI | 60 | 33 | 0.9 [b] | 367 | This chapter |
| 80/20 SPEEK/PI | 60 | 28 | 0.3 [b] | 933 | This chapter |
| 70/30 SPEEK/PI | 60 | 25 | 0.06 [b] | 4167 | This chapter |
| Methyl SPEEK (IEC 1.92 meq/g) | 80 | 134 | 147 [c] | 9 | 6 |
| 75/25 Methyl SPEEK (IEC 1.92 meq/g) / phenoxy resin | 80 | 79 | 54 [c] | 15 | 6 |
| SPEEK copolymer (IEC 2.50 meq/g | 80 | 167 | 261 [c] | 6 | 8 |
| 80/20 SPEEK (IEC 2.50 meq/g)/PAI | 80 | 98 | 85 [c] | 11 | 8 |
| Nafion 117 | 60 | 85 | 9.5 [c] | 89 | 23 |

[a] measured by impedance spectroscopy at the indicated temperature

[b] measured by pervaporation at 55$^{o}$C

[c] diffusion coefficients measured at the indicated temperature

### *5.3.7 DMFC tests*

The polarization curves (DMFC performance) for plain SPEEK and its blends (90/10, 80/20 and 70/30 SPEEK/PI-membranes cast at 130 °C) were obtained and compared in Figure 5.11. It is quite evident from the polarization and power density curves that the difference in performance between the membranes was significant, the blends being superior. This is a result of the reduction of methanol crossover due to the incorporation of polyimide in SPEEK matrix. In accordance to the pervaporation and relative selectivity values, the optimal membranes are those blends prepared with 20 and 30 wt. % of PI and cast at 130 °C. They have higher power density and current density than pure SPEEK membranes. This also confirms low methanol cross-over during the DMFC tests and that in turn enhances the catalytic activity of platinum catalyst on the cathode side with maximum catalytic efficiency due to no or less amount of methanol or water over flooding. No poisoning of catalyst by fuel component enhances the efficiency of a DMFC.

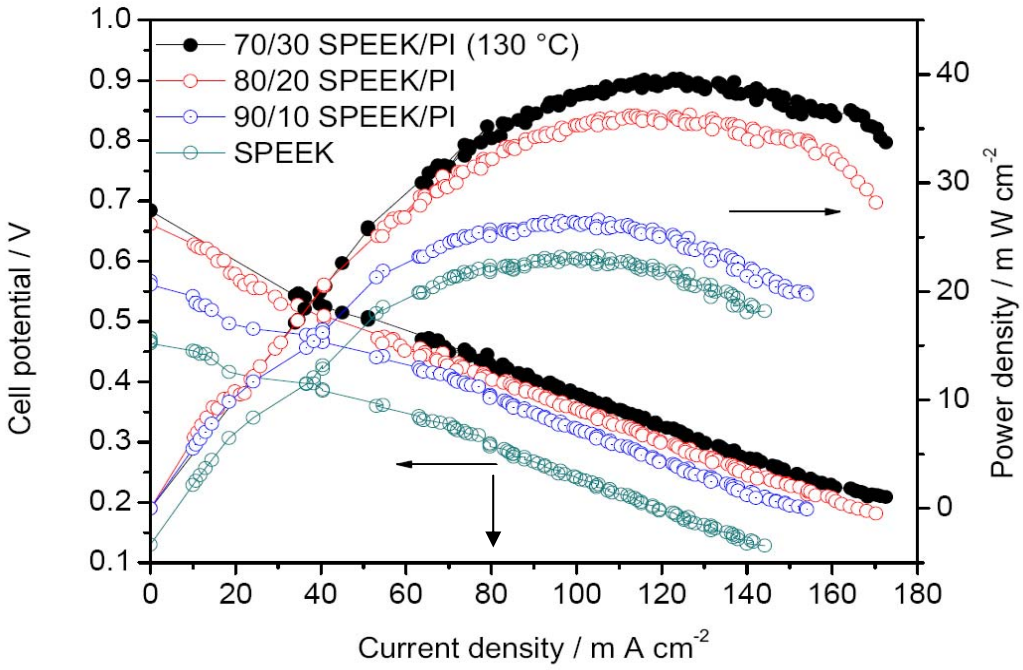


*Figure5.11: Polarization and power density curves for plain SPEEK and SPEEK/PI membranes.*

## 5.4. Conclusions

A series of SPEEK/PI blend membranes was prepared by casting from solution at different temperatures. Structural and thermal characterization of the blend membranes prepared at 110 °C, 120 °C and 130 °C confirmed their homogeneity. Compared to pure SPEEK membrane, the membranes prepared from blends cast at 130$^{o}$C have methanol permeability 4 to 57-fold lower and better performance in DMFC tests.

## 5.5 References


[1] A. Heinzel, V. M. Barragán; A review of the state-of-the-art of the methanol crossover in direct methanol fuel cells. *J. Power Sources* 84 (1999) 70–74.

[2] J. Cruickshank , K. Scott; The degree and effect of methanol crossover in the direct methanol fuel cell. *J. Power Sources* 70 (1998) 40–47.

[3] K. Scott; W. M. Taama, P. Argyropoulos, K. Sundmacher; The impact of mass transport and methanol crossover on the direct methanol fuel cell. *J. Power Sources* 83 (1999) 204–216.

[4] V. S. Silva, B. Ruffmann, H. Silva, V. B. Silva, A. Mendes, L. M. Madeira, S. Nunes; Zirconium oxide hybrid membranes for direct methanol fuel cells - Evaluation of transport properties. *J. Membrane Sci.* 284 (2006) 137–144.

[5] V. Antonucci, A. S. Arico, V. Baglio, J. Brunea, I. Buder, N. Cabello, M. Hogarth, R. Martin, S. Nunes; Membranes for portable direct alcohol fuel cells. *Desalination* 200 (2006) 653–655.

[6] H. Cai, K. Shao, S. Zhong, C. Zhao, G. Zhang, X. Li, H. Na; Properties of composite membranes based on sulfonated poly(ether ether ketone) (SPEEK)/phenoxy resin (PHR) for direct methanol fule cell usages. *J. Membrane Sci.* 297 (2007) 162–173.

[7] M. V. Williams, H. R. Kunz, J. M Fenton. Operation of Nafion(TM)-based PEM fuel cells with no external humidification: influence of operating conditions and gas diffusion layers". *J. Power Sources* 135 (2004) 122–134.

[8] C. Zhao, Z.Wang, D. Bi, H. Lin, K. Shao, T. Fu, S. Zhong H. Na; Blend membranes based on disulfonated poly(aryl ether ether ketone) (SPEEK) and poly( amid imide) (PAI) for direct methanol fuel cell usages. *Polymer* 48 (2007) 3090–3097.

[9] N. W. Deluca and Y. A. Elabd, Polymer Electrolyte Membranes for the Direct Methanol Fuel Cell: A Review. *J. Polymer Sci.: Part B: Polymer Phys.* 44 (2006) 2201-2225.

[10] J.J. Grodzinski, Polymeric materials for fuel cell; Concise review of recent studies, Polym. Adv. Technol. 2007; 18: 785 – 799.

[11] J. A. Kerres. Development of ionomer membranes for fuel cells, *J. Membrane Sci.* 185 (2001) 3-27.

[12] H.-Y. Jung and J.-K. Park, Blend membranes based on sulfonated poly (ether ether ketone) and poly (vinylidene fluoride) for high performance direct methanol fuel cell. *Electrochimica Acta* 52 (2007) 7464-7468.

[13] H. L. Wu, C. C. M. Ma, F. Y. Liu, C.-Y. Chen, S.-J. Lee, C.-L. Chiang, Preparation and characterization of poly (ether sulfone) / sulfonated poly (ether ether ketone) blend membranes. *European Polymer J.* 42 (2006) 1688-1695.

[14] J. Roeder, V. Zucolotto, S. Shishatskiy, J. R. Bertolino, S. P. Nunes, A. T. N. Pires; Mixed conductive membranes: Aniline polymerization in an acid SPEEK matrix. *J. Membrane Sci.* 279 (2006) 70–75

[15] S. Swier, M.T. Shaw, R.A. Swei; Morphology of sulfonated poly(ether ketone ketone) poly(ether imide) blends and their use in proton exchange membranes, J.Membr.Sci. 270 (2006) 22 – 31

[16] J.V. Gasa, R.A. Weiss, M.T. Shaw; Structured polymers electrolyte blends based on sulfonated polyetherketoneketone (SPEKK) and polyether imide (PEI); J.Membr.Sci.320 (2008) 215 – 223.

[17] M. L. Di Vona, A. D. Epifanio, D. Marani, M. Trombetta, E. Traversa, S. Licccia, SPEEK/PPSU-based organic-inorganic membranes: proton conducting electrolyte in anhydrous and wet environments. *J. Membrane Sci.* 279 (2006) 186–191

[18] F. G. Wilhelm, I. G. M. Punt, N. F. A. Vander Vegt, H. Strathmann, M. Wessling. Cation permeable membranes from blends of sulfonated poly(ether ether ketone) and poly(ether sulfone). *J. Membrane Sci.* 199 (2002) 167–176.

[19] S. D. Mikhailenko, S. M. J. Zaidi, S. Kaliaguine; Electrical properties of sulfonated poly(ether ether ketone)/poly(etherimide) blend membranes doped with inorganic acids. *J. Polymer.Sci. Part B: Polym. Phys.* 38 (2000) 1386–1395.

[20] H. L. Wu, C. C. M. Ma, H. C. Kuan, C. H. Wang, C. Y. Chen, C. L. Chiang; Sulfonated poly(ether ether ketone)/poly(vinylpyrrolidone) acid-base polymer blends for direct methanol fuel cell application. *J. Polymer.Sci. Part B: Polym. Phys.* 44 (2006) 565–572.

[21] S. P. Nunes, B. Ruffmann, E. Rikowski, S. Vetter, K. Richau; Inorganic modification of proton conductive polymer membranes for direct methanol fuel cells. *J. Membrane Sci.* 203 (2002) 215–225.

[22] C. S. Karthikeyan, S.P. Nunes, L. A. S. A. Prado, M. L. Ponce, H. Silva, B. Ruffmann and K. Schulte; Polymer nanocomposite membranes for DMFC application. *J. Membrane Sci.,* 254 (2005) 139–146

[23] V. S. Silva, B. Ruffmann, S. Vetter , A. Mendes, L. M. Madeira, S. P. Nunes; Characterization and application of composite membranes in DMFC, *Catalysis Today* 104, (2005) 205–212

[24] R. Gosalawit, S. Chirachanchai, S. Shishatskiy, S. P. Nunes, Sulfonated montmorillonite/ sulfonated poly (ether ether ketone) (SMMT/SPEEK) nanocomposite membrane for direct methanol fuel cells (DMFCs). *J. Membrane Sci.* 323 (2008) 337-346.

[25] H. Maab, S. Shishatskiy, S. P. Nunes, Preparation, characterization of bilayer carbon/polymer membranes. *J. Membrane Sci.* 326 (2009) 27 – 35.

[26] D. Gomes, I. Buder, S. P. Nunes, Sulfonated silica-based electrolyte nanocomposite membranes. *J. Polymer Sci. Part B: Polymer Physics,* 44 (2006) 2278-2298.

[27] A. Dyck, D. Fritsch, S. P. Nunes; Proton conductive membranes of sulfonated poly phenylsulfone, *J. Appl. Polymer Sci.* 86 (2002) 2820–2827.

[28] H. E. A. Brüschke; State-of-art of pervaporation processes in the chemical industry (Part II, Chapter 3). In S. P. Nunes and K. V. Peinemann, editors, "Membrane Technology in the Chemical Industry", Wiley-VCH, Weinheim, Germany, 2001, 2nd edition, 2006.

[29] S. P. Nunes and K. V. Peinemann; Membrane Materials and Membrane Preparations (Part I). In S. P. Nunes and K. V. Peinemann, editors, "Membrane Technology in the Chemical Industry", Wiley-VCH, Weinheim, Germany, 2001, 2nd edition, 2006.

[30] E.M. Woo, K.Y. Cheng, Y. Chen, C.C Su, Experimental verification on UCST phase diagrams and miscibility in binary blends of isotactic,syndiotactic and atactic polypropylenes, Polymer 48 (2008) 5753 – 5766.

[31] R.Horst, calculation of the phase diagrams not requiring the derivatives of the Gibb energy demonstrated for a mixture of two homopolymers with corresponding copolymers, Macromol theory simul, 4 449 – 458 (1995).

[32] R. Horst , B.A Wolf, Calculation of critical points not requiring the derivatives of the Gibb,s energy demonstrated for mixture of two homopolymers with the corresponding copolymers, Macromol theory simul 5, 81 – 92 (1996).

[33] P. A. Small, Some factors affecting the solubility of polymers. *J. Appl. Chem.* 3 (1953) 71-79.

[34] R. J. Karcha and R. S. Porter, Miscible blends of modified poly (aryl ether ketone) with aromatic polyimides, J. Polymer Sci. B: Polym. Phys. 31, 821 (1993)

[35] P. Krishnan, J. Park, C. Kim; Preparation of proton conducting sulfonated poly(ether ether ketone)/boron phosphate composite membranes by in situ sol-gel process. *J. Membrane Sci.* 279 (2006) 220–229.

[36] H. Wu, C. M. Ma, C. Li, T. Lee, C. Chen, C. Chiang, C. Wu, Sulfonated poly(ether ether ketone)/poly(amid imide) polymer blends for proton conducting membranes. *J. Membrane Sci* 280 (2006) 501–508.

[37] T. G. Fox, Influence of diluent and of copolymer on the glass temperature of a polymer system. *Bull. Am. Phys. Soc*. [2] 1 (1956) 123.

[38] L. A. Utracki, *Polymer Alloys and Blends, Thermodynamics and Rheology*, Hanser Publishers, Munich, Vienna, New York, 1989.

[39] D. Pinoit, R. E. Prud'homme, DSC and DTMA characterization of ternary blends, *Polymer* 43 (2002) 2321-2328.

# Chapter 6.

## CMS coated SPEEK bilayer and SPEEK/PI blends membranes for Direct Ethanol Fuel Cell (DEFC) performance

### 6.1. Introduction

Among various types of fuel cell, the direct ethanol fuel cell (DEFC) is still in an early stage of development but it draws much more attention of the research groups all over the world because of its non toxic nature and higher theoretical energy density of (8 kW h $Kg^{-1}$) compared to that of methanol (6 kW k $Kg^{-1}$). DEFC are promising as a power supply for stationeries and portable equipments. DEFC in the form of micro-fuel cell can be the best alternative for the lithium-ion secondary batteries. More over ethanol in the form of a renewable bio-fuel can be produced in large volume by the fermentation of biomass or some common crops like sugar cane and corn through a simple manufacturing process. Ethanol on large scale can be produced by fermentation of sugar cane. The top five ethanol producers in 2006 were USA, Brazil, China, India and France but USA and Brazil accounted for 70 % of the total ethanol production worldwide of 13.5 billions US gallons (40 millions tons). While in 2007 the share of USA and Brazil towards the production of fuel ethanol increased up to 88 % of the total world production of 13.1 Billions US gallons. Ethanol is considered as an alternative to gasoline even today in some parts of the world contributing to a clean environment with a better opportunity for life standard [1 – 3].

As discussed earlier in the introduction part it is evident that much more work is focused on the development of different kind of catalysts for the complete oxidation of ethanol (Breaking of C-C Bond in addition with C-H and O-H bonds) without producing acetic acid, acetaldehyde and etc. with the removal of all 12 electrons [1-10]. Many kinds of polymeric membranes were tested with direct methanol fuel cell (DMFC) since 1960 but now the trend is also to testify the different membranes with direct ethanol fuel cell (DEFC) because of its

unique advantages. Analogously to the development of membranes for DMFC, the main objective is to achieve high proton conductivity with low fuel cross-over through the membrane. Recently a few papers reported on blends/composite membranes for DEFC performance. A simulation study was carried out to determine the ethanol cross-over through the Nafion® membranes in term of different operating temperature and with different ethanol concentration [13].

The two types of membranes reported in chapter 4 and 5 were characterized aiming the application of for DEFC. The first membrane consists of a SPEEK layer and a carbon molecular sieve (CMS) layer (180 and 400 nm). The idea of preparing and using thin layers of CMS is to take advantage of its nonporous structures for stopping alcohols (ethanol) cross-over during the direct ethanol fuel cell (DEFC) performance. The characterization of this membrane applied for direct methanol fuel cell (DMFC) is already presented in chapter 4 and published by our group [14]. The second membrane is based on blends of SPEEK and polyimide (PI) as discussed in chapter 5.

## 6.2. Experimental Work

### 6.2.1 Materials and membrane preparation

Details on materials and membrane preparation for the CMS coated SPEEK bilayer membranes can be read from [14] or from chapter 4. The materials and membrane preparation for the SPEEK/PI blends were discussed in chapter 5. For the fuel cell tests, electrodes and diffusion layers were purchased from E-TEK (BASF).

### 6.2.2 Water and Mixture uptake

Water and solution uptake were measured in de-ionised water and in 5 wt. % ethanol solutions at room temperature 25 °C and at 60 $^{o}$C. All the membranes SPEEK/PI blends, pure SPEEK and Nafion 117 were dried in a vacuum oven at 120 $^{o}$C for 24 hours.

3.0 cm x 3.0 cm films were weighed and then immersed in de-ionised water and in 5 wt. % ethanol solution for 24 hours. After that, and before weighing again, the excess water was quickly removed with tissue paper. The measurements were repeated three times, the results reported being the average values. The water and solution uptake of all the membranes were calculated according to the following equation

$$Uptake(\%) = \frac{mass(wet) - mass(dry)}{mass(dry)} \text{x}100 \qquad \text{Eq. 6.1}$$

Where mass $_{(wet)}$ and mass $_{(dry)}$ are the masses of the fully hydrated and the dry membrane respectively

### 6.2.3 Pervaporation measurements

Pervaporation experiments were performed by using solution of 5 wt % ethanol at 55 $^{o}$C, at a total pressure of 1 bar on the feed side, and vacuum ($10^{-2}$ mbar) on the permeate side. The effective membrane area was 12.5 cm$^2$. After achievement of the steady state, the permeated was collected for 1 hour in cold traps immersed in liquid nitrogen. The compositions of feed and permeate were determined by gas chromatography using a Hewlett Packard 5890

chromatograph equipped with a SUPELCO WAXTM-10 capillary column (30m x 0.53 mm x 1.0 um film thickness) with oven temperature of 280 $^{o}$C and flame ionization detector. Prior to the pervaporation experiments, the membranes were conditioned in the corresponding feed solutions overnight.

The permeabilities (P) and selectivities were calculated according to equations 3.18 and 3.20 respectively as discussed in chapter 3.

### 6.2.4 Membrane Electrode Assembly (MEA) preparation

Membrane electrode assemblies (MEA) for Nafion 117, Pure SPEEK, CMS coated SPEEK and blend SPEEK/PI membranes were prepared by hot pressing of these membranes between two E-TEK electrodes. All the MEA s were prepared by hot pressing at 80 °C for 2 minutes under pressure of 120 Kg $cm^{-2}$. The E-TEK cathode electrode was loaded with 100% pure platinum black catalyst (4 $mg/cm^2$), while the E-TEK anode electrode was loaded with an alloy of 60% Pt Ru (3$mg/cm^2$) on Vulcan XC-72.

### 6.2.5 Direct Ethanol Fuel cell test (DEFC)

Membrane performances were evaluated in a commercial fuel cell stand (Electrochem Inc. CompuCell GM gas management unit, and Scribner Associates computer-controlled fuel cell test load Series 890B). The procedure analogous to that for DMFC experiments as described in chapters 4 and 5; was applied to DEFC test. The cell (25$cm^2$) was fed with a solution of ethanol 5 wt % in water (30mL/min, 1 bar) on the anode side and synthetic air (0.5L/min at 2 to 3 bar) on the cathode side. The operating temperature was 60 °C.

The $CO_2$ concentration at the cathode outlet was monitored by a $CO_2$ sensor (EasyLine IR, Advance Optima EM) to evaluate the ethanol cross over, assuming that all $CO_2$ was resulting from ethanol electro-oxidation at the cathode.

### 6.3. Results and Discussion

#### 6.3.1 Water and mixture uptake

Swellings of membranes in the relevant alcohol solution directly affect the proton conductivity and mechanical properties of membranes. Fig 6.1 represents the percentage of water uptake of membranes in de-ionised water and mixture uptake in 5 wt % ethanol solutions at different temperatures 25 °C and 60 °C. All the membrane samples were immersed in de-ionised water and in 5 wt% ethanol solution at room temperature and then at 60 $^{o}$C. From the values we can conclude that the behaviour is some what the same as observed for 5 wt % methanol solution. It is evident that SPEEK water uptake capacity depends on temperature and PI content in the blend. By incorporation of more hydrophobic polyimide into the blend, the water uptake capacity decreased form 25 to 7 wt % at room temperature and from 36 to 12 wt % at 60 $^{o}$C for the final blend of SPEEK/PI (70/30). The same decreasing behaviour was also observed for mixture uptake from 32 % to 10 wt % and from 50 to 12 for the 5 wt % ethanol solution at room 25 °C and at 60 $^{o}$C respectively. Here again confirming that the water and mixture absorption of 70/30 SPEEK/PI (130 $^{o}$C) blend is lower than that of Nafion 117 when the ethanol solution was used in the experiments.

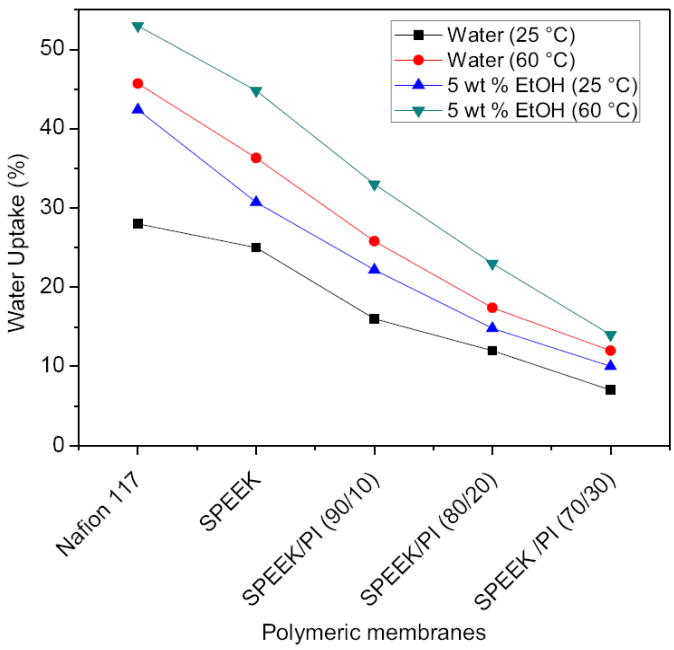


*Figure 6.1: Water and mixture uptake results for Nafion 117, pure SPEEK and (90/10), (80/20), (70/30) SPEEK/ PI blends cast at 130 °C.*

### 6.3.2 Pervaporation of alcohol and water

Water and ethanol permeability of the Nafion 117 , SPEEK, three SPEEK/PI blend membranes and CMS layer (180- and 400- nm) coated SPEEK were measured at 55 °C by pervaporation. The thicknesses of all the membrane samples except Nafion 117 (200 um) were in the range from 65 – 75 µm. Figure 6.2 shows that the permeabilities of ethanol and water for Nafion 117 are 5 to 6 times higher than pure SPEEK membrane.

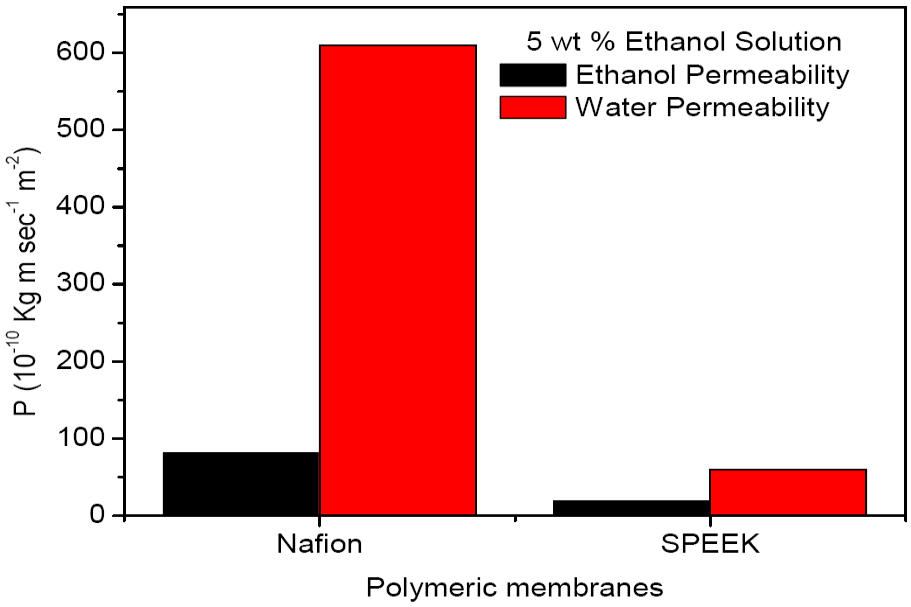


*Figure 6.2: Permeabilities of (ethanol and water) for Nafion 117 and pure SPEEK membranes at 60 °C*

From figure 6.3(a) it is evident that the ethanol permeability was decreased by 50 folds for SPEEK/PI (70/30) blend as compared to pure SPEEK and 150-fold as compared to Nafion 117 with maximum of water permeability of 143 x $10^{-10}$ Kg*m $s^{-1}$ $m^{-2}$. In both cases a gradual decrease of permeability is observed as the polyimide content in the blend increases since it is much less hydrophilic than SPEEK and Nafion 117. The decrease of ethanol permeation is however much more evident than expected when considering just the dilution of sulfonic groups due to introduction of PI. The strong interaction between polymers reduces the

swelling and therefore also the free space for water and ethanol transport. Fig 6.3(b) shows that the water/ethanol selectivity increases up to 300 as the PI content in the blend membranes increases.

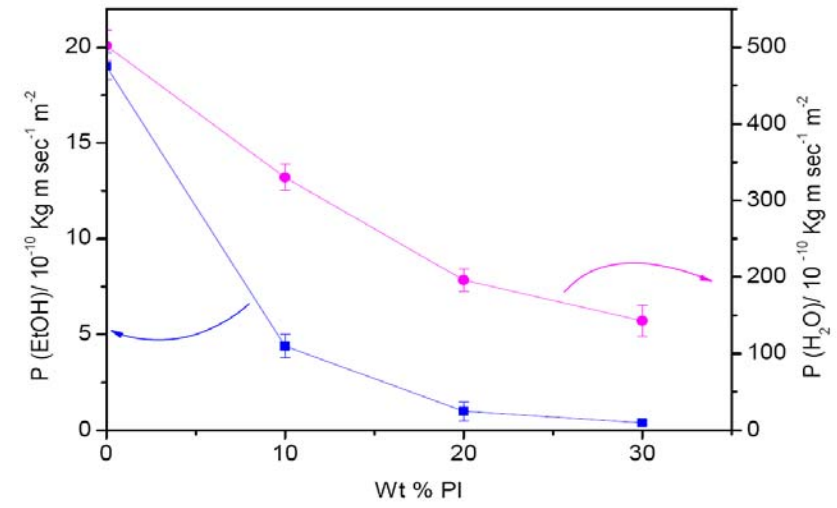


(a)

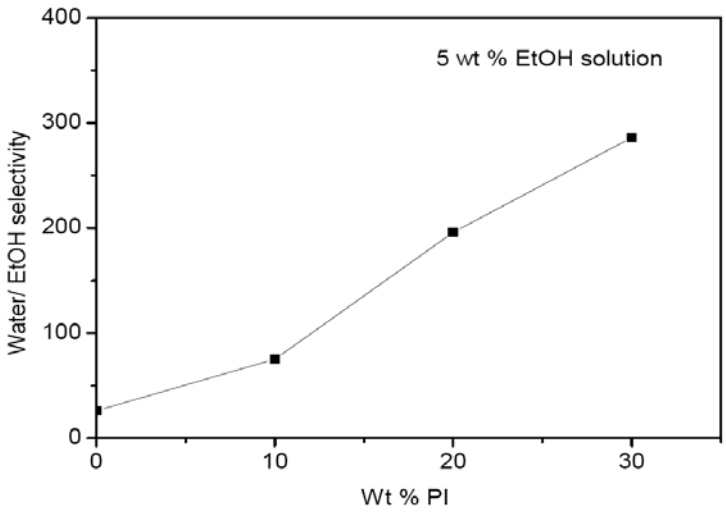


(b)

*Figure 6.3: (a) Effect of polyimide contents on permeability of ethanol and (b) water/ethanol selectivity. Feed solution: 5 wt. % ethanol aqueous solution.*

Figure 6.4 (a) shows the effect of CMS layer for the rejection of ethanol molecules during pervaporation measurements. The permeabilities of ethanol was decreased by a factor of 6-fold and 20-fold for the CMS (400 nm) coated SPEEK bilayer membranes as compared to

pure SPEEK and Nafion 117 respectively and without considerable decrease of proton conductivity. However the selectivity of water/ethanol is not increased in the same order as for SPEEK/PI blends membranes. The maximum value was obtained for the CMS (400 nm) coated SPEEK membrane is nearly 80. This can be observed in Figure 6.4 (b).

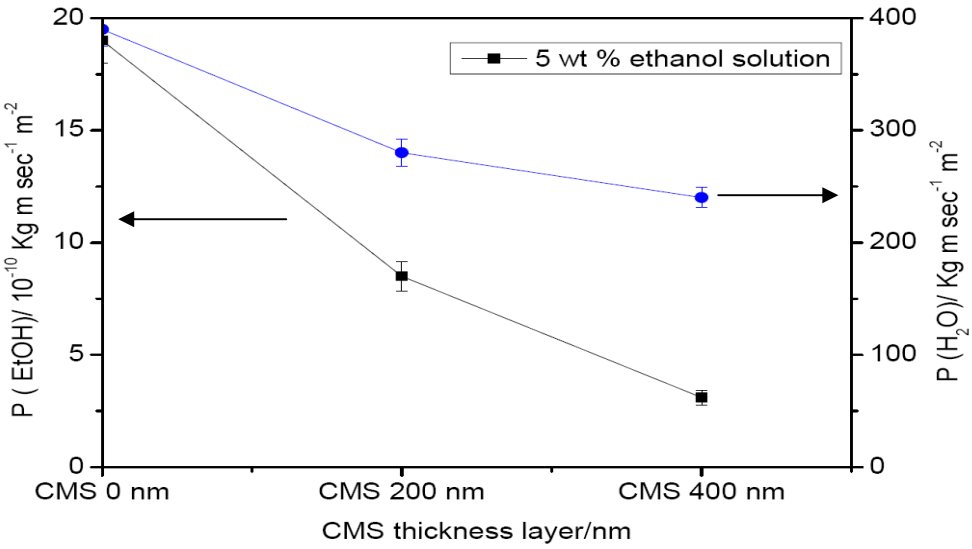


(a)

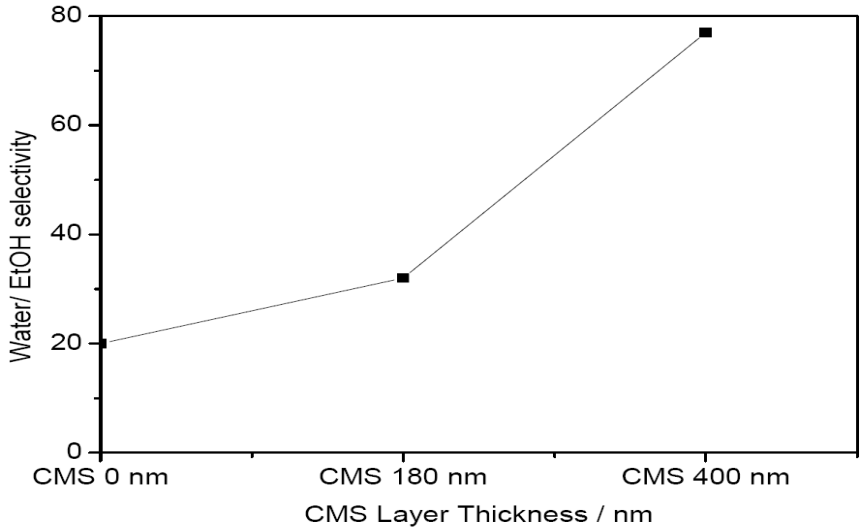


(b)

*Figure 6.4: (a) Effect of CMS layer (180 nm and 400 nm) on permeability of ethanol and (b) water/ethanol selectivity. Feed solution: 5 wt. % ethanol aqueous solution.*

### 6.3.3 Direct Ethanol Fuel cell (DEFC) tests

The polarization curves (DEFC performance) for Nafion 117, pure SPEEK, SPEEK/PI blends and CMS (180 nm and 400 nm ) coated SPEEK membranes were obtained at different temperatures (25 °C , 60 °C and 90 °C) and are compared in Figures 6.5, 6.6 and 6.7. Figure 6.5(a) represents the polarization curves for the Nafion 117 and membranes of pure SPEEK and its three blends. The power and current densities obtained even with Nafion 117 are not that much high and definitely the reason is the high ethanol cross-over and low catalytic activity of catalysts at room temperature. At this temperature the power and current densities for membranes based the three SPEEK/PI blends are higher than for pure SPEEK but lower than for Nafion 117 and the only reason which could be given here is the low ethanol cross-over through the blend membranes as compared to pure SPEEK (Figure 6.8).

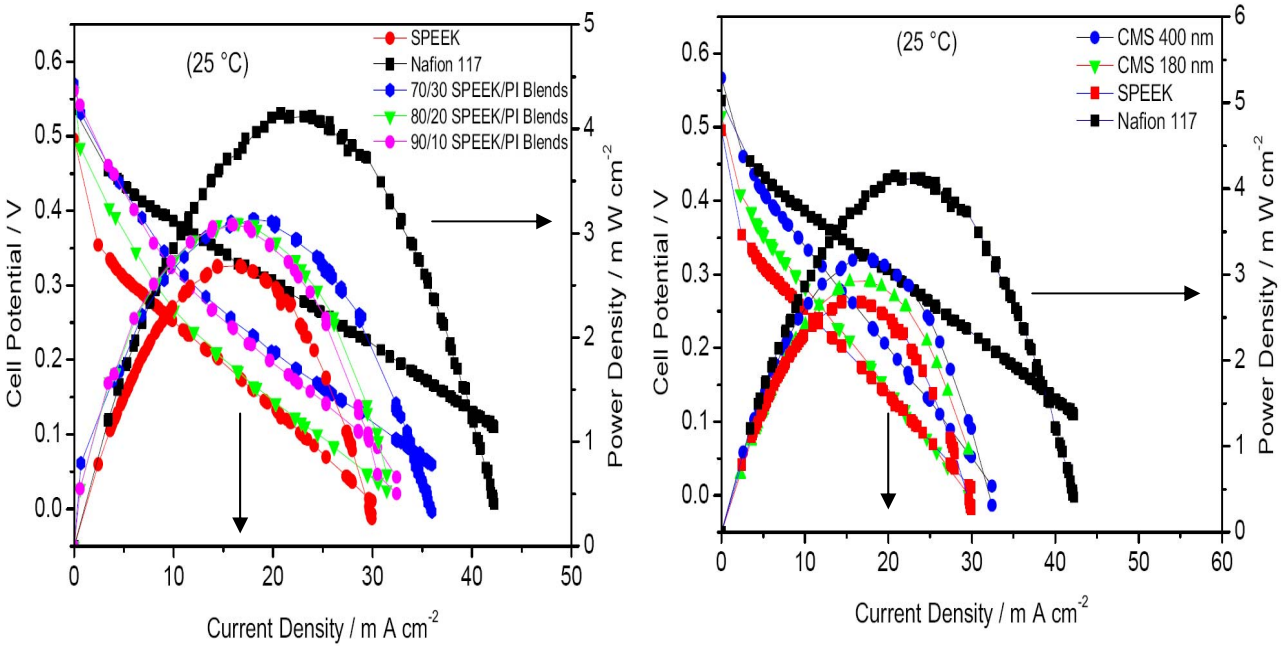


*Figure 6.5: Polarization and power density curves at operating temperature of 25 °C; (a)Nafion 117, pure SPEEK and (90/10), (80/20), (70/30) SPEEK/PI blends and (b) Nafion 117, pure SPEEK, CMS (180 nm and 400 nm) coated SPEEK.*

The same situation is also observed in Figure 6.5 (b) during the DEFC performance tests at 25 °C for the CMS (180 nm and 400 nm) coated SPEEK; the polarization and current densities curve are slightly higher than for the pure SPEEK membrane but lower than Nafion 117. The effect of CMS layer on the ethanol cross-over through the bilayer membranes is compared to pure SPEEK and Nafion 117 in Figure 6.9.

But when the DEFC performance tests were performed at 60 °C then the power and current densities curves for Nafion 117, pure SPEEK and SPEEK/PI blends were higher than those obtained at 25 °C and this confirms the effect of temperature on the catalytic activity of a catalyst. Here a difference can be observed from figure 6.6(a); at high temperature the performances of all three SPEEK/PI blends are better than pure SPEEK and two blends (SPEEK/PI 80/20 and SPEEK/PI 70/30) reached polarization values of 0.63 V and 0.71 V which can be compared to that of Nafion 117(0.65 V). This is a result of the reduction of ethanol crossover due to the incorporation of polyimide in the SPEEK matrix, leading automatically to the enhancement of the catalytic activities. Figure 6.6(b) shows the performance of CMS (180 nm and 400 nm) coated SPEEK at this high temperature of 60 °C in comparasion with pure SPEEK and Nafion 117 membranes. The polarization values of 0.60 V and 0.64 V for the CMS (180 nm and 400 nm) / SPEEK membranes respectively confirms the role of the CMS nanoporous layer rejection of ethanol molecules during the DEFC performances that lead to higher power and current densities as compared to pure SPEEK (0.50 V). The ethanol crossover for both SPEEK/PI blends membranes and CMS / SPEEK membranes are compared in Figures 6.8 and 6.9 respectively. At this temperature (60 °C) the rejection of ethanol by the blends membrane is higher than by the CMS/ SPEEK membranes which enhancing the performances.

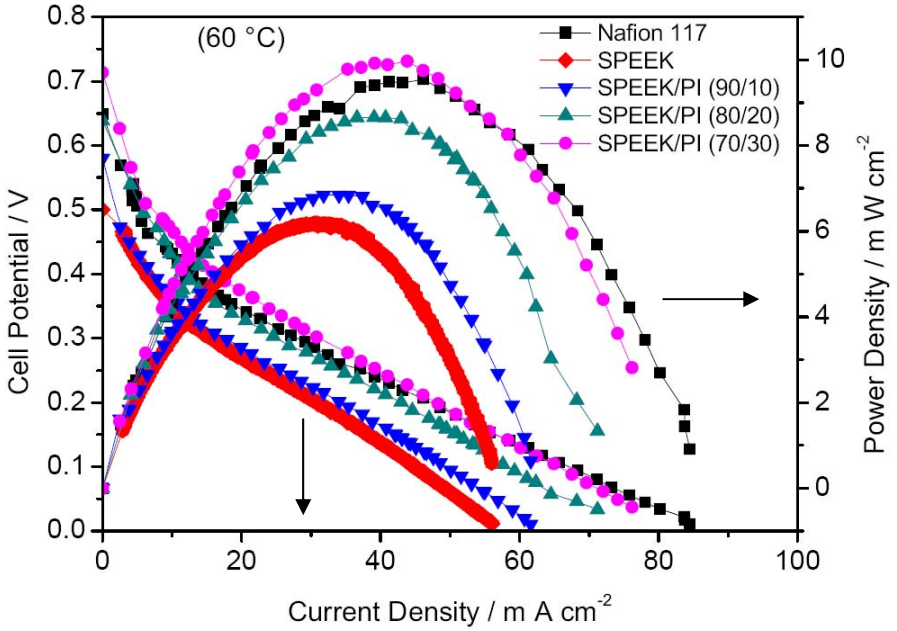


(a)

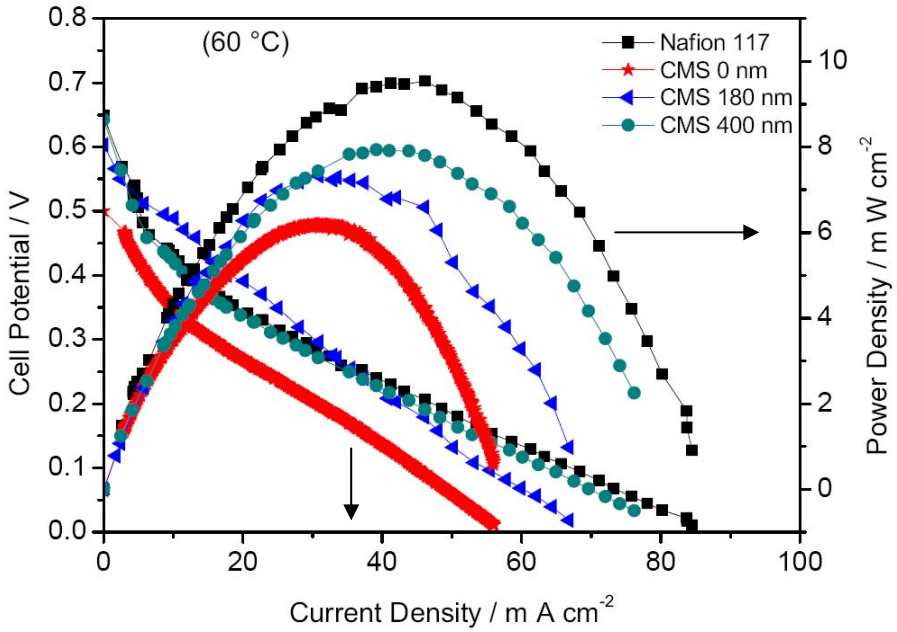


(b)

*Figure 6.6: Polarization and power density curves at operating temperature of 60 °C; (a)Nafion 117, pure SPEEK and (90/10), (80/20), (70/30) SPEEK/PI blends membranes (b)Nafion 117, pure SPEEK, CMS (180 nm and 400 nm)/ SPEEK membranes.*

DEFC tests are usually carried out at higher temperature (even at 100 °C) since the catalytic activities are reported to be much higher at this condition [8 and 9]. Also here the membranes were tested at 90 °C during DEFC performance by using the same E-Tek electrodes. Figure 6.7(a) represents the power densities and current densities for the Nafion 117, pure SPEEK, and SPEEK/PI blend membranes at 90 °C. Except for Nafion 117 (0.65 V), the polarization values for the pure SPEEK and its three blend membranes increased as compared to DEFC performance at 60 °C and two blends membranes SPEEK/PI (80/20) (0.72 V) and SPEEK/PI (70/30) (0.76V) had better performance than Nafion 117 at this high temperature. Compared to DEFC performance at 60 °C, the ethanol crossover observed at 90 °C was much higher for the Nafion 117 and pure SPEEK than for three SPEEK/PI blend membrane as can be seen in Figure 6.8.

A similar behaviour was observed at this high temperature (90 °C) using the CMS / SPEEK bilayer membranes (Figure 6.7b). Bilayer membranes had the same or even better performance than Nafion 117. Here the high power and current densities were obtained because of the low ethanol crossover through the bilayer membranes (Figure 6.9). However the ethanol crossover through the CMS / SPEEK bilayer membranes is higher than for SPEEK/PI membranes. Therefore, the blend membranes might have a high potential of application in DEFC, being also easier to manufacture.

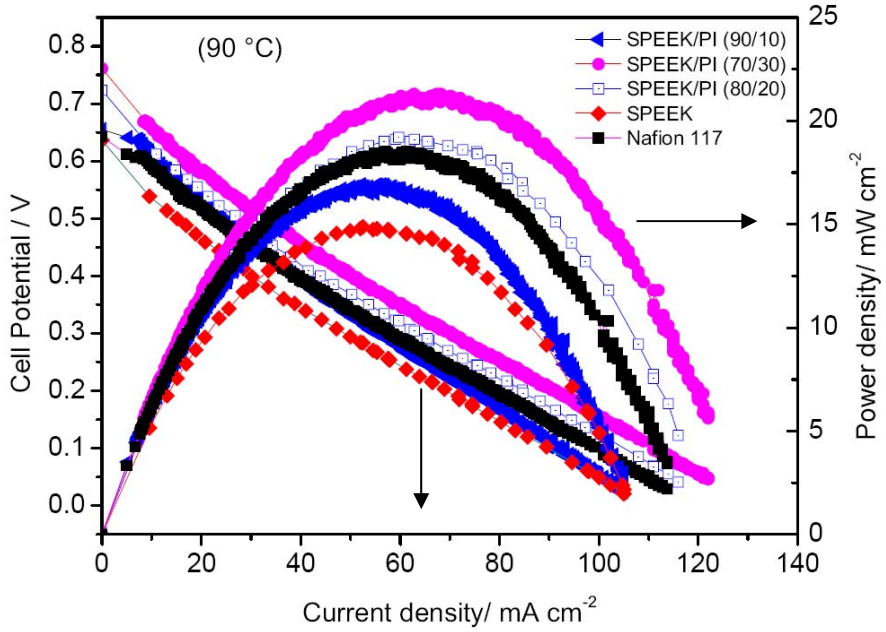


(a)

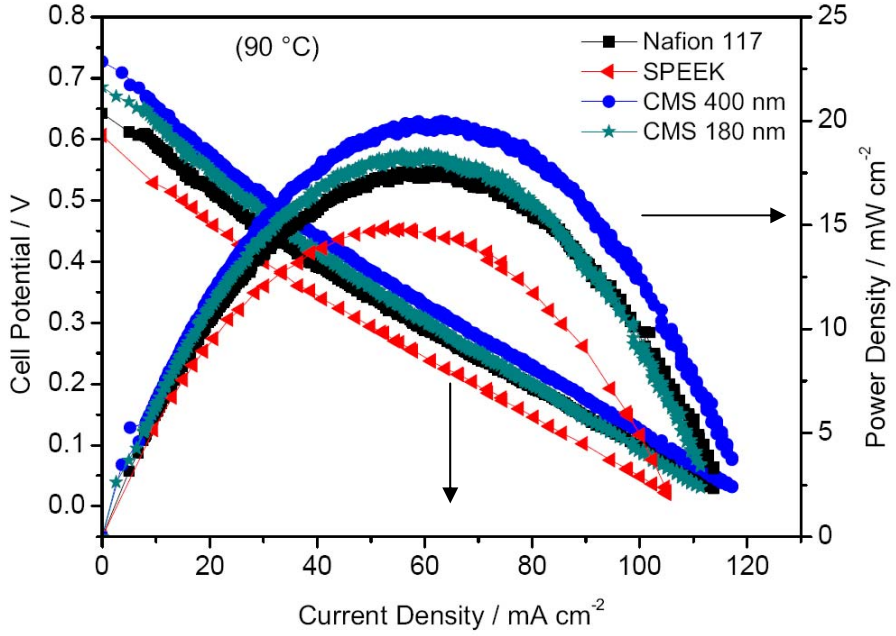


(b)

*Figure 6.7: Polarization and power density curves at operating temperature of 90 °C; (a)Nafion 117, pure SPEEK and (90/10), (80/20), (70/30) SPEEK/PI membranes (b)Nafion 117, pure SPEEK, CMS (180 nm and 400 nm)/SPEEK membranes.*

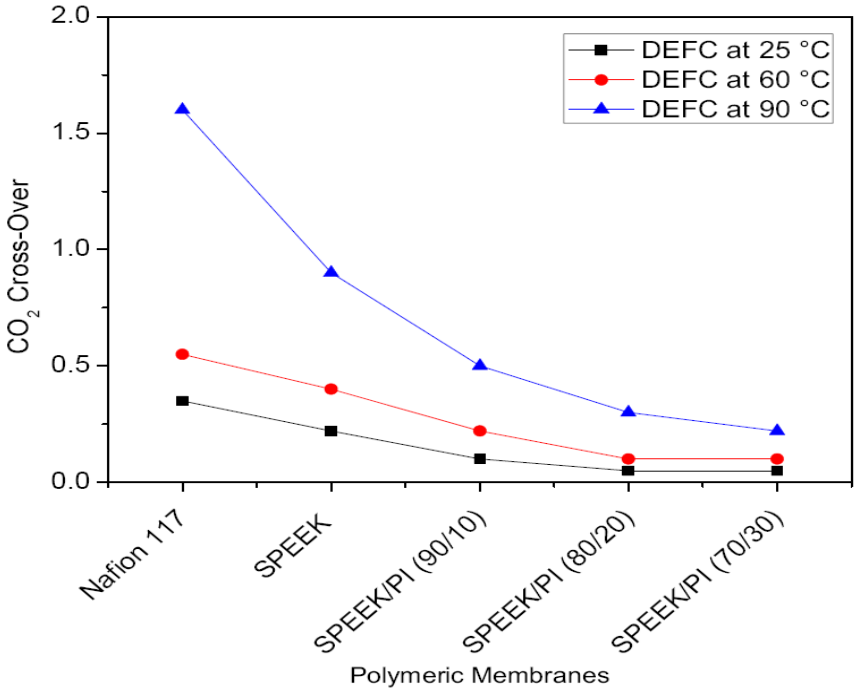


*Figure 6.8: Comparasion of $CO_2$ (crossover) results during DEFC test at 25 °C , 60 °C and 90 °C ; Nafion 117, pure SPEEK and (90/10), (80/20) and (70/30) SPEEK/PI membranes.*

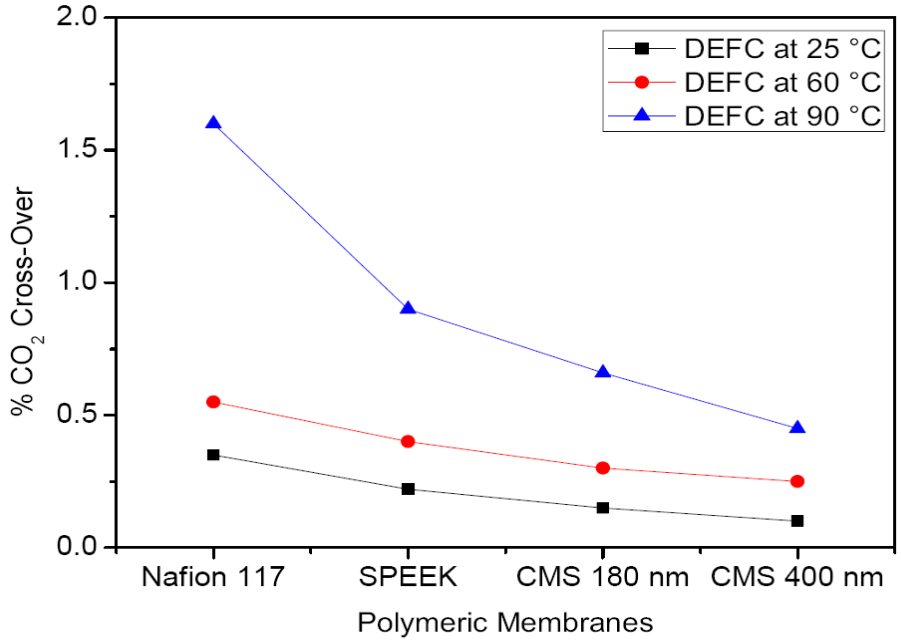


*Figure 6.9: Comparasion of $CO_2$ (crossover) results during DEFC test at 25 °C , 60 °C and 90 °C ; Nafion 117, pure SPEEK, CMS (180 nm and 400 nm)/ SPEEK membranes.*

### 6.4. Conclusions

CMS coated SPEEK and SPEEK/PI blend membranes were prepared and used for water / methanol separation and then for direct methanol fuel cell (DMFC) tests as discussed in previous chapters 4 and 5. In this chapter 6 the same membranes were used for the separation of ethanol / water mixture (5 wt %) in pervaporation and then the performance was also checked in direct ethanol fuel cell (DEFC) and the results were compared with Nafion 117. As can be seen from the results the CMS layer played an important role towards the rejection of ethanol during pervaporation and DEFC performance. But the blends of SPEEK / Polyimide (PI) showed better performance than CMS coated SPEEK membranes in both pervaporation of ethanol / water and in DEFC tests. The selectivity for water / ethanol is higher than for water / methanol of the same concentration (5 wt %). But the power density of DEFC is lower than DMFC and the reason is that for ethanol oxidation an efficient catalyst is needed as it was discussed in chapters 2 and 3. However all the membranes showed a high resistance to fuel cross-over during the DEFC test and at high temperature 60 °C and 90 °C.

## 6.5 References


[1] S.Rousseau , C. Countanceau, C. Lamy , J.-M Leger, Direct ethanol fuel cell (DEFC): performances and reaction products distribution under operating condition with different platinum based anodes *J. Power Sources* 158 (2006) 18–24.

[2] C.B Baretto, R.L.T Parreira, R.R Goncalves, D.C Azevedo, F.Huguenin; Platinum nanoparticles embedded in layer-bi-lyaer films from SnO2/polyallylamine for ethanol oxidation *J. Power Sources* 185 (2008) 6–12.

[3] It's a global thing; Ethanol producer magazine August 2006.

[4] C. Xu, H. Wang, P.K.Shen, S.P Jiang; Highly orderd Pd nanowire arrays as effective electro catalysts for ethanol oxidation in direct alcohol fuel cell. Adv. Mater. 2007, 19, 4256 – 4259.

[5] E.Ribadeneira, B.A.Hoyos; Evaluation of Pt-Ru-N and Pt-Sn-Ni catalysts as anode in direct ethanol fuel cells J.Power.Sources 180 (2008) 238 – 242.

[6] X.Xue, J.Ge, T.Tian, C, Liu, W. Xiang, T.Lu ; Enhancement of electro-oxidation of ethanol on Pt-Sn-P/C catalyst prepared by chemical deposition process, J. Power sources 172 (2007) 560–569.

[7] Q.Wang, G.Q Sun, L. Cao, L.H. Jiang, G.X. Wang, S.L. Wang, S.H. Yang, Q.Xin ; High performance direct ethanol fuel cell with double-layered anode catalysts layer, *J.Power Sources 17*7 (2008) 142–147

[8] F. Colmati, E.Antolini, E.R. Gonzalez; Effect of temperature on the mechanism of ethanol oxidation on carbon supported Pt, Pt-Ru and $Pt_3Sn$ electrocatalysts, *J. Power Sources* 157 (2006) 98–103.

[9] E.Antolini; Catalysts for dierect ethanol fuel cells; J.Power Sources 170 (2007) 1–12.

[10] A. Ghumman, C. Vink, O. Yepez, P.G. Pickup; Continuous monitoring of CO2 yields from electrochemical oxidation of ethanol: Catalyts, Current density and temperature effects. *J.Power Sources 177* (2008) 71–76.

[11] T. Mathuraiveeran, K.Roelofs, Senftleben, T Schiestel; Proton conducting composite membranes with low ethanol cross-over for DEFC. Desalination, 200 (2006) 662–663.

[12] A.R. Tan, L.M. Carvalho, F.G.R. Filho, A.S. Gomes; Nano-composite membranes based on sulfonated poly(etheretherketon) structured with modified silica for direct ethanol fuel cell. Macromol.Symp. 2006, 245-246, 470-475.

[13] G.Andreadis, P. Tsiakaras; Ethanol cross over and direct ethanol PEM fuel cell performance modelling and experimental validation, Chemical Engineering Science 61 (2006) 7497 – 7508.

[14] H.Maab, S.Shishatskiy, S.P. Nunes; Preparation and Characterization of Bilayer carbon/polymer membranes, J.Membr. Sci 326 (2009) 27 – 35.

[15] A. Heinzel, V. M. Barragán; A review of the state-of-the-art of the methanol crossover in direct methanol fuel cells. *J. Power Sources* 84 (1999) 70–74.

[16] P. Jannasch; Recent developments in high-temperature proton conducting polymer electrolyte membranes. *Curr. Opin. Colloid Interface Sci.* 8 (2003) 96–102.

[17] A. Dyck, D. Fritsch, S. P. Nunes; Proton conductive membranes of sulfonated poly phenylsulfone, *J. Appl. Polymer Sci.* 86 (2002) 2820–2827.

[18] K. Scott; W. M. Taama, P. Argyropoulos, K. Sundmacher; The impact of mass transport and methanol crossover on the direct methanol fuel cell. *J. Power Sources* 83 (1999) 204–216

[19] S. Swier, M.T. Shaw, R.A. Swei; Morphology of sulfonated poly(ether ketone ketone) poly(ether imide) blends and their use in proton exchange membranes, J.Membr.Sci. 270 (2006) 22 – 31

# Chapter 7. Summary

## 7.1 Summary

Fuel cells based on direct methanol fuel cell (DMFC) technology are considered as attractive and innovative for portable devices as compared to the current power sources with higher efficiency (10 times higher than the lithium-ion battery), low temperature operation (60 – 120 °C), inexpensive renewable fuel and environmentally friendly. Toshiba, Manhattan Scientific Inc, Smart Fuel Cell (Germany), Medis Technologies and many more are working to develop a micro-fuel cell based on the DMFC technology for application in portable devices like cell phone, laptops and etc. Smart fuel cell (Germany) EFOY (Energy for You) has also developed a bigger DMFC stack with high power generation for transportation, motorhome, CCTV and environmental monitoring applications. Another advantage is that the fuel (methanol) can be added in few seconds even during the operation of the device and the DMFC can start generation soon and continuously. In direct ethanol fuel cell (DEFC), ethanol is used as fuel instead of methanol which is toxic, flammable, volatile with a distinctive odour but slightly sweeter than ethanol. The direct ethanol fuel cell (DEFC) draws much more attention of the researcher groups all over the world because of its non toxic nature and high theoretical energy density of (8 kW h $Kg^{-1}$) to that of methanol (6 kW k $Kg^{-1}$). The system and design of the fuel cell (DEFC) is the same like for DMFC but a more effective catalyst for electro-oxidation of ethanol is required. In both systems the role of membrane is the same i.e. partition between the two electrodes, proton conductor and barrier to fuel.

DMFC and DEFC having polymer electrolyte membranes (PEM) as electrolyte are the most advanced systems of the fuel cell technologies. The sulfonated poly (ether ether ketone) (SPEEK) membrane possesses the properties for future development of fuel cell based on PEMFC, DMFC and DEFC technologies. For this purposes many research groups around the world are now focussing to make it free from any kind of disadvantages; most important one

the fuel cross-over through the membranes from anode towards cathode side. Therefore, the target is to modify the SPEEK membranes by other substance with reduced fuel cross-over but in any case the proton conductivity must not be lower than 10 mS/cm at working temperatures as well as the requirement of high mechanical, thermal stability and chemical stability at the applied conditions.

This research work is based on the preparation of membranes from SPEEK with reduced fuel cross-over following two different approach: 1) the preparation of bilayer membranes from in-home sulfonated PEEK (Vitrex) and a thin layer of in-home prepared carbon molecular sieve (CMS) from polyimide (Matrimid 5218); 2) blending of SPEEK with polyimide polymers. In both ways, it was possible to decrease the fuel cross-over in both direct methanol fuel cell (DMFC) and direct ethanol fuel cell (DEFC) without compromise on proton conductivity. In this research work, a SPEEK with 56 % sulfonation degree was prepared and then used for making polymeric membranes.

The specific modifications made to SPEEK polymeric membranes can be summarized as follows:

*(1) CMS coated SPEEK bilayer membranes:*

The idea was to take advantage of molecular sieving effects of the CMS for the rejection of bigger fuel molecules from the fuel mixture (water/alcohols) during pervaporation, DMFC and DEFC tests. The CMS layer was prepared by pyrolysis at (500°C-1000°C), under inert ($N_2$ gas) atmosphere, of a thin film prepared from a polyimide (Matrimid 5218) solution in chloroform. The complete pyrolysis to carbon was confirmed by FTIR-ATR analysis. CMS prepared at 800 °C for 8 hours were chosen for further characterization because of high water/alcohols selectivity and easily detached from the quartz glass without any damage to them. Based on the thickness of CMS layer resulted from polyimide solutions with different concentration (1 and 2 wt. %), two types of bilayer membranes (CMS/SPEEK) were prepared.

i. SPEEK coated with 180 nm CMS thick layer (from 1 wt. % solution) (CMS/SPEEK 1).

ii. SPEEK coated with 400 nm CMS thick layer (from 2 wt. % solution) (CMS/SPEEK 2).

Another approach was the preparation of a membrane electrode assembly (MEA) by the incorporation of platinum as catalyst into the CMS layer in order to take advantage of both fuel barrier and electron conducting properties of the CMS layer.

In order to determine fuel-crossover through plain SPEEK and CMS/SPEEK bilayer membranes, pervaporation experiments were carried out with methanol solutions at different concentrations (5, 10 and 20 wt. %) as well pervaporation of ethanol, n-propanol and iso-propanol solutions each with different concentrations (5 and 10 wt. %) were also carried out to investigate the pore size of the thin CMS layer. Table 1 shows the pervaporation results using both methanol and ethanol solutions with the same concentration (5 wt. %) and the proton conductivity measured at 60°C and 100% relative humidity (R.H.). It can be seen that fuel cross-over through the CMS/SPEEK bilayer membranes is quite low as compared to plain SPEEK and at the same time the proton conductivity remains almost constant. These results highlight the fuel barrier properties of the CMS layer.

Table 7.1: Methanol and Ethanol permeability at 55 °C and proton conductivity at 60 °C and 100% R.H.

| **Membrane** | **CMS layer thickness (nm)** | **P ($10^{-10}$ Kg m $s^{-1}$ $m^{-2}$)** | | **Proton conductivity (mS $cm^{-1}$)** |
|---|---|---|---|---|
| | | **MeOH** | **EtOH** | |
| **SPEEK** | 0 | 28 | 19 | 34 |
| **CMS/SPEEK 1** | 180 | 18 | 8.5 | 33 |
| **CMS/SPEEK 2** | 400 | 10 | 3.1 | 35 |

*(2) SPEEK/PI Blends membranes:*

The idea was to take advantage of hydrophobic property of polyimide by incorporating it into SPEEK matrix for rejection of alcohols/water mixture during pervaporation, DMFC and DEFC performances.

Three types of homogeneous SPEEK/PI blends were prepared at high temperatures (80°C, 90°C, 100°C, 110°C, 120°C and 130°C) based on the amount of polyimide (Matrimid 5218) added to the blend solution using dimethyl sulfo-oxide (DMSO) as solvent.

- SPEEK/PI (90/10)
- SPEEK/PI (80/20)
- SPEEK/PI (70/30)

It was observed that homogeneous membranes were obtained at casting temperatures higher than 110 °C independent of the PI concentration in the SPEEK/PI blend solution. The same solutions rendered non-homogeneous membranes when cast below this temperature. For further characterization, homogeneous membranes from the above mentioned SPEEK/PI blend solutions were prepared by casting the solution at 130°C. The methanol and ethanol permeation through these membranes was determined by the pervaporation of methanol and ethanol solutions (5 wt % concentrations) at 55°C (Table 2).

Table 7.2: Methanol and Ethanol permeability at 55 °C and proton conductivity at 60 °C and 100% R.H.

| **Membrane** | **P ($10^{-10}$ Kg m $s^{-1}$ $m^{-2}$)** | | **Proton conductivity (mS $cm^{-1}$)** |
|---|---|---|---|
| | **MeOH** | **EtOH** | |
| **SPEEK** | 28 | 19 | 34 |
| **SPEEK/PI (90/10)** | 7.21 | 4.4 | 33 |
| **SPEEK/PI (80/20)** | 2.61 | 1 | 28 |
| **SPEEK/PI (70/30)** | 0.55 | 0.4 | 25 |

The hydrophobic role of PI towards fuel rejection through the blend membranes as compared to plain SPEEK membranes is the reason for the low permeability values when increasing the concentration of PI in the blend solution. The proton conductivity (mS $cm^{-1}$) at 60 °C is also

shown in Table 2. About the effect of the blend composition onto the proton conducting properties of the membranes, just a slight decrease of the proton conductivity has been observed when increasing the PI concentration.

Other functional characterizations of all the CMS/SPEEK and SPEEK/PI membranes prepared in this work included water and mixture uptake, direct methanol fuel cell (DMFC) and direct ethanol fuel cell (DEFC) performance tests. The morphology of the CMS/SPEEK and SPEEK/PI membranes (both homogeneous and non-homogeneous) was analysed by atomic force microscopy (AFM) and scanning electron microscopy (SEM). While attenuated total reflectance (ATR-FTIR), dynamic mechanical thermal analysis (DMTA), thermogravimetric analysis (TGA) and differential scanning calorimetry (DSC) were performed for the SPEEK/PI blend membranes to analyse the homogeneity of these membranes as compared to the pure constituents (polyimide and SPEEK).

**7.2 Zusammenfassung:**

Brennstoffzellen, die auf der Direktmethanolbrennstoffzellen-Technologie (DMFC) basieren, sind interessant und zukunftsweisend für portable Geräte. Im Vergleich mit herkömmlichen Energiequellen weisen DMFC-Brennstoffzellen eine 10-mal höhere Energieeffizienz als Lithium-Ionen-Batterien auf, arbeiten bei niedrigeren Temperaturen (60 – 120 °C), lassen sich kostengünstig erneuern und sind umweltfreundlich. Toshiba, Manhattan Scientific Inc., Smart Fuel Cell (Germany), Medis Technologies sowie zahlreiche weitere Unternehmen arbeiten an der Entwicklung von Mikrobrennstoffzellen auf Basis der DMFC-Technologie zur Anwendung in tragbaren Geräten wie Mobiltelefonen, Notebooks u. ä. Smart Fuel Cell (Germany) und EFOY (Energy for You) haben einen größeren DMFC-Brennstoffzellenstack für den Einsatz in Lkw, Wohnmobilen, Video- und Umweltüberwachungseinrichtungen entwickelt. Ein weiterer Vorteil ist, dass der Brennstoff (Methanol) innerhalb kürzester Zeit und auch während der Anwendung hinzu gegeben werden kann. In Direktethanolbrennstoffzellen (DEFC) kommt Ethanol anstelle des giftigen, leicht

entzündbaren und instabilen Methanol, das einen starken Geruch hat und geringfügig süßer als Ethanol ist, zum Einsatz. Weltweit beschäftigen sich weitaus mehr Forschungsteams mit Direktethanolbrennstoffzellen (DEFC), weil Ethanol nicht giftig ist und eine höhere theoretische Energiedichte von (8 kW h $Kg^{-1}$) im Vergleich zu Methanol (6 kW k $Kg^{-1}$) aufweist. System und Design von Direktethanolbrennstoffzellen (DEFC) und Direktmethanolbrennstoffzellen (DMFC) sind in etwa gleich – allerdings ist für die Elektrooxidation von Ethanol ein effektiverer Katalysator erforderlich. In beiden Brennstoffzellenarten ist die Rolle der Membran dieselbe: sie wirkt als Trennschicht zwischen den beiden Elektroden, fungiert als Protonenleiter und gleichzeitig wirkt sie als Sperrschichtfolie für den Treibstoff.

Als besonders geeignete lonen leitende Membran für PEMFC-, DMFC- and DEFC-Anwendungen hat sich eine Membran aus sulfoniertem PoIyetheretherketon (SPEEK) erwiesen. Wesentlicher Nachteil dieser Membran ist ihre Methanoldurchlässigkeit insbesondere bei höheren Methanolkonzentrationen, was zu einer Minderung der Leistungsfähigkeit führt. Es besteht in der Tat die Notwendigkeit an neuen und besseren Membranmaterialien, die gute Barriere-Eigenschaften für den Treibstoff, hohe Protonenleitfähigkeit sowie ausreichenden thermische und chemische Widerstandfähigkeit aufweisen.

Die Aufgabe der vorliegenden Arbeit ist es, eine auf SPEEK-basierte Membran zu entwickeln, die eine verbesserte mechanische Stabilität und/oder ein wesentlich verbessertes Methanolrückhaltevermögen aufweist. Dafür werden zwei verschiedene Strategien verfolgt: 1) Herstellung von Doppelschichtmembranen aus SPEEK (die Protonleitende Schicht) und Kohlenstoffmolekularsiebe (CMS) (die trennaktive Schicht). In dieser Arbeit sind auch die Sulfonierung von kommerziell erhältlichen PEEK (Vitrex) sowie die Herstellung des CMS aus Polyimid (PI) (Matrimid 5218) eingeschlossen. 2) Herstellung von Blendmembranen aus

SPEEK und PI. Eine Beschreibung der beiden Strategien kann wie folgt zusammengefasst werden:

*(1) CMS/SPEEK Doppelschichtmembranen:*

Das Konzept ist, die Vorteile der Trennungseigenschaften der CMS zur Verringerung der Alkoholdurchlässigkeit während DMFC- und DEFC-Tests nutzen zu können. Die CMS wurden durch Pyrolyse einer dünner Polyimid-Membran bei hohen Temperaturen (500 °C-1000 °C) unter Inertgasatmosphäre ($N_2$) erhalten. Die so hergestellten CMS wurden danach mittels FTIR-Spektroskopie untersucht. Nach 8 Stunden Karbonisierung bei 800 °C wurde ein CMS mit einer hohen Wasser/Alkohol-Selektivität hergestellt, das für weitere Charakterisierungen und die Herstellung der Doppelsichtmembranen verwendet wurde. Aus PI-Chloroform-Lösungen mit zwei verschiedenen Konzentrationen wurden folgende Doppelschichtmembranen hergestellt:

i. Beschichtung einer 180 nm dicken CMS-Schicht, die aus einer 1 Gew.-% PI-Chloroform-Lösung hergestellt wurde, mit einer SPEEK-Schicht (CMS/SPEEK 1).
ii. Beschichtung einer 400 nm dicken CMS-Schicht, die aus einer 2 Gew.-% PI-Chloroform-Lösung hergestellt wurde, mit einer SPEEK-Schicht (CMS/SPEEK 2).

Wegen ihrer elektrischen Leitfähigkeit und Trennungseigenschaften eigneten sich CMS für die Herstellung von Gasdiffusionselektroden; daher wurden auch mit Platin dotierten CMS (Pt-CMS/SPEEK) Membran-Elektroden-Einheiten hergestellt.

Pervaporation Tests mit MeOH-Wasser (5 Gew.- %) und EtOH-Wasser (5 Gew.- %) Lösungen wurden durchgeführt um den Stofftransport durch die hergestellten Membranen zu bestimmen. Tabelle 1 zeigt, dass Methanol- und Ethanoldurchlässigkeit den CMS/SPEEK Membranen erheblich niedriger war als die der Ausgangsmembran (SPEEK), während kein negativer Einfluss auf die Protonenleitfähigkeit beobachtet wurde. Diese Ergebnisse heben die Brennstoff-Barriere-Eigenschaften der CMS-Schicht hervor.

Tabelle 7.3: Methanol- und Ethanoldurchlässikeit (P) bei 55 °C und Protonenleitfähigkeit bei 60 °C und 100% r.F.

| Membran | CMS- Schichtdicke (nm) | P ($10^{-10}$ Kg m $s^{-1}$ $m^{-2}$) | | Protonenleitfähigkeit (mS $cm^{-1}$) |
|---|---|---|---|---|
| | | MeOH | EtOH | |
| **SPEEK** | 0 | 28 | 19 | 34 |
| **CMS/SPEEK 1** | 180 | 18 | 8.5 | 33 |
| **CMS/SPEEK 2** | 400 | 10 | 3.1 | 35 |

*(2) SPEEK/PI Blend Membranen:*

Andere Versuche zur Verringerung des Stofftransportes waren die Herstellung von homogenen Polymer-Blend-Membranen aus einer SPEEK/PI-Polymerlösung. Weil PI beachtlich wasserabweisend (hydrophob) ist, erwartet man eine Verringerung der Methanol- und Ethanoldurchlässikeit.

Für verschiedene der PI-Konzentrationen in der SPEEK/PI-Polymerlösung wurden drei verschiedene homogene SPEEK/PI Blend-Membranen bei hohen Temperaturen (80 °C, 90 °C, 100 °C, 110 °C, 120 °C and 130 °C) hergestellt:

- SPEEK/PI (90/10)
- SPEEK/PI (80/20)
- SPEEK/PI (70/30)

Ein Zusammenhang zwischen Homogenität der SPEEK/PI-Blend-Membranen und Giess-Temperatur wurde festgestellt. Homogene SPEEK/PI-Blend-Membranen wurden nur bei Temperaturen über 110°C, bevorzugt 130 °C, erhalten. Methanol- und Ethanoldurchlässikeit der SPEEK/PI-Blend-Membranen wurde mit Pervaporation Tests (bei 55 °C mit 5 Gew.- % Alkohol) gemessen (Tabelle 2).

Tabelle 7.4: Methanol- und Ethanoldurchlässikeit (P) bei 55 °C und Protonenleitfähigkeit bei 60 °C und 100% r.F.

| Membran | P ($10^{-10}$ Kg m $s^{-1}$ $m^{-2}$) | | Protonenleitfähigkeit (mS $cm^{-1}$) |
|---|---|---|---|
| | MeOH | EtOH | |
| **SPEEK** | 28 | 19 | 34 |
| **SPEEK/PI (90/10)** | 7.21 | 4.4 | 33 |
| **SPEEK/PI (80/20)** | 2.61 | 1 | 28 |
| **SPEEK/PI (70/30)** | 0.55 | 0.4 | 25 |

Die in Tabelle 2 dargestellten Ergebnisse heben die Wasserabweisenden-Eigenschaften des PI in SPEEK/PI Blend-Membranen in Vergleich zu der Ausgangsmembran (SPEEK) hervor. Ein leichter Einfluss der PI-Konzentration in der SPEEK/PI-Blend-Membran auf die Protonenleitfähigkeit wurde festgestellt, je höher die PI-Konzentration desto geringer wurde die gemessene Protonenleitfähigkeit.

Andere funktionelle Charakterisierungen wie Wasseraufnahme, DMFC- und DEFC-Leistungstests wurden durchgeführt. Die Membranmorphologie für alle hergestellten CMS/SPEEK und SPEEK/PI Membranen wurde durch Rasterkraftmikroskopie (RKM) und Rasterelektronenmikroskopie (REM) untersucht. Außerdem wurde die Homogenität der SPEEK/PI-Blend-Membranen bei Abgeschwächter-Totalreflektion Fourier-Transformations-Infrarotspektroskopie (ATR-FTIR), thermogravimetrische Analyse (TGA), Differential-Wärmefluß-Kalorimetrie (DSC) und dynamisch-mechanisch-thermischer Analyse (DMTA) untersucht.

# Chapter 8. Acknowledgment

## 8.1 Acknowledgment:

*Working as a Ph.D Scholar in Germany was an excellent plus a challenging experience after 9 years of my Master. During this period many people from Germany and Pakistan pushed and helped me re-shaping my academic & research carrier for competing the 21st century with new technologies.*

*First of all I am greatly thankful to Prof.Dr. Volker Abetz, Director Institute of Polymer Research and Professor at Faculty of Technology University of Kiel; for being my university supervisor and allowing me to come to Germany and work at GKSS Research Center (Geesthacht) one of Helmholtz (HGF) centres. Numerous thanks for his continuous support, fruitful technical and creative discussion during our routine progress report meeting and now supervising my Ph.D dissertation in Kiel University.*

*I feel immense pleasure to say thanks to my research supervisor Dr. Suzana Pereira Nunes, Head of Department Membranes for Energy-technology (PME); for supervising all of my Ph.D research, technical advice and guideline during the whole period. I was really influenced by her technical expertise, creativity and basic knowledge in the field of Membranes Sciences; and tackling any research problem in time during the work I faced.*

*A special thanks to my co-supervisor Dr. Sergey Shishatskiy, the most responsible person who guided and helped me all the time during my research work at the laboratories and then evaluating the results and writing in the form of papers for publications. Without his encouragements and support I would not be able to finish this gigantic task in time. I should not forget the moral and technical support of my previous group members Dr. Irmgard Buder and Dr. Jun Qiu who helped me a lot during my early difficult days. Also I wish to thank all of my present group members (PME) who directly or indirectly helped me in some ways during our weekly group meetings. They are Dr. Mariela Ponce, Dr. Wilfredo R.Yave, Dr. Anja Car, Dr. M.Schieda, A.Petersen, J.R.Pauls, Y.Treekamol, I. Kusumawardhana, Pradeep NC, G.Johansson and I.Ternes. Many persons from other department of this institute also helped me regarding my research work. Therefore, special thanks to Dr. K. Ebert, Dr. G.Bengston & S.Dargel (GC), Dr. P.Simon (GPC), M.Aderhold & K.M. Prause (SEM), G.Lührs & Clarissa Abetz (AFM),*

*H. Böttcher (DMTA), Silvio Neumann (TGA & DSC), C.Scholles and H. Pingel. My deep hearted thanks to every member of this Polymer Institute. Scientists and Researchers from all over the world tend to come and work at GKSS because it is amongst the world famous research centres including Polymers, Materials and Coastal Research institutes with almost all kind of facilities. Therefore I had the opportunities to make friends like Mustafa Volkan Uz, Shahrokh Danishpour, Shaheen Homaeigohar, Tariq Abu Leil, Ibrahim Taha, Zahid Chaudhary, Ashak Pervez, M.Rakib ul Kabir, Shaik Bashir, Weimin Gan, T.Dai, R.Zeng, B.Kannan, C.Nistor, Plamin Iliev and many more. I found Christine Plath quite helpful in the time of need and a lot of thanks for her so nice attitude. A lot of thanks to Mr. P. Kummerow (a responsible person for foreigners in GKSS) for solving my residential, visa related and many more problems. I am thankful to P.K.Kapoor and all of his family members for moral support and ensuring any kind of help I needed from them.*

*I missed a lot the company of my parents, sisters and brothers, Yasar Arafat and Durre- Maab. I am grateful of the best wishes and prayers of my Aunts & Uncles Amir Ferosh Aasi and Fazal Mabood Zia. On this happy occasion I really miss my late Uncle Prof. Aurang Zeb who motivated and encouraged us towards higher education. Also I wish to thank my cousins Haroon Khan Aasi, Adnan Amir Aasi, Numan Aasi, Javed Iqbal, Shafqat Shahab, Afrasiab, Zatul Amin, Shafqat Seir, Akbar Ali and my friends Bashir Iqbal, Abdus Salam, Hamayun Khan, Zafar Ali Khan and Mati Ur Rahman for having online contact with me most of the time to encourage and to treat my home sickness. Special thanks to the Directors of CESAT Institutes (Pakistan) Javed Raza Khan and Saleem Khalid for allowing me for higher studies abroad and continuation of their help regarding my service matters through out this period. And finally my best friend and my spiritual teacher Dr.Hussain Ahmad Director EPA-NWFP Peshawar Pakistan; who found this position for me looking to my long time desire for Ph.D degree. He proved himself to be a best friend and honestly guided me through out this whole period.*

*I greatly acknowledge the financial support from GKSS during this whole period of my Ph.D research that helped me a lot during my stay in Germany.*

**8.2 Curriculum Vitae (CV)**

# Husnul Maab

***Wald Strasse 5, Geesthacht 21502 Germany***
***Phone No. +49-4152872467***
***E-Mail: mhusnul@hotmail.com***
***husnul.maab@gkss.de***

---

## Professional / Employeement History & Experiences

**1** **Department of Membranes for Energy Technology (PME) Institute of Polymer Research GKSS Research Centre Geesthacht GmbH, Germany**

*Research Scientist (April 2006 – October 2009).*

*Membranes for Energy Technology / Membranes & Membranes Electrode Assembly (MEA) for:*

- *Direct Methanol Fuel Cell (DMFC)*
- *Direct Ethanol Fuel Cell (DEFC) and*
- *Hydrogen Fuel Cell (PEMFC) Applications*

**2** **Environmental Protection Agency (EPA) North West frontier Province (NWFP) Pakistan; (Environmental Protection and Resource Conservation project (EPRC) of Pakistan; funded by World Bank).**
**(Inventory of Industrial Discharges and Pollution profile (IIDP) of NWFP)**

*Field Officer / Research Officer (05-11-1997 – 12-30 1999)*

**3** **Investigation of a Re-cyclic method for solubility of polyethylene shopping bags based on its dissolution in selected solvents.**

*Master of Science (M.Sc) Theises (1995 – 1997)*

**4** **Teaching Experiences**

*Islamiya English medium School & College Swabi (15-02-2000 to 31-08-2000)*

**5** **National Centre of Excellence Islamabad Pakistan.**

*Manager (Chemical laboratories) (11-09-2000 till Now)*

## EDUCATION

*1* Faculty of Engineering, Christian-Albrechts-University (CAU) of Kiel Germany

**Ph.D Membranes Technology for Fuel Cells (2009).**

2 University of Peshawar, Peshawar, Pakistan (1996 – 1997)

**M.Sc. Chemistry (Analytical chemistry).**

3 University of Peshawar, Peshawar, Pakistan (1993 – 1994)

**B.Sc. (Chemistry, Zoology and Geography).**

## Publications

1 H. Maab, S. Shishatskiy, S. P. Nunes; Preparation, characterization of bilayer carbon / polymer membranes. *Journal of Membrane Science* 326 (2009) 27 – 35.

2 H. Maab, M. Scheida, W.Y. Rios, S.Shishatskiy, S.P. Nunes; SPEEK / polyimide (PI) blends for proton conductive membranes, *Fuel Cell 09, 2009, No 4, 401 - 409*

## International Conferences and Posters Presentations

1. Zahner Impedance days March 2006 Germany.
2. Marrie-Currie workshop"New Materials for Membranes Technology" June 2007 GKSS Research Centre Geesthacht Germany.
3. 24th EMS Summer School (Membranes for Reactive Processes), September 2007 Genoa Italy.
4. NanoMemCourse 3rd Event "Nano-structured Materials and Membranes for Energy". March 2009 Norway.

**Personal Information:**

| | |
|---|---|
| Name: | ***Husnul Maab*** |
| Father's Name: | *Fazli Wahab* |
| *Religion* | *Islam* |
| Passport No. | AA0098791 |
| NID No. | 16202-0878879-3 |
| Date of Birth: | April 10, 1974 |
| Place of birth | Turlandi (District Swabi) NWFP Pakistan |
| Gender | Male |
| Marital Status: | Single |
| Hobbies | Reading, Travelling in mountainous areas. |
| Present Address: | GKSS Wohnheim Otto-Hahn-Strasse 1<br>Geesthacht 21502 Germany<br>**Ph: +49-4152872467(Office.)** |
| **E-mail:** | **mhusnul@hotmail.com**<br>**husnul.maab@gkss.de** |
| **Permanent Address**: | Mohallah Ali Khan Khel, Village & Post office<br>Turlandi; Tehsil & Dist. Swabi (N.W.F.P) Pakistan<br>Ph: 0092-938-311836 |

**References:**

**Prof.Dr. Volker Abetz**
***Director Institute of Polymer Research;***
*GKSS Research* Centre Geesthacht
GmbH 21502 Germany.
**Professor at Faculty of Technology,**
University of Kiel Germany
Ph: +49-4152872461
E-mail: volker.abetz@gkss.de

Dr. Suzana Periera Nunes
***Head Department of Membranes***
***for Energy Technology (PME)***
Institute of Polymer Research;
GKSS Research Centre
Geesthacht GmbH 21502 Germany
Ph: +49-4152872440 (Office)
E-mail: suzana.nunes@gkss.de

## 8.3 Declaration on application for doctoral admission

I declare hereby that this doctoral theses was prepared by myself and all the publications are correctly cited here as references.

This work is neither published before by any other body nor is copied from other sources.

This doctoral theises has never been submitted in the present form or similar to any other University or board of examiners.

Husnul Maab

GKSS Research Center Geesthacht, April 2009

## 8.4 Pictures



WORLD ENERGY DIALOGUE
Where Future meets Solutions
22-23 April 2008
BDI
dena
Fast Lane
Besucher Visitors


Arbeitsgruppe
Numerische Feldb


MICHIGAN


HOLSTEN
HOLSTEN